

Heidelberg University
Faculty of Chemistry and Earth Sciences
Institute of Geography

Master Thesis

**Discussion of the thermo-insulation effect of a seasonal snow
cover on permafrost soil in Bayelva, Svalbard (1998 - 2017)
with respect to current knowledge**

Sabrina Ebenhoch

Matriculation Number: 2905457

ebenhoch@stud.uni-heidelberg.de

Supervision:

Prof. Dr. Bernhard Höfle (Ruprecht-Karls-Universität Heidelberg)

PD Dr. Julia Boike (Alfred-Wegener-Institut für Polar- und Meeresforschung)

Date:

January 29, 2018

Statutory Declaration

I declare that I have authored this thesis independently, that I have not used other than the declared sources / resources and that I have explicitly marked all material which has been quoted either literally or by content from the used sources. This work was not previously presented to another examination board and has not been published.

Heidelberg, January 29, 2018

Abstract

Bayvelva is a High-Arctic research site on Spitsbergen Island in the Svalbard archipelago (78.551 ° N; 11.571 ° E) where climate, soil and snow components are recorded since 1998 by the Alfred-Wegener-Institute. This study site is underlain by permafrost with average temperatures around -2.8 °C and seasonally snow-covered from October to May. The snow pack thermally insulates the soil temperatures from air temperature signals, a connection which is not well understood yet. To gain better understanding of these thermal relationships, long-term analyses of air, radiation, soil and snow characteristics were examined in this study.

Air temperature has increased by 0.14 °C per year for the period from 1998 to 2016 which is higher than the global average temperature increase in the same period. Radiation balance trend analyses are characterized by an increase in longwave radiation during winter months. Results of snow characteristic studies show that the last day in the year with a snow cover has been moving to earlier dates with 0.5 days per year from 1998 to 2016, extending the snow-free season. Thus more time for soil warming is supplied. This aligns well with warming trends of all soil temperature sensors to a depth of 9 m as well as the thickening of the active layer (ALT). The ALT is estimated to have reached a depth of 2 m in 2016 for the first time, following an increase of 0.05 per year. Since it is difficultly to measure the exact ALT, we used the 'Stefan-Model'.

To account for different magnitudes of snow cover insulation, an effective snow depth ($S_{\text{depth,eff}}$) was calculated for each year. High $S_{\text{depth,eff}}$ values represent high thermo-insulation, due to early snowfall and long periods with snow depths over 0.4 m, and can be linked to years in which re-freezing of the whole active layer took until early March of the next year.

The results of this study support the importance of snow physical characteristics for the permafrost thermal regime, as also detailed in the Arctic Monitoring and Assessment Programme - an Arctic Council Working Group.

Contents

Statutory Declaration	I
Abstract	III
1 Introduction	1
1.1 State of Research	3
1.2 Variables and techniques	4
2 Study Site	7
2.1 Climate Stations	8
2.2 Soil Stations	9
2.3 Data Quality Control	10
3 Background on thermal relations in permafrost regions	11
3.1 Surface Energy Budget	12
3.2 Heat Flow in Frozen Soils	13
3.2.1 Thermal Conductivity and Heat Capacity	14
3.2.2 Progression of Temperature Waves	14
3.2.3 The Stefan-Model	15
3.2.4 Near-Surface Ground Temperature	16
4 Methods	18
4.1 Air Temperature	18
4.2 Radiation	19
4.3 Snow Cover Timing Variation	19
4.4 Thermal-Insulation Effect	23
4.5 Active-Layer	27
4.6 Permafrost	27
4.7 Precipitation	28
5 Results	29
5.1 Climate	29
5.1.1 Radiation Component Characteristics	29
5.1.2 Air Temperature Characteristics	32
5.2 Snow	34
5.2.1 Duration of the Snow Cover	34
5.2.2 Measured versus Effective Snow Depth	36
5.3 Soil	40
5.3.1 Active Layer	40

5.3.2	Permafrost	42
5.4	Linkage between Climate, Snow and Soil Characteristics	44
6	Discussion	47
6.1	Comparison to other sites	47
6.1.1	Climate	47
6.1.2	Soil	50
6.1.3	Snow Cover Characteristics	53
6.2	Difficulties in snow cover modeling	55
7	Summary and concluding remarks	60
	Acknowledgment	62
	Bibliography	63
	Appendix	69

List of Figures

1	Aerial orthoimage	7
2	Temperature Profile	11
3	Freeze-Back and Zero-Curtain	15
4	Snow Cover Variables	20
5	Snow Cover onset and offset	22
6	Soil vs. Air Temperatures	24
7	Monthly mean values four radiation components	30
8	Annual Air Temperatures	32
9	Monthly Air Temperatures	33
10	Freezing/Thawing Degree Day Index	34
11	End of Snow Cover	35
12	Effective Snow Depth	37
13	Relation $S_{\text{depth,eff}}$ and A_{norm}	39
14	Date and duration of active layer freeze-up	41
15	Active Layer Thickness after Stefan-model	42
16	Permafrost Temperature Trends	43
17	Positive Correlations	45
18	Comparison A_{norm}	56
19	Daily air and soil amplitudes vs. Snow Height	58
20	Climate Station 1998 to 2009	69
21	Climate Station 2009 to now	70
22	Soil station 1998 to now	71
23	Soil station 2009 to now	71
24	Comparison Borehole and Soil Profile Temperatures	72
25	Seasonal Air Temperatures	72
26	Active Layer Temperature Trends	73
27	Linking the Parameters	77
28	Meteorological Stations Svalbard	79
29	Seasonal trends of Net Radiation	80
30	Permafrost Temperatures SWIPA	81

List of Tables

1	Quality control	10
2	Effective Snow Depth:	38
3	Maximum Soil Temperatures:	74
4	Minimum Soil Temperatures:	75
5	Permafrost Temperatures:	76
6	Correlation Variables:	78

1 Introduction

In 2014, the Intergovernmental Panel on Climate Change (IPCC) published the Contribution of Working Group II to their Fifth Assessment Report: Impacts, Adaptation, and Vulnerability [Larsen et al. 2014]. The authors gathered research results on climate change and summarize impacts of climate change on the environment as well as humankind, give adaptation suggestions as well as vulnerability aspects of the Earth. The report states that amongst many other challenges humankind has to face in the coming years, like water scarcity or sea-level rise, changes in the Arctic and Antarctica permafrost due to climate change will have a direct impact on the lives of people in those regions. Degradation of this frozen ground may even put lives at risk [Larsen et al. 2014]. The Physical Science Basis published one year earlier reported that both the temperature of continuous permafrost (covering >90% of a geographic region) as well as the freeze and thaw pattern of seasonally frozen ground are highly sensitive to climatic changes. Resulting changes in landscapes, ecosystems, hydrology, and the gas exchange between atmosphere and the lithosphere are drastic and the full extent is not yet fully understood [IPCC 2013b].

Warming temperatures in most regions of continuous permafrost as well as the thickening of seasonally thawing and freezing ground are both observed with *high confidence*, showing high agreement of the evidence. The extent of the snow cover on the Northern Hemisphere (NH) was decreasing since 1950 with *very high confidence* [IPCC 2013c]. While the evidence of those trends is very clear and there is high agreement amongst the contributing scientists, the degree of change rates is provided with uncertainties, due to high variations between different research sites. Emphasizing the importance and urgency to gain deeper understanding of those processes, the IPCC has decided on publishing a Special Report on the Ocean and Cryosphere in a Changing Climate (SROCC) by the end of 2019.

In addition to the IPCC reports on the state of frozen ground, the Arctic Monitoring and Assessment Programme – an Arctic Council Working Group published their second report on Snow, Water, Ice and Permafrost in the Arctic (SWIPA), focusing only on Arctic regions, giving an even closer insight in recent research developments [AMAP 2017]. A significant gap of knowledge identified by the authors, exists on snow related processes in the Arctic. Uncertainties occur especially on the role a seasonal snow cover plays as boundary layer on the temperature profile between the atmosphere and lithosphere. The effect a snow cover has on soil temperatures was modeled by Cook et al. [2008]. The authors run a state of the art climate model (CAM3-CLM3) in a first round with two cases of thermal conductivity of the snow layer: at first setting the thermal conductivity equal to the underlying soil pack, thus eliminating an insulation effect, and second setting the thermal conductivity as a function of snow density. Both cases are run with minimal and maximal observed thermal conductivity values, leading to the result of soil cooling up to 20 K in winter for the high conductivity/low insulation scenario. This example for a climate model including a seasonal snow cover shows

how intense the thermal insulation can be but on the other hand is based on the density of snow, a property that is highly difficult to determine.

To gain better knowledge on the big-scale developments (Arctic, Global) profound understanding of regional processes needs to be achieved. This study contributes to this, by characterizing snow-related processes of a High-Arctic research site on Svalbard. Meteorological and energy balance parameters as well as subsurface components were recorded since 1998 in Bayelva, a river bank, situated on the west coast of Svalbard. Long-term trends of the variables connected to the thermal regime of the atmosphere-lithosphere interaction are examined in a first step of this work. Comparing them to other Arctic sites gives insight on the high variability of results of climate change on frozen ground regions. In a second part, the role of the seasonal snow cover on air and soil temperature differences is inspected more closely, applying an exponential fit defined by Slater et al. [2017]. Before an introduction to recent techniques and research results of permafrost regions is given, the three most important terms for this work will be defined:

The term **permafrost** is used, where the average soil temperature is below 0 °C for at least two consecutive years,

the term **active layer** is used for the soil layer underlain by permafrost, that thaws and re-freezes in the course of a year. The maximum thaw depth during summer is referred to as active layer thickness (ALT).

after Harris and Permafrost Subcommittee [1988], and:

climate describes the current state of the atmosphere statistically in terms of the mean and variability of relevant quantities. The classical time period is 30 years,

after IPCC [2013a].

The IPCC works with confidence intervals when judging evidence of a specific climate topic. Confidence intervals are based on both the evidence itself and the agreement with other sources. The evidence itself is judged on type, amount, quality and consistency. *Very high confidence* is reached when evidence occurs multiple times independently and is of high quality [Mastrandrea et al. 2010]. Thus, when the IPCC states a relationship between two climate parameters, several studies have produced the same results and the research community reached a consent on one particular issue. In the following section, the state-of-the-art on meteorological, energy budget, subsurface and snow parameters is presented together with knowledge gaps and uncertainties. Organized climatological measurements can be dated back to the late 19th century, being limited to recordings of air temperatures, atmospheric pressure and precipitation mostly. In 1873 the World Meteorological Organization (WMO) was founded, building a worldwide network to describe the current state of the atmosphere [ZAMG 2018]. Today the aim for standardized measurement techniques and a consistent dense network is tackled by committees like the IPCC on a global scale, the AMAP on a regional scale or the World Radiation Monitoring Center – Baseline Surface Radiation Network (WRMC -

BSRN) on a topical scale. A common goal is to understand climate change processes from the past and project them to the future [Boike et al. 2017]. To understand global processes, regional characteristics need to be quantified precisely to account for regional climatological differences. The following section presents the current state of research in Bayelva.

1.1 State of Research

Improving modeling the future state of permafrost requires in-situ measurements for verification. Still, field work in permafrost regions is a big challenge, since ground temperatures below 0 °C for more than two consecutive years require air temperatures below 0 °C for most of the year, leading to harsh conditions when researching in those areas. Being exposed to extreme climate conditions is challenging for both humans and the measurement equipment. Nonetheless, research in Bayelva today covers a broad range of climatological relevant processes ranging from soil physics and hydrology, to soil chemistry, surface energy balance, vegetation patterns to surface gas exchange fluxes. Essential for soil thermal properties are fluvial hydrology processes, that origin in the glaciers surrounding the research site, feeding the Bayelva river during ablation with sediments. Hodson et al. [2002] report that solute elution due to snow pack melt-off is one major controlling factor in the Bayelva river basin, regarding its hydrochemistry. In-situ hydrochemical water sampling for their study was conducted in 1991 and 1992. Research on the surface energy budget, containing radiation, latent, and ground heat flux measurements in Bayelva is profound even though the system is highly complex [Westermann 2010]. Continuous data recordings in Bayelva started in 1998, when the study site also used for this study was set up. In the nearby village of Ny-Ålesund radiation measurements already started in 1993, covering a 25-year period by now. These long-term trends are valuable in permafrost research, since ground temperature phenomena are long-ranging [Westermann 2010]. The energy surface balance in Bayelva is strongly connected to the presence or absence of a snow cover. Several applications of surface energy budget models were made to this point, aiming on quantifying the role of the snow cover as energy supplier to the underlying soil. Boike [2003] attributed 30-50 % of the total net radiation energy to be supplied to the ground for the spring melt seasons of 1998 to 2000. A one-year study from March 2008 to March 2009 using radiation, sensible, latent and heat fluxes as well, accredited 15 % of the supplied energy to the thawing of the active layer in July and August [Westermann et al. 2009]. Directly related to the annual course of radiation components are surface gas exchanges like the CO₂ and H₂O. Those are measured together with sensible and latent heat fluxes at the eddy covariance tower, installed in 2007 [Westermann 2010]. Lloyd [2001] identifies solar radiation as well as soil temperatures as controlling physical variables for changes in carbon dioxide fluxes in the Bayelva flood plain. Both variables activate plants and soil microorganisms. A simple combined photosynthetic assimilation-soil respiration model

is able to capture CO₂ fluxes during summer but lacks in accuracy for spring snow melt and early autumn snow fall seasons. The authors recommend more complex models at that point. The complexity of biotic and abiotic CO₂ processes through a snow cover were quantified for the years 2008 and 2009 by Lüers et al. [2014]. The snow pack acts as mediator during the snow season together with mesoscale wind and pressure forcings.

To capture the spatial and temporal distribution as highly resolved as possible recent trends in snow cover research on Bayelva are both ground based high resolution photography and satellite remote sensing [Winther et al. 1999; Boike et al. 2017; Aalstad et al. 2017]. Resolutions below 1 km are already set with high errors when averaging, due to the microscopic variability of the snow distribution. An ensemble-based assimilation scheme, relating the timing of snow cover melt up received from satellite products to snow water equivalent of the pre-melt situation proved valuable for hydrometeorological reanalyses [Aalstad et al. 2017]. Derksen and LeDrew [2000] attribute the snow cover a multidisciplinary role, which is reflected in the research fields in Bayelva presented above. They all have in common, that the snow cover states a physical variable, that interacts with intensely with its surroundings. At the same time it is a major source of variability thus leading to uncertainties in permafrost modeling [AMAP 2017]. Long-term analyses of the broad physical components is named as one approach to provide deeper insight in the role of the snow cover in Bayelva [Westermann 2010; Lloyd 2001]. The motivation for this study is therefore to use the almost 20-year recordings of snow cover related physical components from Bayelva and describe their trend developments from 1998 to 2017. More precisely, this study aims to give insight on the vertical temperature profile in Bayelva, Svalbard, focusing on the role of the snow cover as thermo-insulation between atmosphere and lithosphere. The variables considered in this thesis and the most common measurement techniques will shortly be introduced in the next section, including the specific research questions asked for this study.

1.2 Variables and techniques

Permafrost temperatures are recorded through boreholes installed at various sites all over the Arctic which reach depths of 26 m below surface [AMAP 2017]. Active layer temperatures are often recorded by digging a soil profile. Here, temperature sensors (as well as volumetric water content sensors) can be positioned along the material layering of the soil, presenting a 2D-grid, giving insight on the procession of temperature waves in the soil [Boike et al. 2017; Hinzman et al. 2005; Boike et al. 2013]. ALT is measured manually by inserting a steel probe into the soil until resistance of the frozen soil occurs [Åkerman and Johansson 2008; Klene et al. 2001]. Snow depth measurements were conducted manually for the longest part of snow depth recordings. That method limits observations to easy accessible areas, whereas remote locations were underrepresented in the Arctic network. In-situ installed infra red measure-

ments of the depth of the snow/soil surface started in the early 1990, automating snow depth recordings in most countries [AMAP 2017]. Higher spatial as well as temporal resolution of snow cover measurements brought an intense increase on knowledge of snow related processes. Vital for snow hydrological processes is the measurement of the snow water equivalent (SWE), showing the amount of water stored in a snow pack. Those measurements are still mostly conducted manually as well. The GlobSnow product by Takala et al. [2011] maps snow depth and SWE all over the Arctic. Their algorithm combines weather station data with satellite passive microwave radiometry to generate a 30-year time-series for the NH. It is the best available method to date to collect snow depth and SWE data in such quantity as well as quality [AMAP 2017]. Nonetheless, the uncertainties are still limiting, when applying snow cover models. Remote sensing is used more and more to detect fractional snow covers, estimate the SWE, measure albedo values or determine the melt state of the snow pack [AMAP 2017]. The quality of remotely collected information on snow covers increases, when being validated with in-situ measurements. The more knowledge on regional differences is available, the better transregional models work.

The archipelago of Svalbard is in the very north (78° N) of the Arctic Ocean. The islands represent the unique feature of a comparatively warm climate, with average air temperatures in January being -13°C and $+5^\circ\text{C}$ in July (compared to -29°C and $+11^\circ\text{C}$ on Baffin Island in the Canadian Arctic Archipelago, 70° N [meteoblue 2018] or the Lena River Delta in Siberia with -30°C and $+10^\circ\text{C}$ in January and July [Boike et al. 2013]). The moderate annual air temperature amplitudes result from the West Spitsbergen Ocean Current, the northernmost branch of the North Atlantic Current, transporting warmth to the high latitudes in the Arctic Ocean [Boike et al. 2017]. Understanding permafrost thermal processes of this unique place could be transferred to other regions with currently colder conditions, which in the future reach warmer temperatures and permafrost degradation proceeds.

The introduction highlighted the importance of characterizing the snow cover in Bayelva in order to improve permafrost models. The following questions will be answered in this thesis:

A) Trend Detection

- How did climate parameters proceed from 1998 to 2017?
 - * Air Temperature
 - * Radiation Components
- How did soil parameters proceed from 1998 to 2017?
 - * Soil Temperatures
 - * Active Layer Thickness
- How did snow cover characteristics proceed from 1998 to 2017?
 - * Timing and Duration
 - * Snow Depth

B) Thermal Insulation Relationship

- How does the correlation of $S_{\text{depth,eff}}$ and A_{norm} behave in regard to the thermal insulation effect of a snow cover?
- What influence of the snow cover on temperature amplitudes can be identified?

To begin with, the study site of this work will be introduced in chapter 2. Subsequently a background on the thermal relationships in permafrost regions will be given in chapter 3, followed by the explanation of the analysis methods in chapter 4. The results are presented in chapter 5 and will be discussed concerning uncertainties and comparison to other Arctic sites in chapter 6. The final part summarizes the findings of this study and gives an outlook for further research (chapter 7).

2 Study Site

All data used for this study was recorded in Bayelva on the archipelago of Svalbard, 78° N. Bayelva is a small research site 2 km west of the town of Ny-Ålesund, the northern-most settlement in the world. Two stations, Koldewey (from the German-based Alfred-Wegener-Institut, Helmholtz-Zentrum für Polar- und Meeresforschung (AWI)) and Rabot (French Polar Institute Paul Emile Victor (IPEV)) joined their forces in 2003 and founded the AWIPEV Base.

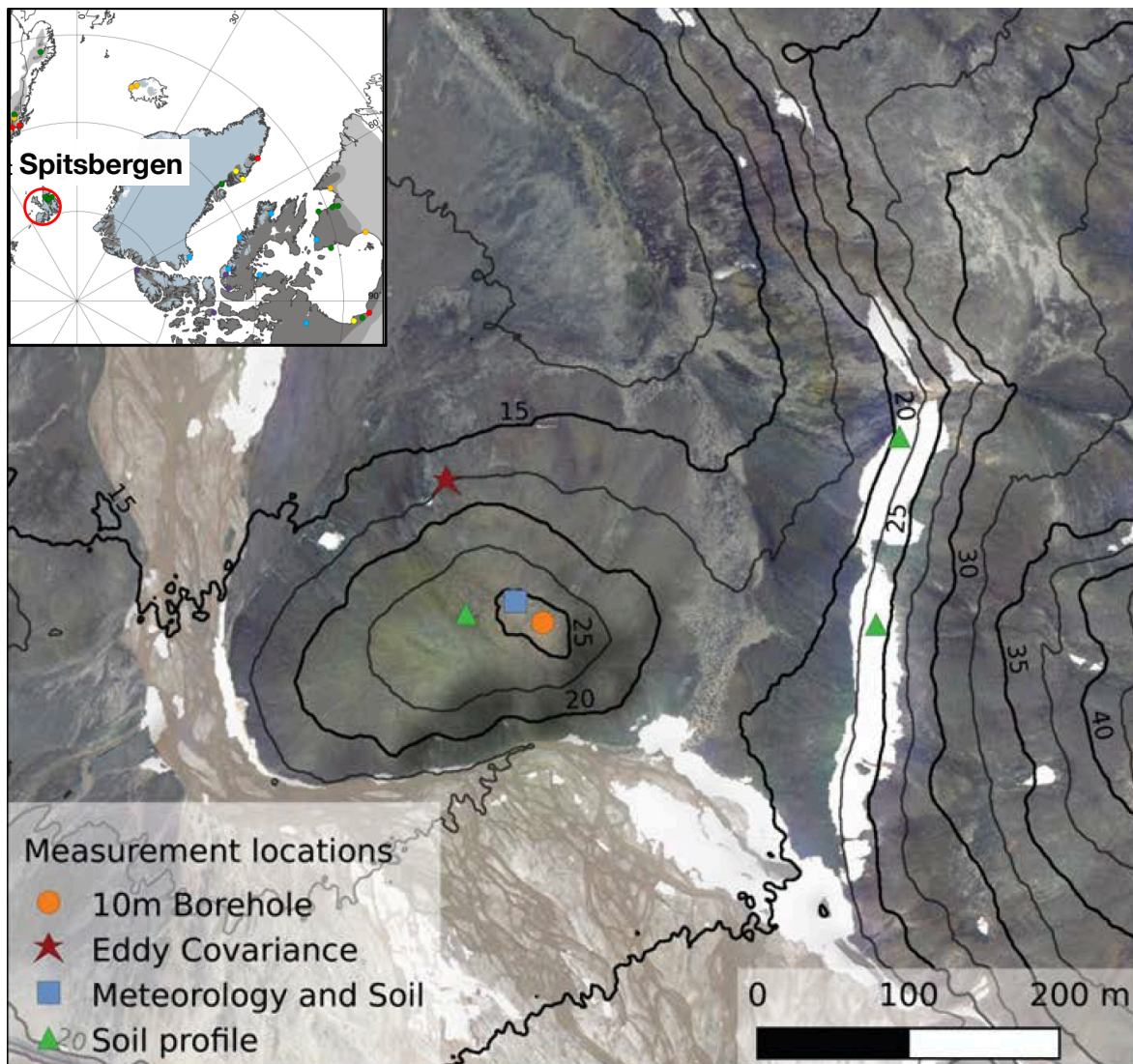


Figure 1: Location of Spitsbergen in the Arctic Ocean (78.551° N; 11.571° E) and aerial orthoimage (20 cm/px) of the study site with the locations of the different stations used in this study. [Boike et al. 2017].

Climate data measurements are collected since 1993, leading to a broad data network over a timespan of 24 years by now. These long-term measurements can provide detailed information on the various processes in soil and atmosphere and their connections to each other. The Bayelva research station is running since 1998. Today over 50 sensors measure different components, that describe the complex interactions of atmosphere, active layer and permafrost. This chapter starts with a description the setup of the climate station, focusing on air temperature, radiation and precipitation. Other measurements are shortly mentioned but will not be discussed in detail, since they are not part of the analyses made in this work. Two high-resolution soil profiles, recording soil temperatures and volumetric water content installed in 1998 and 2009 are described in the second section. Permafrost temperatures are recorded since 2009 with temperature sensors in a bore-hole and are depicted in the third section. Snow depth measurements are taken by the climate station. All data was provided by the working group of Dr. Julia Boike of the AWI.

2.1 Climate Stations

Both climate and soil stations described in the following are located on a small hill and are fenced to protect sensors from reindeer disturbance.

Climate data in Bayelva was collected by two stations. The first one was installed in 1998, running until August 2009 (for schematic set-up see Fig. 20). In that year a new station was installed, which is still running (for schematic set-up see Fig. 21). Air temperature is measured half-hourly (since 2009, before: hourly) in a height of 2 m. Radiation components are recorded separately (incoming/outgoing shortwave and incoming/outgoing longwave radiation) only since 2009. Before the net radiation budget was recorded. In 2003 a downward-looking pyrgeometer to detect reflected longwave radiation was installed additionally, thus a longer time-series for this component exists. At the AWIPEV station in Ny-Ålesund, meteorological data is recorded since 1992 as part of the worldwide Baseline Surface Radiation Network (BSRN). In this study, the Bayelva dataset was complemented with AWIPEV data at some points which will be commented on the respective sections. Snow depth measurements are part of the climate station and are recorded since 1998 with a sonic ranging sensor (SR50). Raw distance from the sensor to the surface (either ground surface or snow surface) is measured. In 2006 an additional sensor of the same type was installed in approx. 85 m distance. In 2013 a third snow depth sensor was installed next to the climate station. The three different data-streams were merged to the so-called 'snow product', complementing each other by filling respective gaps and then obtain one long time-series. The distance between one of the sensors to the two others may result in snow depth changes due to microtopographic differences of the locations.

2.2 Soil Stations

Active Layer Temperatures Similar to the time-line of the climate stations, a first high-resolution soil profile was installed in 1998. The sensor are still running but their data is only used up to 2009 in this work (for schematic set-up see Fig. 22). For the installation a 1.4 m deep and 2 m wide trench was excavated, cross-sectioning a mudboil. The soil consisted mainly of silty clay, the stone content being less than 10 %. Below 0.85 m the soil was rich in coal. Temperature as well as volumetric water content (with time-domain reflectometry (TDR)) was measured in a 2D-profile, with a total of 32 sensors. Due to degradation of sensor quality (offset of about 6°C in 2009, compared to 1998 and 1999), a second profile was installed in 2009 (for schematic set-up see Fig. 23). All values with an offset higher than 0.5°C were flagged accordingly (see section 2.3). The new profile also measures soil temperatures and volumetric water content, but to a depth of 1.41 m (11 sensors), and only in a 1D profile.

Permafrost Temperatures In March 2009 a 9 m deep borehole was installed in close proximity to the soil and climate stations. Nine temperature sensors measure temperatures below ground on a thermometer chain. Due to sensor failure, the chain was replaced several times. Following the advice of the AWI staff, data-streams below 1.5 m were used in this thesis. Sensors above 1.5 m are marked with higher uncertainties due to air exchange from the surface.

2.3 Data Quality Control

All data used in this study was pre-processed and flagged by the AWI. The different flags are listed in Table 1, where 0 declares good data. Flags ranging from 1 to 8 describe different situations, which lead to no or bad data, which is excluded from analysis. Flagging routines were either based on automatic algorithms, run over the different datasets, or executed manually by engineers (e.g. flag 6, check for plausibility). Since analyses in this study mostly contain monthly or annual data aggregations, excluding all flags is justified by the large amount of data available. For other studies a closer look and weighting of the different flags might be useful to limit data-gaps.

Study site, sensor and flag descriptions are based on Boike et al. [2017].

Table 1: Quality control Description of flags of the Bayelva data-set.

Flag	Meaning	Description
0	Good data	All quality tests passed
1	No data	Missing value
2	System error	System failure led to corrupted data, e.g. when the power supply broke down, sensors were removed from their proper location, sensors broke or the data logger saved error codes
3	Maintenance	Values influenced by the installation, calibration and cleaning of sensors or programming of the data logger; information from field protocols of engineers
4	Physical limits	Values outside the physically possible or likely limits, e.g. relative humidity should be in a range of 0-100 %
5	Gradient	Values unlikely because of prolonged constant periods or high/low spikes; test within each single series
6	Plausibility	Values unlikely in comparison with other series or for a given time of the year; flagged manually by engineers
7	Decreased accuracy	Values with decreased sensor accuracy, e.g. identified when thawing soil does not have a temperature of 0°C
8	Snow covered	Good data, but the sensor is snow covered

3 Background on thermal relations in permafrost regions

Correctly describing soil physics in permafrost regions is highly challenging. It depends on soil characteristics such as texture, layering, moisture, thermal state, and many more, thus differing from location to location. This study focuses on the processes behind heat exchange between atmosphere and lithosphere in continuous permafrost regions.

After a typical temperature profile in permafrost regions (Fig. 2) is introduced, the relevant physical laws are described. Beginning in the atmosphere, the Surface Energy Budget (SEB) is explained in chapter 3.1, then moving to the soil, the Ground Thermal Regime (chapter 3.2) will be discussed. The role of a snow cover as boundary between atmosphere and lithosphere is explained simultaneously.

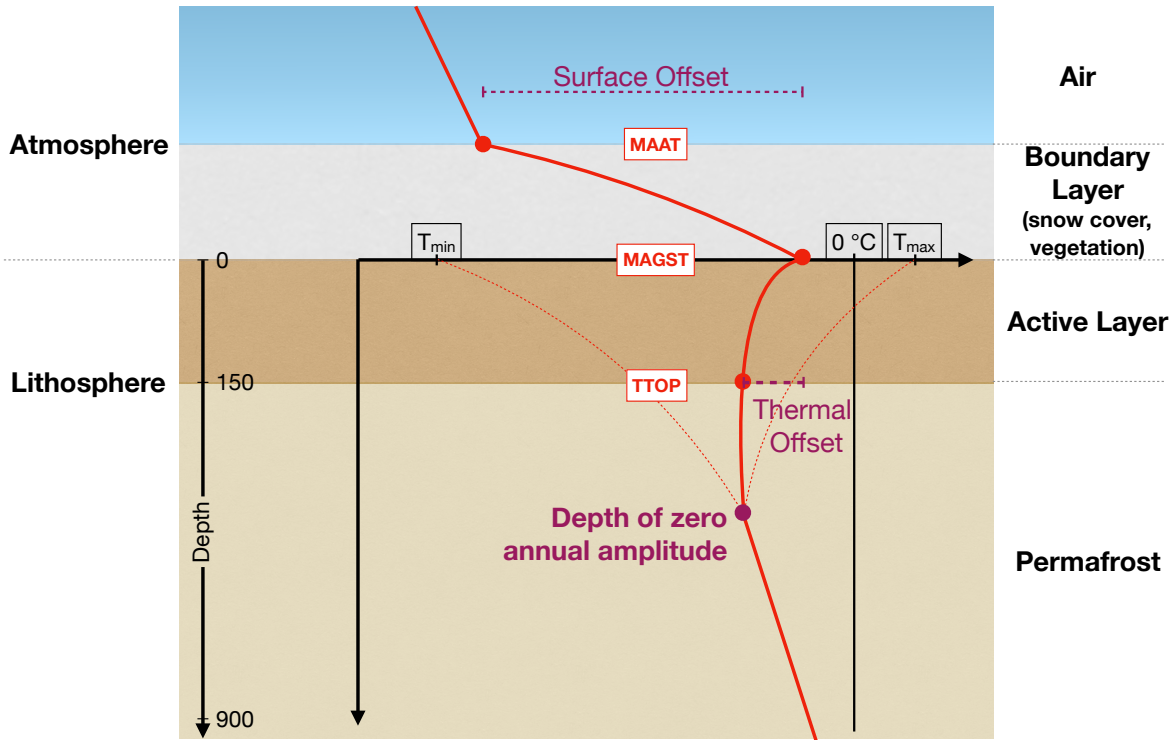


Figure 2: The Temperature Profile through atmosphere and lithosphere is characterized by a **surface offset** due to a boundary layer (seasonal snow cover or vegetation) and a **thermal offset** between MAGS and TTOP temperatures. Schematic draft based on Smith and Riseborough [2002].

Figure 2 shows a schematic profile of the atmosphere and lithosphere found in Bayelva. Those two main components interact in a complex system. To describe the temperature progression, we define the following variables.

The temperature of the atmosphere on Svalbard is characterized by the **mean annual air temperature** (MAAT), describing the mean thermal state of the atmosphere. Typical for the Northern Hemisphere (NH) a seasonal snow cover posts a boundary between atmosphere and lithosphere acting as disturbance in the temperature profile. MAAT and **mean annual ground surface temperature** (MAGST) thus show a **surface offset**, meaning that MAAT are colder than MAGST (during snow season). This offset can also be observed during snow free seasons, due to vegetation acting as the boundary. Surface offset due to vegetation is smaller than that due to snow cover. An attempt of understanding the relationship of air and surface (and soil) temperatures is one subject of this study. A second temperature progress offset, in the opposite direction, is given between MAGST and **temperatures at the top of permafrost** (TTOP). Mean temperature from the ground surface gets colder as it proceeds to deeper depths of the active layer, meaning that the **thermal offset** is opposite to the surface offset. Permafrost temperatures stay below 0°C for the whole permafrost layer, gradually (**geothermal gradient**) moving towards zero degrees at the bottom of permafrost. Changing air temperature signals lead to MAGST temperature variations between T_{\min} and T_{\max} that are being transferred into the soil to a **depth of zero annual amplitude** (see Fig. 2). Below this point seasonal temperature changes have no more impact.

3.1 Surface Energy Budget

The temperature course described in the previous section is the result of energy transfer between an atmospheric volume and an underlying land volume. The interface is set to be an infinitesimally thin surface with no energy storage (in theory). This assumption is not valid for all surfaces (e.g forests), but for tundra with only little vegetation the approximation is justified. All energy fluxes are closed at all times, resulting in the following equation:

$$0 = S_{in} + S_{out} + L_{in} + L_{out} + Q_h + Q_e + Q_g \quad (1)$$

The difference between incoming (S_{in}) and reflected (S_{out}) shortwave radiation is the net shortwave radiation, while the difference between downward (L_{in}) and upward (L_{out}) facing longwave radiation is called net longwave radiation. Q_h is the sensible heat flux, Q_e the latent heat flux and Q_g the ground heat flux or snow heat flux during snow-covered periods. For a complete surface budget, the water budget equation needs to be factored in. This includes water transport in the soil, rainfall and evapotranspiration and is coupled with the surface energy budget through the latent heat flux. In this thesis the water budget will be mentioned but is not focused on further [Westermann 2010].

The relationship of incoming and outgoing shortwave radiation is given by the **albedo** ($\alpha = S_{out}/S_{in}$) of a surface. Values differ between 0 and 1, where snow-free tundra on Svalbard ranges between 0.1 and 0.2 and snow cover between 0.8 and 0.9 [Maturilli et al. 2015]. Both

shortwave and longwave radiation budgets are influenced by cloud cover. Shortwave through the cloud albedo and longwave through the emission and absorption characteristics of the surface, described by the Stefan-Boltzmann-Law:

$$L_{out} = \varepsilon\sigma_{sb}T_{surf}^4 - (1 - \varepsilon)L_{in} \quad (2)$$

with σ_{sb} being the Stefan-Boltzmann constant. Equation (2) describes the coupling of surface temperature and outgoing longwave radiation, which is based on the blackbody radiation of the ground. Since the tundra on Svalbard behaves differently than a black body, the Kichhoff's Law emissivity ε needs to be introduced.

3.2 Heat Flow in Frozen Soils

This chapter presents theories that describe the thermal processes in the soil. The focus lies on heat propagation from the surface to deeper depths, thaw and freeze-back properties and the thermal state of permafrost on Svalbard. Precipitation plays an important role as it adds water to the system, thus being able to change the temperature regime on a short scale through one single event (e.g. rain on snow event). Therefore, this chapter introduces precipitation development on Svalbard. Several approaches to describe heat flow dynamics exist, with differing levels of complexity. Here only the ones used for this work are introduced. Loosely following Woo [2012], basic concepts of thermal conductivity and head capacity will be explained (section 3.2.1), as well as the progression of temperature waves (section 3.2.2). In section 3.2.3 an approach to estimate the maximal thawing depth of the active layer will be described. This approach is only based on air and soil temperatures and the volumetric water content of the soil. Temperatures at the exact surface are basically impossible to measure, thus one method of approximation will be explained (section 3.2.4). With this physical background, the data were analyzed and the steps will be explained in the next chapter.

3.2.1 Thermal Conductivity and Heat Capacity

The connection of atmosphere and lithosphere is given by the surface energy budget (1). This section describes thermal processes in the active layer. Soil properties, for example mineral and organic material fractions, as well as air, water and ice content are the factors determining thermal conductivity of a soil volume. Estimations for dry and wet soils are:

$$K_{dry} = \frac{(0.135\rho_b + 64.7)}{(2700 - 0.947\rho_b)} \quad (3)$$

$$K_{sat} = \prod_{j=1}^5 K_T(j)^{f(j)} \quad (4)$$

with ρ_b being bulk density, $K_T(j)$ and $f(j)$ the thermal conductivity and volumetric fraction of different type of soil (j), including ice, water, air and mineral and organic materials, as defined by de Vries, Nichollson and Oke in Woo [2012]. The heat capacity is then calculated by:

$$C_T = \sum_{j=1}^5 C(j)^{f(j)} \quad (5)$$

where C_T is the bulk heat capacity and $C(j)$ the heat capacity of the different soil types. The thermal diffusivity is yielded by dividing the thermal conductivity by the heat capacity:

$$D_T = \frac{K_T}{C_T} \quad (6)$$

3.2.2 Progression of Temperature Waves

As temperature signals from the atmosphere travel deeper into the soil, they are dampened over time. Analytical solutions face the following difficulties:

1. The annual amplitude of the air temperature is distorted by a seasonal snow cover.
2. Soil temperature rise in spring caused by melt water infiltration is hard to describe.
3. Zero-curtain effects during thawing and re-freezing are not always accounted for.

The thawing period happens gradually during late spring to summer. Freeze-back on the other hand occurs in stages in late autumn to winter. There are different stages, that can be followed in Figure 3a) where the temperature processions during freeze-back in 2011 of all depths measured in the soil profile are shown. Positive temperatures in the active layer start dropping towards 0°C in the first stage. This phase is referred to as **zero-curtain** effect

(Outcalt et al. [1990] in Roth and Boike [2001]). The effect generates through water vapor transport and mechanisms of internal distillation, caused at the soil surface by freeze/thaw events. It is followed by a couple of days where conductive heat flow is close to zero, thus temperatures stay roughly between 0 and -3°C . This isothermal state ends with the cold front from the surface intervening, leading to a rapid decrease of soil temperatures.

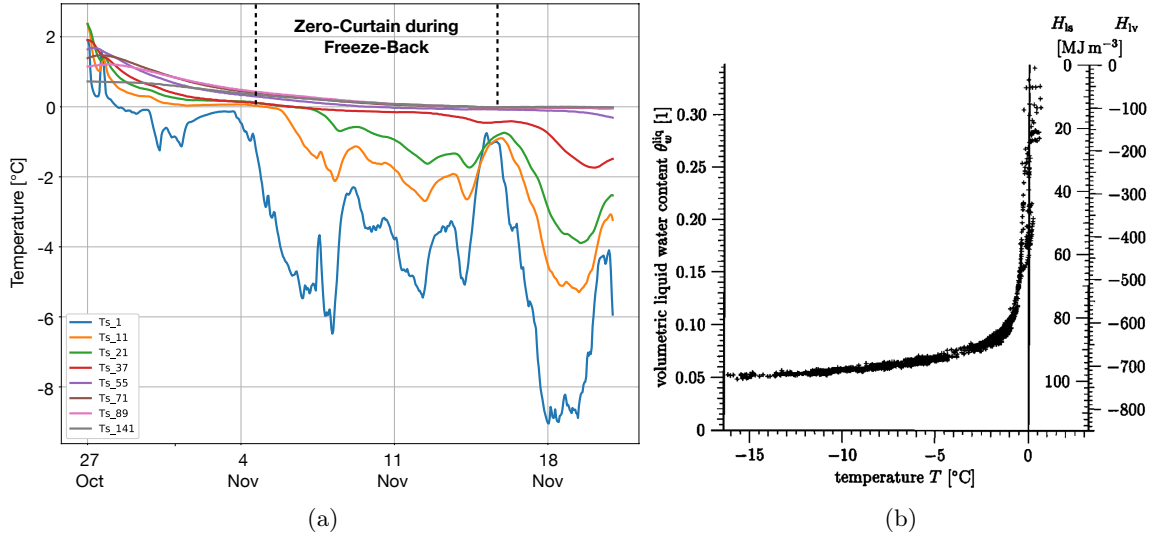


Figure 3: a) Active Layer Temperatures during freeze-back in October 2011. The Zero-Curtain phenomenon is indicated (dashed black lines), where temperatures linger just below 0°C until they start dropping rapidly. b) Empirical freezing characteristic obtained from plotting measured values of liquid water content versus temperature for the probes at 0.245 m depth. The axes on the right indicate the latent heat associated with the change of θ_w^{liq} if the excess water freezes (H_{sl}) or if it evaporates (H_{sv}) [Roth and Boike 2001].

3.2.3 The Stefan-Model

The **Stefan-Model** is a simplified description of heat transfer in permafrost regions, assuming that sensible heat is negligible. Energy consumption or release during thaw or re-freeze respectively is set equal to the conductive heat flux, which is approximated by interpolating the freezing temperature of water T_f and the surface temperature T_{surf} to the freeze-thaw interface. This leads to

$$-\rho_w L_{sl} \theta_w \frac{\partial Z_{thaw}(t)}{\partial t} = -K_h \frac{T_{surf}(t) - T_f}{Z_{thaw}} \quad (7)$$

for thawing with the thawing depth Z_{thaw} (positive below surface). Integration gives the analytical solution:

$$Z_{thaw} = \sqrt{\frac{K_h |TDD(t)|}{\rho_w L_{sl} \theta_w}}. \quad (8)$$

K_h denotes the thermal conductivity of soil in [$\frac{W}{m}K$], $-\rho_w L_{sl} \theta_w$ can be summarized to the volumetric latent heat of soil Q_t and a thawing index TDD:

$$TDD(t) = \int_{t_0}^t (T_{surf}(t) - T_f) dt. \quad (9)$$

The following three assumptions are made to simplify heat progression:

- Conduction is the only way of heat transport from the soil surface to the thawing front.
- A constant temperature gradient lets temperatures relax immediately after any disturbance.
- At the thawing front heat is consumed completely for melting water.

The Stefan-Model was applied on the Bayelva dataset by Weismüller et al. [2011] and Stern [2017]. The results will be discussed in section 6.1.

3.2.4 Near-Surface Ground Temperature

As mentioned before, temperature measurements directly on the ground surface are impossible to measure automated. In Bayelva, the uppermost sensor of the high-resolution soil profile is located just under the surface, thus giving a good estimate. Analytical methods are formulated, to get an estimate for ground surface temperatures, and one simple empirical approach is introduced.

Lunardini defined the freezing/thawing **n-factor** in 1978, to link air and surface temperatures, also accounting for a seasonally disturbing snow cover. By building the ratio between freezing/thawing degree days in the air and at the surface [Smith et al. 2016; Klene et al. 2001; Phillips et al. 2003; Woo 2012]

$$n_{thaw} = \frac{TDD_{surface}}{TDD_{air}}, \quad (10)$$

$$TDD_{surface} = \sum [T_j(surf) - T_b], \quad (11)$$

T_j being the mean surface temperature on day j , and the freezing temperature T_b of 0°C . For the freezing n-factor, freezing degree days (FDD) are being used. TDD_t is usually given in degree · days and restricted to days where temperatures are above T_b , for FDD to temperatures below the freezing temperature. Equation (11) can be verified by inserting in equation (8).

The **Thawing or Freezing Degree Days** divide the year into warming and cooling regimes, based on positive or negative (above or below 0°C) air temperatures. The balance of that annual regime contains consequences on thermal soil-properties and was used in this work to apply the Stefan-model.

Going one step further, Nelson and Outcalt (1987) calculate the Surface Frost Number F_+ to derive frontiers between continuous, discontinuous, sporadic and no permafrost regions [Barry and Gan 2011].

4 Methods

In the following chapter the methods used to analyze the Bayelva regarding different aspects are described. The analysis of the data-set is based on the physical theory/background that was introduced in the previous chapter and aimed to answer the scientific questions stated in chapter 1. The results will then be presented in the following chapter 5.

4.1 Air Temperature

Annual mean air temperatures from 1998 to 2016 were calculated for the whole dataset. At the point of data-analysis, the year 2017 was only recorded until 30th April and is thus excluded from annual aggregations. Since there are several gaps in the Bayelva time-series, air temperature records from the neighboring AWIPEV station were used to fill the gaps. The AWIPEV station is located about 3 km further east and air temperatures are measured at 2 m height, same as in Bayelva. Examining differences of the two datasets gives a mean of 1°C temperature difference of the whole period overlapping. A gap-filling with the AWIPEV temperatures is thus justified. The monthly means were calculated by the daily means, filtering out months with more than 5% missing values, in case the AWIPEV data-streams didn't catch all gaps. No months had to be excluded from further analysis though. Calendar years (1st January to 31st December) were used when aggregating annual means to simplify the comparison to literature (e.g. Maturilli et al. [2013]). For inter-annual variation analysis, **monthly** as well as **seasonal** mean values were calculated. The seasons were defined following Maturilli et al. [2013]:

spring: March, April and May

summer: June, July and August

autumn: September, October and November

winter: December, January and February.

Winter 2013 for example refers to the months December of 2012, January and February of 2013. Seasonal aggregations have the advantage of a better representation of climatic conditions such as cooling or warming, but monthly values permit a more detailed description of the year.

4.2 Radiation

Radiation balance trends were computed for annual net radiation from 1999 to 2016. Parallel to air temperature aggregations in chapter 4.1, seasonal and monthly averages were computed. The four single components (incoming/outgoing shortwave, incoming/outgoing longwave) were aggregated monthly, to monitor annual variations. Single components were only recorded since 2009, so this analysis is limited to this timespan. According to the radiation data representation of Maturilli et al. [2015] which analyses AWIPEV data, daily aggregations were excluded if more than 5 hours a day were missing. Monthly mean values were based on daily aggregations and excluded if more than 4 days were missing. Since data collection at the AWIPEV station has only little gaps, annual aggregations is possible for all years. In Bayelva years with more than four months missing were excluded from averaging. This threshold is justified, since there are either years with only one month missing, or years with four or more months missing. One missing month is assumed to have only little effect on the annual average.

4.3 Snow Cover Timing Variation

For most of the years of the Bayelva data-set the months October to May are covered with snow. The average timespan of seasonal snow cover on the NH is from October to March [Slater et al. 2017], i.e. the average duration at Bayelva is usually two to three months longer than the NH mean. The timing of the beginning and ending of the snow cover are on one hand dependent on air temperature and the radiation budget, and on the other hand influence soil characteristics like volumetric water content or temperature. This chapter describes the variables that were used to sketch the course of a snow-layer over the year. In Figure 4 these variables are shown as an example on the snow cover of 2015/2016. Two kinds of maxima were differentiated. The **global maximum** describes the maximal measured snow height of one snow period. To be able to quantify the duration of the snow cover ablation the global maximum is misleading, since there might follow more snowfall afterwards, and thus the ablation process is prolonged or even disturbed. For this reason the **last maximum** is defined, i.e. the snow depth after which no snowfall event occurs. From this day on, snow depth change rates were either negative or stayed the same.

When detecting the beginning and end of snow covers, two different approaches were used. The first one uses snow depth measurements, the second one changes in the reflection of shortwave radiation. Both approaches will be explained in the following.

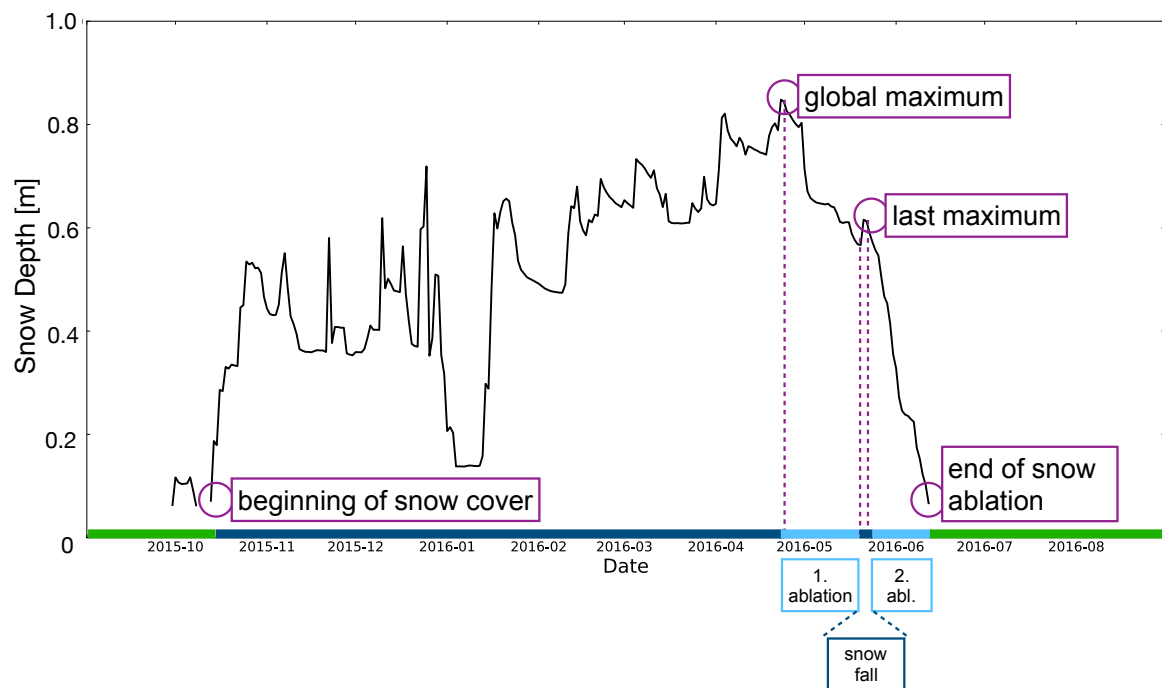


Figure 4: Snow Cover Variables for an example snow cover in 2015/2016. Variations in the beginning of the snow cover, the end of snow ablation as well as global and last maximum snow cover values change the insulation effect on soil temperatures.

Snow Depth

After first visual examinations of the data, false detections of the sensor during summer periods can be observed. Following a snow ablation period to 0.0 m snow depth, an increase to around 0.05 m snow depth followed. The measurements stayed at this depth until autumn, when first snow-fall was detected (increase over a few hours to values over 0.1 m). The measured 5 cm during summer were identified as vegetation that started growing as soon as all snow was melted in spring. Thus all data below 0.05 m was excluded in all years from further analysis. This step facilitates the detection of the **end of snow ablation**. The **start of the snow cover** was defined as the point when a continuous (no more values below 0.05 m) snow cover has built up. The snow cover in Figure 4 started building up in the middle of October for the first time, but melted off to below 0.05 m after a couple of days again. Since short snow periods like these are assumed to have no influence on the soil temperatures [Sokratov and Barry 2002], they weren't accounted for in further analysis. Some years show incomplete recordings or gaps due to filtering (see section 2.3), and start as well as end dates could not (with high uncertainty) be analyzed this way, so a second approach was used, following Maturilli et al. [2015].

Reflection

This approach is based on the different albedo of vegetation, tundra or rocks (between 0.1 and 0.2) and snow (0.8 to 0.9). During onset/offset of a snow cover, albedo values change with the transition of the surface texture. Figure 5 shows an exemplary course of albedo values (black solid line) during snow cover ablation, summer and snow cover built up in 2003 (exemplary year) as well as the snow depth in meter (blue area). A rapid decrease in Albedo follows the melt-of in the end of June, and Albedo values stay below a threshold of 0.2 (black dashed line) for the duration of summer. The threshold was chosen after Maturilli et al. [2015] (Fig. 8 and 9), to have a solid basis for comparison. The assumption, that snow depth records over 5 cm during summer is vegetation is supported by Albedo values lower than 0.2. First snow-falls in September change the short-wave-ratio immediately, leading to spikes in the course of the black solid line. These first snow-fall-events are so small and vanish after a few hours already, that they don't show up in the daily averaged snow depth measurements of Figure 5. Due to the frequent jumps in Albedo values, a threshold respective to the one for the ablation dates is not generated in this thesis (neither in [Maturilli et al. 2015]) to determine the beginning of the snow cover.

Results of the detection of variation in beginning and end of the Bayelva snow cover are presented in chapter 5.2.1.

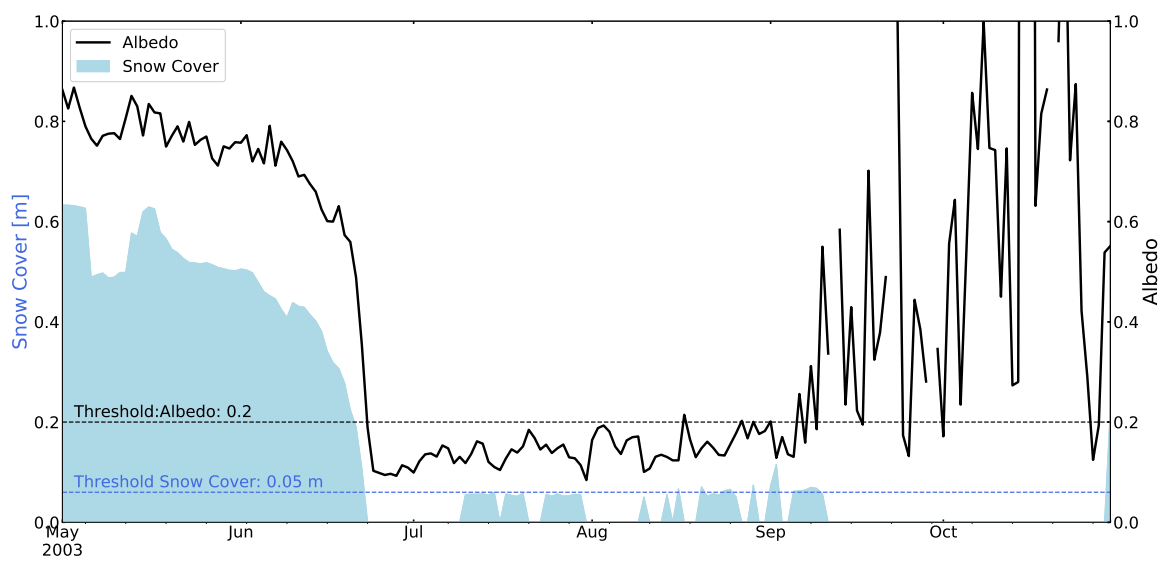


Figure 5: The blue area shows the snow cover in 2003 (left y-axis), the black line the albedo (right y-axis) in the same year. Thresholds to determine the end of the snow cover for the two approaches are shown with dashed lines: dashed blue determines the end where snow depth measurements stay below 0.05 m for the summer period; dashed black determines the end where albedo values stay below 0.2 for the summer period.

4.4 Thermal-Insulation Effect

For a first inspection of the effect of a snow cover on soil and atmosphere, daily averages were calculated from 1998 to June 2017 and plotted against each other. The results for depths 0.01, 0.71 and 1.41 m are presented in Figure 6. Proceeding days of the year (doy) are color-coded, with beginning and end of the year both being red, to connect the transition of years. Horizontal and vertical lines at 0°C as well as a diagonal line where air and soil temperatures are the same are added to the figures. Divergences from the diagonal line show more temperature differences between air and soil, when temperatures are below 0°C . This observation vanishes with deeper depths, until there almost never the same at a depth of 1.41 m. Soil temperatures at depth 0.01 m varies between 15 and -15°C , while temperatures at depth 1.41 m varies only between 4 and -8°C , reflecting the dampening of air temperature signals with depth. During summer months (blue and turquoise) and beginning of autumn, as defined in chapter 4.1, both air and soil temperatures are positive at the uppermost layer, while in spring and early summer (doy 100 to 150) at depths 0.71 and 1.41 m, soil temperatures are still below zero.

The snow covered part of the year, approximately doy 300 to doy 170 (red and green colors), show high variability below 0°C . The area under the horizontal and above the diagonal black lines shows the temperature measurements where soil are warmer than air temperatures. Here highest variations are shown of mostly winter and spring temperatures. The influence of a boundary layer between soil and air is clearly visible, but only through this visualization no clear pattern can be followed. One distinctive feature at depths 0.71 and 1.41 m are winter soil temperatures (red) that linger close to 0°C , even though air temperature drops below -2°C , represents the zero-curtain effect, explained in chapter 3.2.2. One approach to describe the relationships between seasonal air and soil amplitudes during winter and spring is introduced by Slater et al. [2017]. In three steps, data from over 100 study sites on the Northern Hemisphere, adding up to 2049 observed study years, was analyzed. In this chapter the steps will be described, chapter 5.2.2 presents the results of the analysis with the Bayelva data and finally in chapter 6, advantages and difficulties with such estimates will be discussed.

4.4 Thermal-Insulation Effect

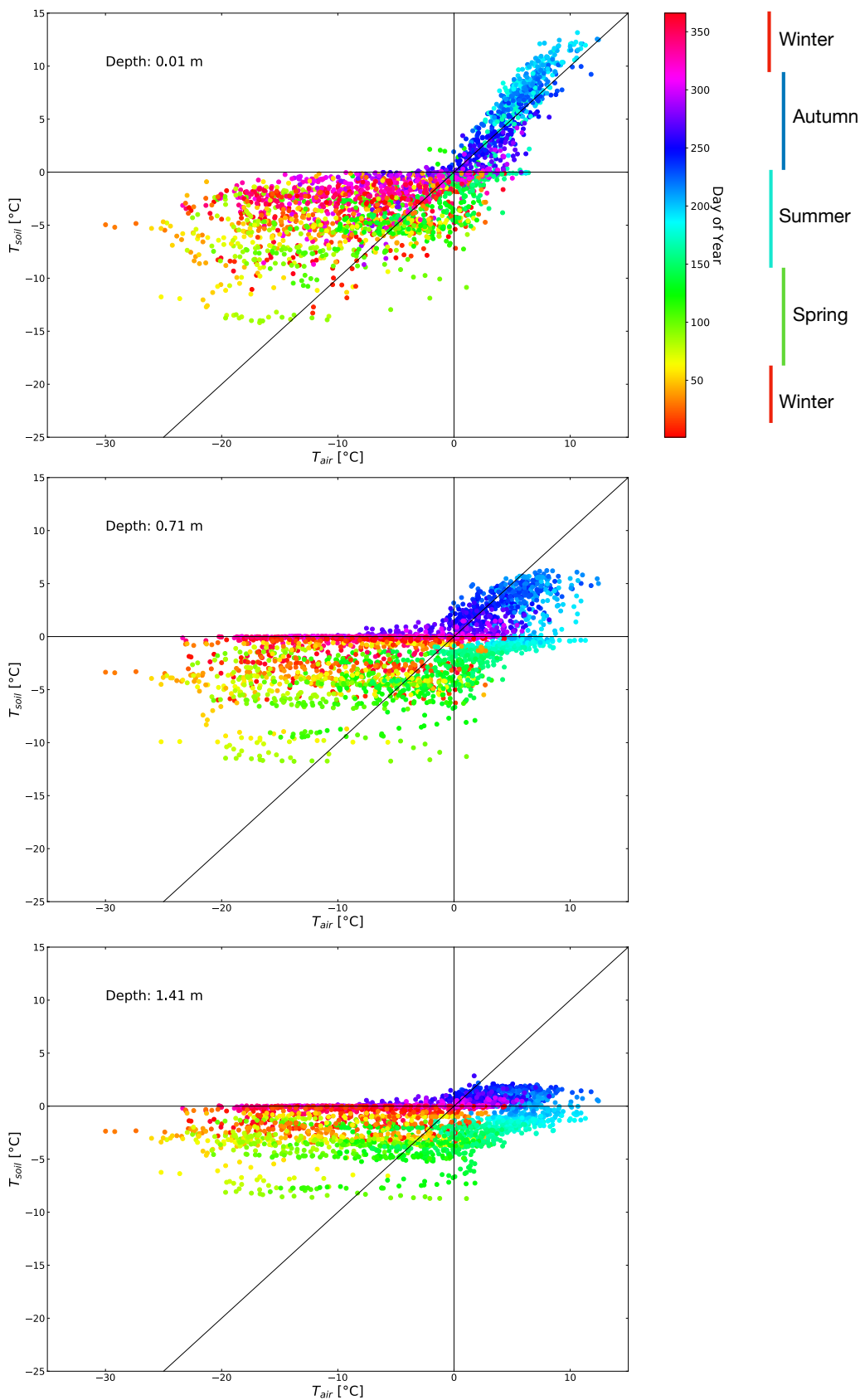


Figure 6: Daily mean air temperature versus soil temperatures at depths 0.01, 0.71 and 1.41 m. Color-code differentiates day of year, with seasons marked for orientation. Diagonal black line shows where air and soil temperature are the same.

The authors use monthly mean values of air temperatures as well as soil temperatures at a depth of 0.2 m. Using temperatures at 0.2 m is used since this is the depth in which most study sites have continuous data recordings. The aggregation of monthly mean values is explained as a consequence of being the most common output of large-scale land-models. The cooling season is defined from October to March, being the average duration of snow covers on the NH. In step one, a normalized temperature amplitude is generated as follows:

$$A_{air/soil} = MAX(T_{air/soil}) - MIN(T_{air/soil}) \quad (12)$$

Seasonal amplitudes of air and soil temperatures are being calculated as shown in equation (12) respectively. Eliminating climatically driven influences (e.g. large scale seasonal cycles in deep continental regions and more moderate cycles in coastal regions), as well as describing the process of heat transfer A_{norm} is derived from that:

$$A_{norm} = \frac{A_{air} - A_{soil}}{A_{air}} \quad (13)$$

Values between 0 and 1 distinguish between minimal difference between soil and air temperature amplitudes of one cooling season (values close to 0), and soil temperatures that basically do not change over the timespan (values close to 1). Equation (13) constitutes an inflexible approach, neglecting the impact of snow cover, soil inhomogeneities or phase changes. A_{norm} is thus extended by the parameters P, Q and R. P describes the offset arising from differences in air and soil amplitudes even in snow-free periods (e.g. through imperfect thermal properties of the soil or phase change during freeze-back and thawing). Q is a multiplier accounting for temporal aspects of the snow cover. Cooling of the soil is not only due to a snow cover, but also due to atmospheric forcing. The last parameter R describes the damping effect of temperature signals through a soil column, as a result of a snow cover. Before estimating the non-linear parameter with the Levenberg-Marquardt algorithm (LM), an **Effective Snow Depth** $S_{depth,eff}$ is introduced, to account for the timing aspects on the insulation properties of the snow cover. The final equation for A_{norm} is:

$$A_{norm} = P + Q \left(1 - e^{-\left(\frac{S_{depth,eff}}{R}\right)} \right) \quad (14)$$

$S_{depth,eff}$ defines as follows:

$$S_{depth,eff} = \frac{\sum_{m=1}^M (S_m \cdot (M + 1 - m))}{\sum_{m=1}^M m} \quad (15)$$

where S is the mean snow-depth of one month, M the maximum duration of the cooling period, defined in the study as 6 (October to March) and m the index of each month (1 to 6). Calculations begin with the mean snow-depth S_1 in October ($m = 1$). The hypothesis behind $S_{\text{depth,eff}}$ is, that early snowfall has a bigger insulation effect on the air and soil temperature amplitudes. The result will thus be higher than from a snow cover that reaches maximum depths late in the cooling season. These assumptions are backed by observations made on many research sites around the NH. Woo [2012] summary the insulation role of the snow cover as follows:

- A seasonal snow cover reduces heat loss from the soil to the atmosphere. At the same time the snow cover experiences a net loss of energy, resulting in cold snow temperatures.
- The effectiveness of the snow cover comes from the amount of air locked in the snow-pack, meaning the porosity. Roth and Boike [2001] (in [Woo 2012]) state that the effectiveness is higher with a reduced snow cover.
- Thick snow covers require more melting-time which leads to near-surface temperatures below 0°C until the whole snow is gone. Thus influencing soil thermal regimes.

Results of the effective snow depth analysis with the Bayelva data are presented in section 5.2.2.

4.5 Active-Layer

Active Layer temperatures are recorded in a high-resolution soil profile, that has been renewed in 2009 (see chapter 1). To exclude seasonal over-representation, annual means with more than 5% of data gaps longer than 48 hours were excluded from the trend analysis [Boike et al. 2017]. Smaller gaps were interpolated linearly. Annual, summer and winter trend were calculated by the AWI and are shown in Figure 26.

The deepest point of boundary between the seasonally thawing and re-freezing soil layer and permafrost is defined by the Active Layer Thickness ALT. To get the exact transition depth, gap-less temperature or volumetric water content measurements would be needed. With temperature and volumetric water content sensors with known distances like in Bayelva, the ALT can be assessed by interpolating between the deepest sensor that still thaws in summer (1.41 m from the soil profile) and the first one that doesn't rise above 0°C anymore (2.5 m from the bore-hole data). A different simple modeling estimate was achieved by applying the Stefan-Model (see chapter 3.2.3).

Freeze-Back

Figure 3b) shows freezing the correlation of temperatures to the volumetric liquid water content θ_w^{liq} at 0.245 m depth. This relationship is used to determine the duration of complete freeze-up of the active layer. The limiting value for total frozen state condition is not set to 0°C, but to -2°C since there the volumetric liquid water content is below 8% and total freeze-up commenced. The day of the year where soil temperatures at depth of 0.1, 0.71 and 1.41 m are below -2°C is determined for each year from 1998 to 2017 and presented in Figure 14.

4.6 Permafrost

Permafrost temperatures are gathered from borehole data below 1.5 m. Sensors in depths of 2.5, 3.5, 5.5, 7.5 and 9 m are aggregated to annual mean values for the years from 2010 to 2016. The years 2009 and 2017 were excluded from annual trend analysis since both years have not been recorded in total at the time of this study. As mentioned before, the rest of the borehole sensors were not used in this study, since temperature records that rise above 0°C contain high uncertainties, probably connected to air temperature influences in the sensor set-up. Sensors at depths of 0.5 and 1.5 m are compared to temperatures recorded at the soil profile in similar depths (see Fig. 24). Soil temperatures measured in a depth of 0.5 m in the borehole show high day-to-day amplitudes, which can not be seen at the record in the soil profile at a similar depth (0.55 m). When adding daily air temperature values, the amplitudes could be explained by high amplitudes in the air temperature, which travel to a depth of 0.5 m in the borehole. Borehole records at a depth of 1.5 m do not show these amplitudes, suggesting that the influence of air temperatures vanishes with depth. Since these uncertainties need further

investigation, temperature records above 2.5 m from borehole measurements are excluded from analyses in this study.

4.7 Precipitation

One of the challenges in recording precipitation on Svalbard is the distinction between liquid (rainfall) and solid (snowfall) state precipitation. In Bayelva, measurements only represent rainfall due to the measuring instrument (see chapter 1). Additionally wrong detections occur during wind-speeds above 12.5 m/s, which lead to vigorous shaking of the installation, falsely detecting rainfall. The affected measurements are flagged in the data-set. The Norwegian Meteorological Institute (formerly: eklim) measures precipitation in Ny-Ålesund with a heated and shielded bucket, eliminating false detection through high wind-speeds as well as snowfall consideration. Precipitation measurements from Bayelva were completed with the eklim-data-set for this study, to be able to regard both cases. Important for the snow energy budget are rain-on-snow events, in which case the combination of eklim and Bayelva data would not be necessary [Westermann 2010].

5 Results

The results chapter consists of four parts. The first two sections present the results of the data-sets provided by the two stations in Bayelva: climate and soil. Since the snow cover is analyzed in more detail in this work, section three contains all results of snow-analyses. In the final part the individual components will be cross-correlated to each other, to try and find links in the complex system.

5.1 Climate

From the many climate components recorded in Bayelva, radiation and air temperatures were analyzed in detail in this study. The focus on these two variables was chosen, based on their importance in energy budget calculations (see chapter 4).

5.1.1 Radiation Component Characteristics

A data-stream from 1998 to 2017 only exists for net radiation values. The four component sensor was installed in August 2009. Thus presented here are monthly mean values from 2010 to 2017 for incoming (downward) and outgoing (upward) shortwave and longwave radiation. The nomenclature in Figure 7 is based on Maturilli et al. [2015], to simplify comparison. The Bayelva data-set used incoming/outgoing, which is why it is used for the rest of this work.

Downward shortwave radiation is characterized by being zero for the months November to February (11 to 2), the polar night. It reaches maximum values in June (month of summer solstice) which have been varying between 148 W/m^2 (in 2013) and 201 W/m^2 (in 2015). Inter-annual variations are mainly caused by the varying occurrence of clouds during polar day seasons. The results of downward shortwave radiation analysis aligns well with the results of Maturilli et al. [2015]. Directly connected to downward shortwave radiation is the shortwave radiation reflected from the earth surface, the upward shortwave radiation. Obviously it is zero during polar night as well (reflecting moonlight is too weak to be displayed in monthly mean values), maximum values are reached in May and June. They range from 135 W/m^2 (in May 2016) to 182 W/m^2 (in June 2014). Since reflected shortwave radiation depends on the structure of the earth surface, which differs greatly between snow and snow-free tundra, the variations of monthly mean values in these two months is high. The abrupt decline after maximum values were reached is also explained through this effect. In 2014 for example (purple line in Fig. 7c)) a thick snow-layer stayed until late June, explaining this year to differ from the others. In contrast, 2016 (pink) has the lowest values in almost all months, which can not be explained through surface differences and will thus be picked up in the discussion chapter of this study. Downward longwave radiation is the incoming thermal radiation, that

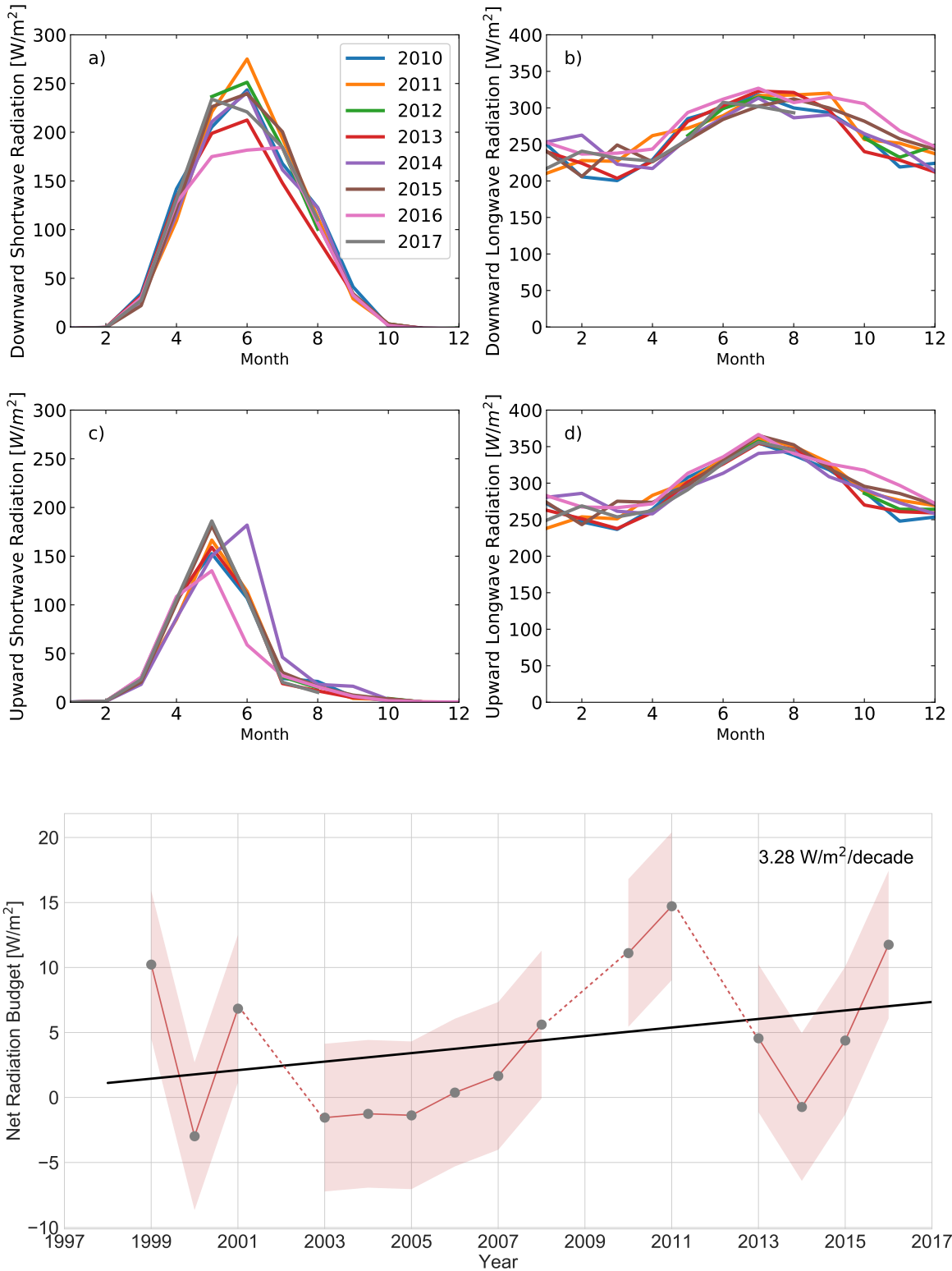


Figure 7: Bayelva monthly mean values for the years 2010 to 2017 for **a)** downward shortwave radiation, **b)** downward longwave radiation, **c)** upward shortwave radiation and **d)** upward longwave radiation. The legend in **a)** applies to all plots. **e)** Shows the annual mean net radiation from 1999 to 2016 in 95% confidence interval. Linear regression suggests a trend of 3.28 W/m^2 per decade (with standard error of $\pm 2.7 \text{ W/m}^2$ per decade).

dominates the radiation budget during polar night. It is dependent on atmospheric temperature and humidity. The variability seen in Figure 7b) arises from different cloud situations and atmospheric water content over the months and years. Maximum values during summer (JJA) result of higher atmospheric temperatures in these months. The Bayelva dataset shows similar inter-annual variability ($\pm 50 \text{ W/m}^2$) for all months, which doesn't support observations made in Ny-Ålesund (see further: section 6). Winter downward radiation shows higher variability, connected to high variation in winter air temperatures and humidity as well as different cloud-covers. The small sample size of the Bayelva dataset could explain the absence of those connections. Upward longwave radiation depends on surface temperatures and properties, which is described in equation (2). Here the difference of month-to-month variations for winter and summer months is visible. In January, highest variations between 238 W/m^2 (in 2011, orange) and 284 W/m^2 (in 2012, green) occur, while maximum values in July only range between 341 W/m^2 (in 2014, purple) 367 W/m^2 (in 2016, pink). Annual mean values for the net radiation budget were averaged next and are shown in Figure 7e). The years 2002, 2009 and 2012 were excluded from annual aggregations by the filter introduced in chapter 4.2. In 2002 no data was recorded until 14th May, in 2009 a big data-gap occurred in the second half of the year and in 2012 the time between February and May is missing. Each data-gap is flagged with 1, meaning no data/missing value. A linear increasing trend in net radiation of 3.28 W/m^2 per decade with a standard error of 2.7 W/m^2 per decade results the trend analysis. The high error is explained by high variations of annual averages over the years and the three missing years. Nonetheless the trend aligns with the trend Maturilli et al. [2015] published, that is 4.9 W/m^2 per decade with a standard error of $\pm 2.9 \text{ W/m}^2$ per decade. The timespan of their study is from 1993 to 2012, with positive annual mean net radiation values after 2000. The Bayelva dataset shows positive values only after 2005, with an exception year 2014, where the annual average is -0.7 W/m^2 . Maximum net radiation value in Bayelva is reached in 2011 with 14.7 W/m^2 , minimum in 2000 with -3 W/m^2 . Net radiation data from 1998 to 2009 is estimated to have field accuracies between $\pm 10\%$ (sensor from 1998 to 2003) and $\pm 20\%$ (sensor from 2003 to 2009) because they were unattended for most times and could not be checked for condensation, physical damage, hoar frost or dirt [Boike et al. 2017] (see further: section 6).

5.1.2 Air Temperature Characteristics

Annual mean air temperatures

were aggregated and are shown in Figure 8. The annual mean air temperatures vary between -7 and -1.8°C from 1998 to 2016. The coldest year recorded at the climate station in Bayelva was 2003, the warmest 2016. An increasing trend of $1.4 \pm 0.4^{\circ}\text{C}$ per decade can be observed over the 18-year period.

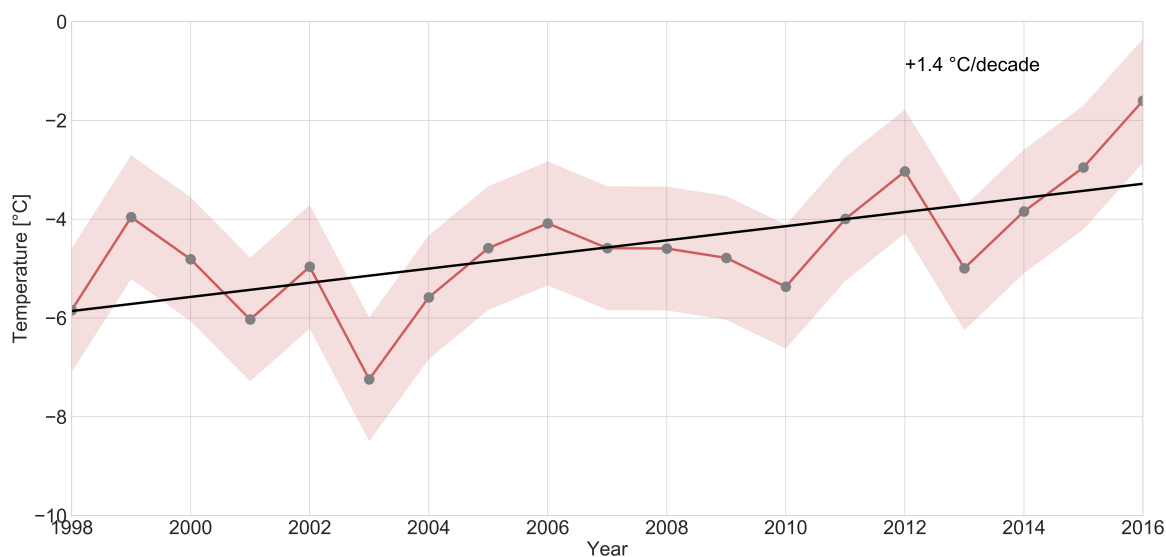


Figure 8: Annual mean temperatures in Bayelva (grey points) from 1998 to 2016 with a 95% confidence interval (red shading) and the linear regression (black line). A positive trend of 1.4°C per decade is visible.

It needs to be looked at inter-annual air temperature processes, to gain deeper understanding of the observed year-to-year variations. **Monthly mean temperatures** were aggregated to distinguish months that show high variability over the observed time span from months with little variations. The results are plotted in Figure 9a), similar to figure 2a) in Maturilli et al. [2013]. During the cold months January, February, March, April as well as November and December variations are greatest and range from 11°C in October (-9 to 2°C), 15°C in January (-19 to -4°C) and 15°C in April (-17 to -2°C). Lowest temperature differences occur in July ($\Delta T = 4^{\circ}\text{C}$) and August ($\Delta T = 3^{\circ}\text{C}$). Mean values of all months over the years are shown in a separate Figure 9b) with absolute minimum and maximum temperatures recorded in each month. Again the highest month-to-month differences occur during winter months. Monthly mean temperatures between 1998 and 2017 show coldest values in March (-11°C) and warmest in July (6°C). The absolute warmest month was recorded in July 2005, with 14°C average air temperature, whereas January 2004 was the absolute coldest month (-31°C) recorded in Bayelva.

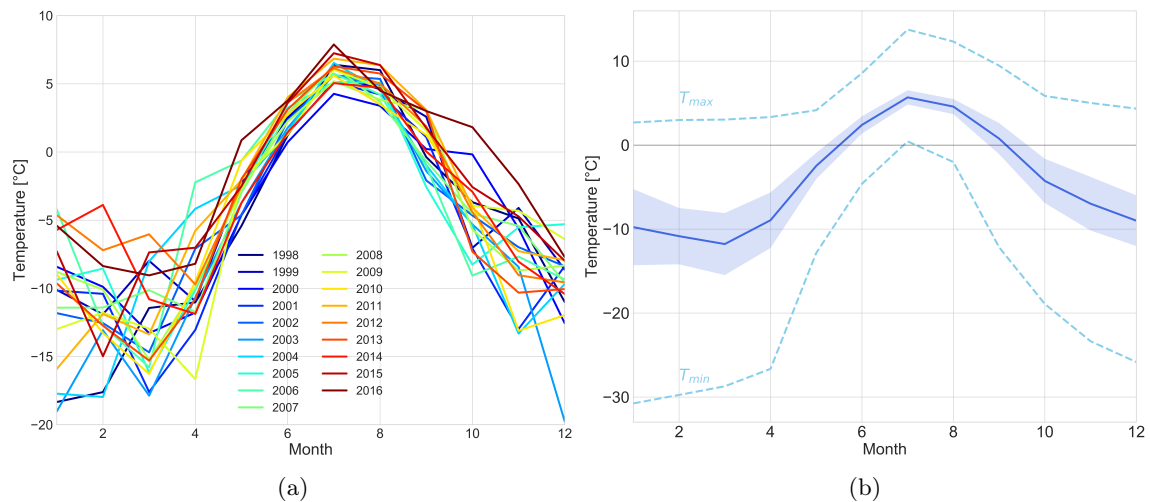


Figure 9: **a)** Averaged monthly mean air temperatures of all years show greatest variations during winter months (1,2,3,4 and 11,12). **b)** Averaged monthly mean air temperatures (dark blue line) with standard error (shading) as well as observed minimum and maximum temperatures (light blue dashed lines) from 1998 to 2017.

While monthly mean values help differentiate the years in an intuitive way, generating mean values for each climatological season (spring, summer, autumn, winter) allows interpretations of changes in the climate system (results see Appendix, Figure 25). Winter temperatures have been following the steepest positive trend with 2.7 ± 1 °C per decade. Maturilli et al. [2015] observed a trend of 3.1 K per decade. The difference in air temperature trends is due to cold winter temperatures (around -13 °C) in Ny-Ålesund for the years before air temperature recordings in Bayelva began (1994 to 1998). Mean winter temperatures in Bayelva are -11 ± 0.1 °C.

Freezing/Thawing Degree Day Index

To be able to compare the different years, regarding freezing and thawing degree-days, an index was calculated by taking the square root from equation 11 for TDD and FDD. The results are presented in Figure 10a) and b). 2003 has the highest freezing degree-day index with 55, 2016 the lowest with 35.5. The thawing degree-day index is lowest in 2000 (19.2) and highest in 2016 (27). After first visual examination and comparison with air temperatures (see Figure 8), the results correlate in the way that extreme years, like 2003 as the coldest year observed, also has the highest freezing degree-day index. Whereas the warmest year so far, 2016, has the highest thawing degree-day index and lowest freezing degree-day. Detailed

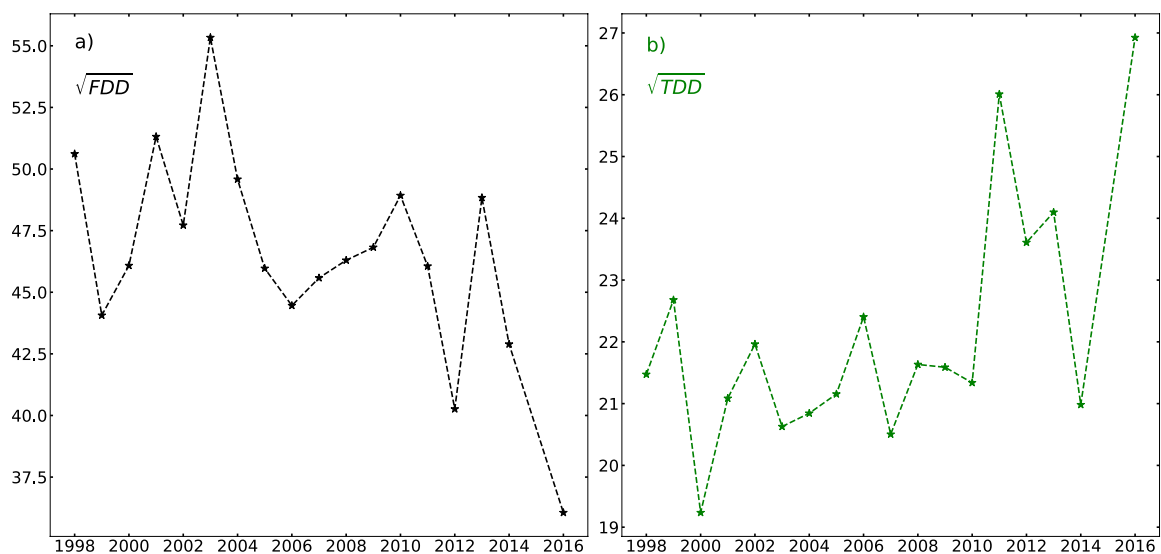


Figure 10: Freezing/Thawing Degree Day Index

relations of freezing/thawing degree-day indices to air and soil temperatures, as well as snow cover characteristics will be presented in chapter 5.4.

5.2 Snow

The snow cover in Bayelva show high spatial variability, comparable to many arctic seasonal snow covers [Maturilli et al. 2013; Boike et al. 2013]. Irregular topography and redistribution due to wind-blow are the two main reasons. Point measurements like the one in Bayelva thus only represent a snap-shot of the overall snow situation. However, a characterization is still possible and the results are presented in the following.

5.2.1 Duration of the Snow Cover

In a first analysis step, the end date of the ablation was determined by extracting the day in spring/summer where the snow height is lower than 0.05 m and shows no further build up

over July and August. The results show great variability over the years. The years 2001 and 2008 could not be defined clearly due to data gaps in the measurements. Extreme values, like 2014 or are due to a very long snow cover duration. To verify the results of this method, the approach Maturilli et al. [2013] used with their data was applied additionally. They used the different albedo of snow and tundra ground to define the end point of snow cover. Values around 0.1 are typical for tundra, as it is found around the snow height sensor during snow free periods, so a filter of 0.2 was applied to the albedo dataset. Albedo values for fresh fallen snow are around 0.8 (see Fig. 5). The first day in spring/summer below this filter was set to be the end of snow cover. Applying this to the Bayelva dataset results in the dates shown in Figure 11. To determine beginning and end of the snow cover, the two methods described in chapter 4.3 were applied to the dataset from 1998 to 2016. The results show that a continuous snow cover builds up between 11th September (in 2005) and 15th November (in 2016). Most build-ups are in the last week of September and the first two weeks of October. The great variation on these dates is partly due to the filter applied on snow depth measurements (see chapter 4.3). In some years, first snowfall occurred earlier then the detected beginning, but several periods of melt-off cuts the snow-period shorter. A clear definition of the beginning of a snow cover that has a significant effect on soil temperatures is thus difficult. The offset of the snow cover in Bayelva happens between 3rd June (in 2006) and 9th July (in 2014). Most offset-dates vary in the last two weeks on June. Variations here are less, since there is no more snowfall in spring and the distinction between the snow-covered and snow-free period is clearer. Average duration of the snow cover is eight months. The results of the offset-analysis are presented in Figure 11.

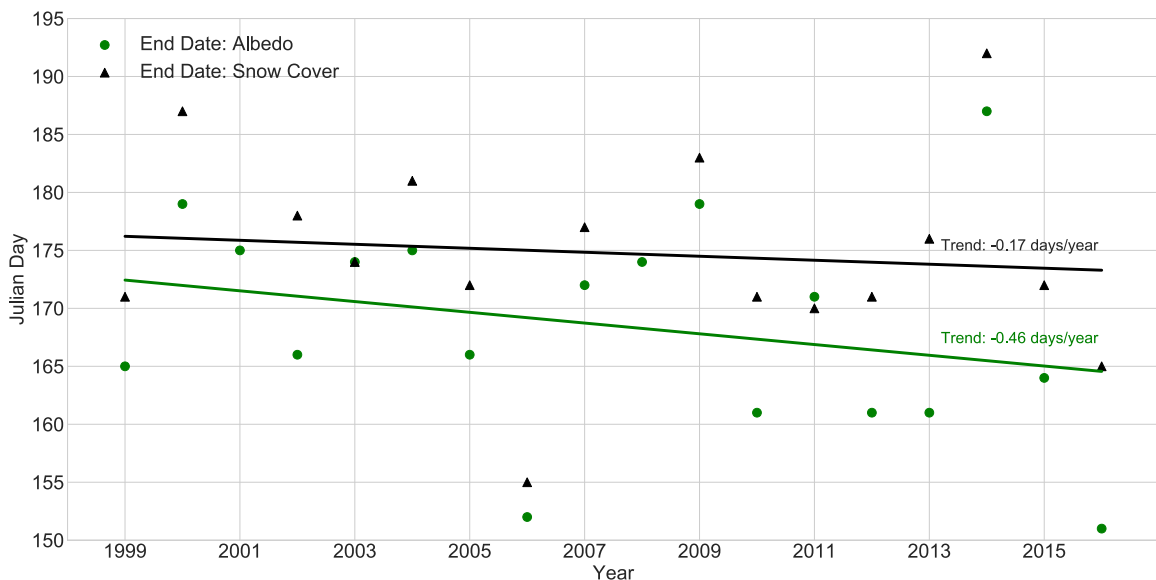


Figure 11: Comparison of end date of the snow cover (julian day) determined through filter, where snow cover stays lower than 0.05 m (black) and through filter where albedo stays lower than 0.2 over the summer (green) with respective linear regressions.

The second approach, to retrieve the end date over the albedo is shown with the green data points with the corresponding linear regression. The trend of this analysis -4.9 days/decade, which supports the theory that the snow covered period is getting shorter and the end of ablation happens earlier in the year. Not just the trends of the two analyses differs greatly. Only in two years (2003 and 2011) the approaches ended the snow period around the same day (± 1 day). For the most years the difference is between 3 to 10 days, the biggest divergence are for the years 2001 and 2008, which were already detected as outliers due to measurement insecurities of the snow height measurements. Differences between 3 to 10 days can be the result of comparing data that is measured on just one point (snow height sensor) and data that represents the snow situation on a bigger region. During ablation, some landscape patches clear earlier than other ones. This influences the albedo but is not as clear as if the snow sensor measures 10 cm of snow or none. To set the albedo threshold to 0.2 results in this difference.

5.2.2 Measured versus Effective Snow Depth

Seasonal variations in the snow depth disturb the linear distance between air and soil temperatures and influences the net radiation budget. This chapter presents the results of snow cover analyses, and focuses on the difference between measured snow depths and calculated effective snow depths after Slater et al. [2017]. Table 2 presents monthly mean snow depths for the cooling months October to March as well as the mean snow depth of each cooling period and $S_{\text{depth,eff}}$, which was only calculated if no months were missing for the calculation.

The effective snow depth after Slater et al. [2017], introduced in chapter 4.3 weights the monthly mean snow depths by their timing, this helps to gain insight to the insulation effect of snow. The cooling period in Bayelva is defined from October to May. During these months most of the recorded years are snow covered, differing from the average snow cover duration of the terrestrial Northern Hemisphere, which lasts from October to March. Mean snow depths for the cooling periods 1998, 2011 and 2016 are similar around 0.5 m (Fig. 12), their behavior over the cooling period shows great differences though. In November 2016 heavy snowfall built up the cover almost to its maximum height and only grew more until May. The snow cover in 2011 reached around the same maximum height in April/May but took more time to built up. Almost continuous snowfall over the whole period shows a smoother evolution. In 1998, high snowfall from October to January built a snow cover as thick as in 2016. Melting periods and small snowfall rates for the rest of the cooling period follow. The early snow cover built-up in 2016 lead to greater values of $S_{\text{depth,eff}}$ than in 2011 and 1998. Steady snowfall in 2011 results in a higher effective snow depth than in 1998, even though early snowfall occurred during that year.

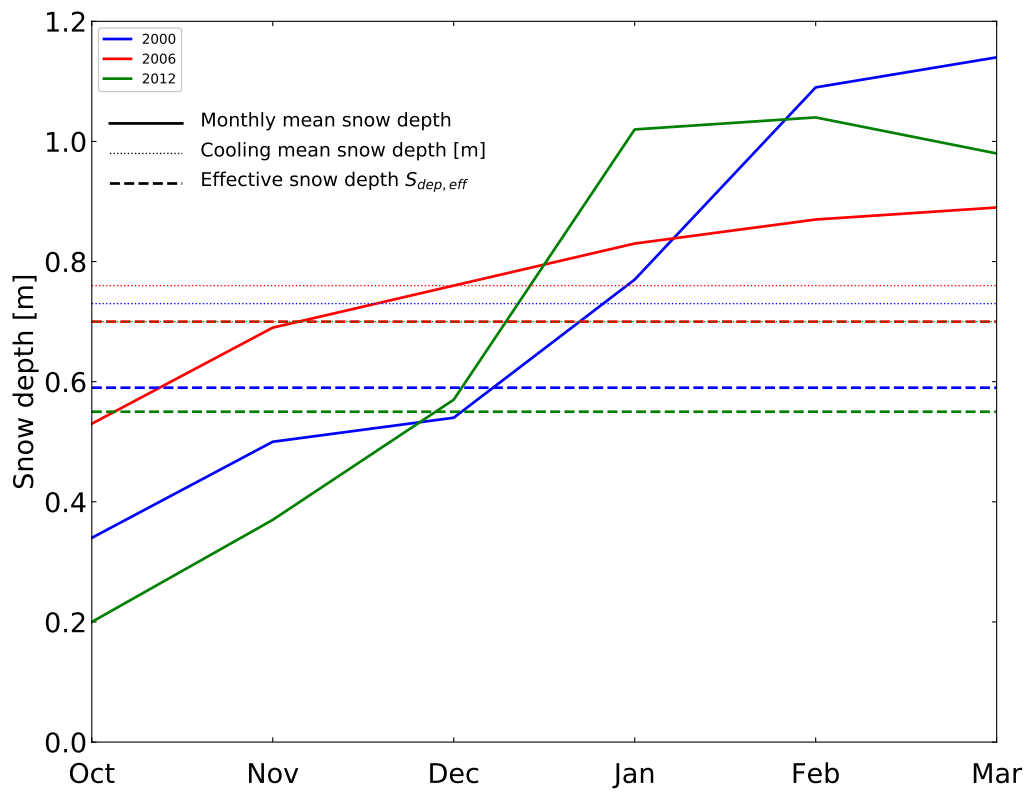


Figure 12: Effective snow depth after Slater et al. [2017] of three different snow regimes (2000, 2006 and 2012) that have similar mean values over the period October-May.

Table 2: Effective Snow Depth: Monthly mean snow depths of cooling period (Oct to May) with mean snow depth in meter and Effective Snow Depth.

Year	Oct	Nov	Dec	Jan	Feb	Mar	Mean	$S_{\text{depth,eff}}$
1998	0.17	0.25	0.42	0.65	0.56	0.62	0.45	0.36
1999	0.19	0.11	0.29	0.28	0.27	0.3	0.24	0.22
2000	0.34	0.5	0.54	0.77	1.09	1.14	0.73	0.59
2001	0.25	0.38	-	-	-	-	0.32	-
2002	0.08	0.25	0.26	0.2	0.33	0.55	0.28	0.22
2003	0.23	0.2	0.49	0.73	0.91	1.01	0.59	0.45
2004	0.26	0.6	0.62	0.64	0.68	0.74	0.59	0.53
2005	0.4	0.51	0.54	0.6	0.89	0.93	0.65	0.55
2006	0.53	0.69	0.76	0.83	0.87	0.89	0.76	0.7
2007	0.3	-	0.68	0.6	0.91	0.82	0.66	-
2008	-	0.82	0.8	0.79	0.89	0.98	0.86	-
2009	-	0.39	0.54	0.5	0.51	0.55	0.5	-
2010	0.14	0.46	0.64	0.84	0.9	0.88	0.65	0.52
2011	0.18	0.35	0.38	0.47	0.65	0.66	0.45	0.37
2012	0.2	0.37	0.57	1.02	1.04	0.98	0.7	0.55
2013	0.41	0.71	0.79	1.03	1.06	1.39	0.9	0.75
2014	0.19	0.37	0.47	0.54	0.66	0.71	0.49	0.41
2015	0.3	0.41	0.45	0.38	0.58	0.66	0.46	0.41
2016	0.11	0.15	0.57	0.69	0.74	0.71	0.5	0.38

Maximum mean snow depth for the cooling period is recorded in 2013 with 0.9 m in average. The result is due to a high snow cover in March 2014, where other years started to melt off already. That snow cover already had high values in October 2013, resulting in the maximum value for $S_{\text{depth,eff}}$ calculations of 0.75. A slightly lower $S_{\text{depth,eff}}$ results in 2006 with 0.7, the mean measured snow depth here being 0.76 m. The difference here results of over 10 cm higher snow depths at the beginning of the cooling period (0.53 m in 2006 and 0.41 m in 2012). Minimal mean measured snow depth occurs in 1999 with 0.24 m, leading to a $S_{\text{depth,eff}}$ of 0.22, which also occurs in 2002, where the mean depth is 0.28 m. In 1999 snow depth in October was higher than in 2002, both years lingered around 0.3 m for the following months and in March of the 2002 cooling, late snow-fall led to a monthly mean of 0.55 m compared to 0.3 m in the 1999 cooling. For verifying whether the $S_{\text{depth,eff}}$ of the two cooling periods

in fact had the same insulation effect on air and soil temperatures, the amplitudes following equation (13) were compared. The results are shown in Figure 13.

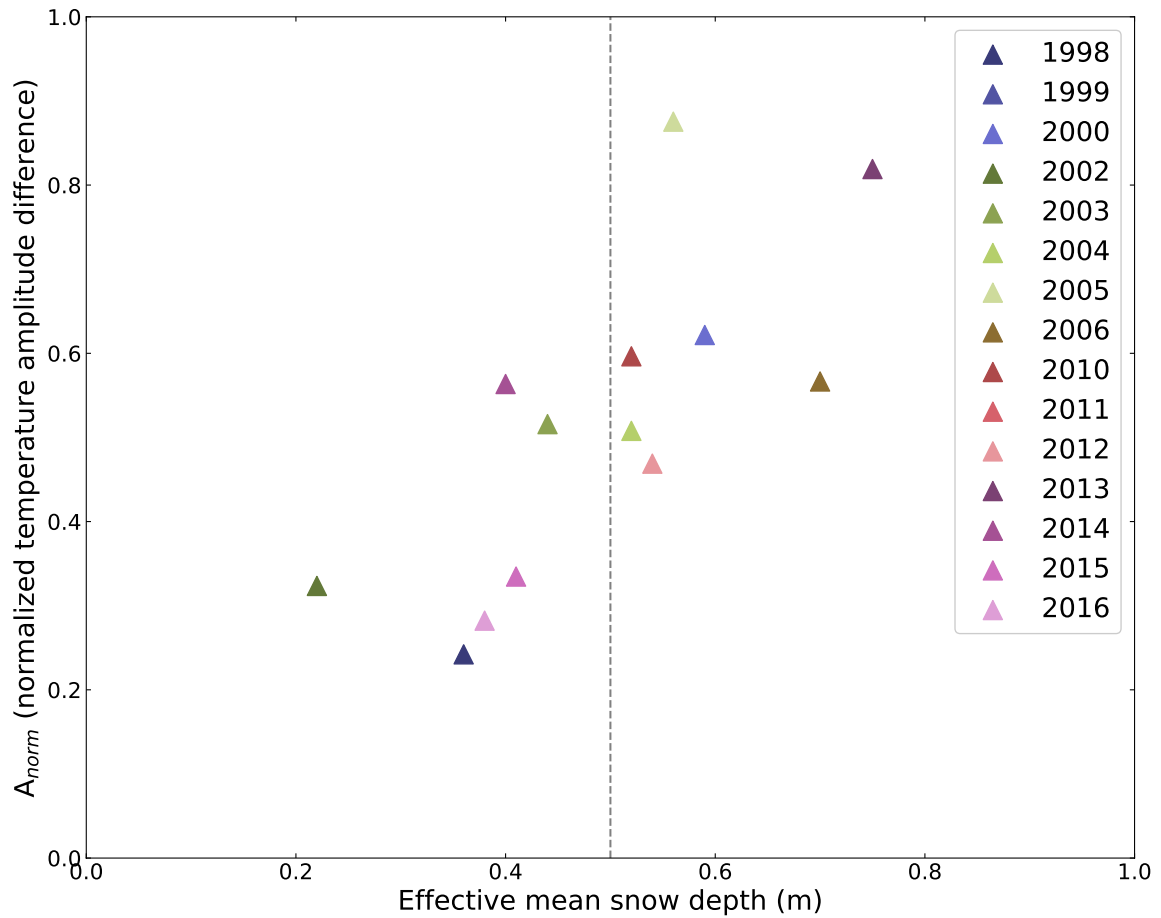


Figure 13: Observed relation of observed $S_{depth,eff}$ and A_{norm} in Bayelva, for the years 1998 to 2016 with 2001, 2007 and 2008 excluded due to missing data.

The years 2002, 2007 and 2008 were excluded from the Figure, since no $S_{depth,eff}$ values were calculated. Due to the very limited samples with high scattering, parameter-estimation of equation (14) was not possible.

A comparison and discussion with the results from Slater et al. [2017] will follow in chapter 6.1.3.

5.3 Soil

Results of the soil characteristics analysis are presented for active layer and permafrost features separately.

5.3.1 Active Layer

Active Layer Temperatures

Absolute minimum and maximum temperatures at depths 0.01, 0.71 and 1.41 m for each year with the respective dates are presented in Table 4 and 3 in the appendix separately. Mean temperatures over the recorded timespan are -1.23°C (0.01 m depth), -1.55°C (0.71 m depth) and -1.20°C (1.41 m depth) with an absolute maximum temperature of 16.88°C measured at a depth of 0.01 m and absolute minimal temperature of -16.10°C measured at the same depth. Absolute maximum temperature of 16.88°C was measured in July 2016. Maximum temperatures in that depth vary with $\Delta T = 9^{\circ}\text{C}$. In a depth of 0.71 m, maximum temperature occurred in August 2007, with 6.6°C (ΔT being 4°C) and in the lowermost sensor, warmest temperature was measured in September 2016 with 3.29°C (ΔT being 4°C). The uppermost temperature sensor shows highest absolute values as well as highest ΔT between the years. Coldest temperature in one year was measured in March 2000 at a depth of 0.01 m. Minimum temperatures in the uppermost sensor vary between $\Delta T = 10^{\circ}\text{C}$. At a depth of 0.71 m, coldest temperature was measured in February 2003 with -13.1°C (ΔT being 12°C). The sensor at a depth of 1.41 m recorded -11.7°C in February 2003 as well, ΔT here being 10°C . Year-to-year variations are higher for minimum temperatures, where the sensor in a depth of 0.71 m shows highest fluctuations. When looking at the date of minimum/maximum temperatures in one specific depth, the general trend is, that ΔT is always in the direction of highest absolute temperatures being in the recent past, suggesting a warming trend. For a closer look at trends, temperatures were aggregated annually as well as seasonally for three different depths (44, 58, 133) by the AWI [Boike et al. 2017]. Trend analysis for the three depths each show increasing temperatures. From 1998 to 2017 temperatures in all three depths have been rising with $0.18^{\circ}\text{C}/\text{year}$ (± 0.07 , 0.06 , $0.05^{\circ}\text{C}/\text{year}$ standard error respectively). Aligning with air temperatures, active layer temperatures show most warming in the winter months: 0.25 , 0.25 and $0.23^{\circ}\text{C}/\text{year}$ (± 0.12 , 0.11 , $0.07^{\circ}\text{C}/\text{year}$) for the three depths analyzed. The results of trend analyses are shown in the appendix Figure 26.

A warming trend in the cold seasons results in a longer duration of re-freezing of the active layer in the Alaskan Arctic [AMAP 2017]. To examine this hypothesis on the Bayelva active layer, the day of year, on which all temperature sensors recorded temperatures below -2°C was extracted. Figure 14a) shows the results of this analysis. To get an even better understanding of freezing-patterns, the total duration (first sensor below -2°C to final sensor below -2°C) of freezing of the active layer was measured and are presented in Figure 14b). The years 2001 and 2013 show the latest day until final freeze-up, day 496, which refers to the middle of May.

In 2002, the active layer was completely frozen on the 11th November, showing the earliest day of final re-freeze, day, 315. The years 2001 and 2013 also show the longest duration of re-freeze with 189 and 227 days respectively. In 2005 it took only eleven days for the soil to re-freeze. Low maximum temperature at depth 1.41 m of 0.4 °C reacted quickly to the cooling signal from overlaying layers, shortening the re-freeze duration.

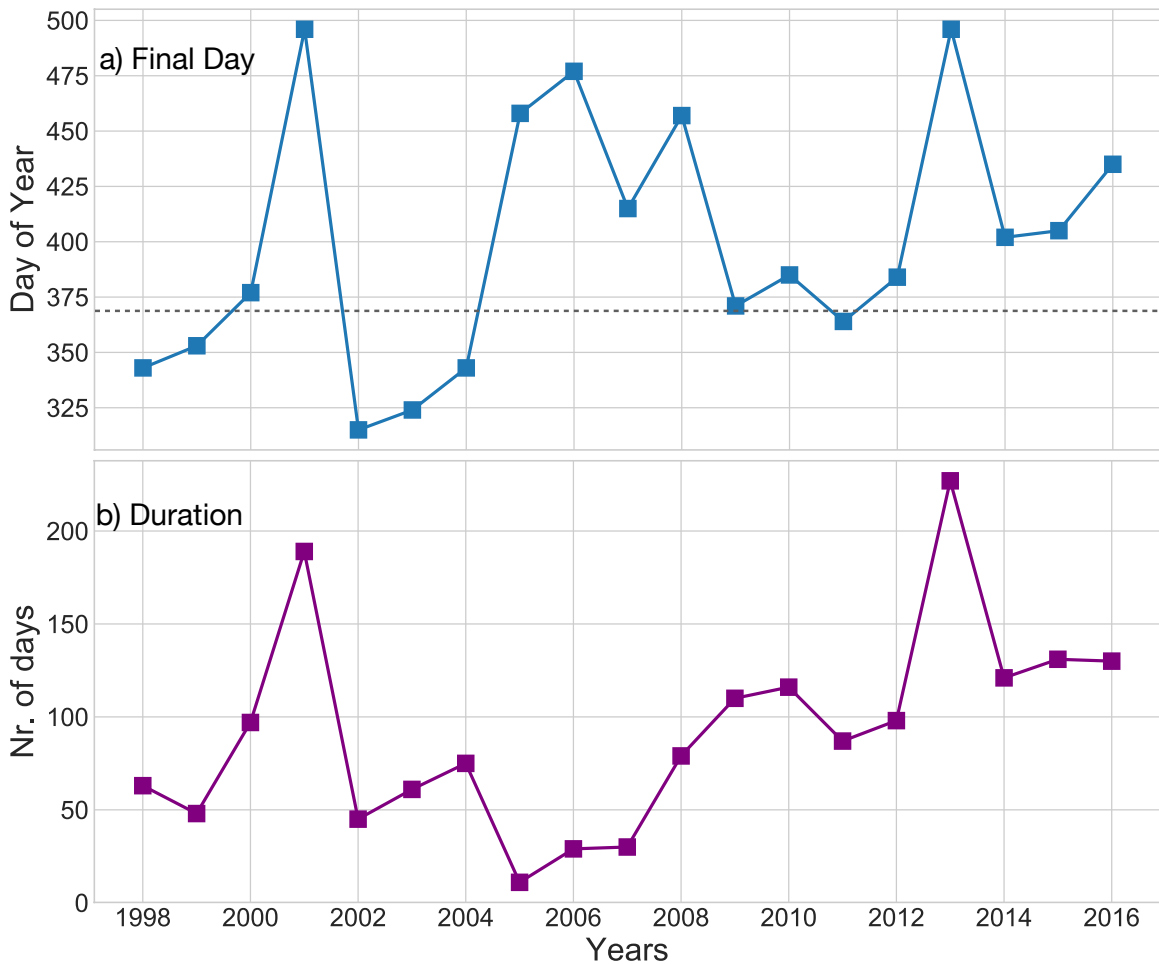


Figure 14: a) Final day of active layer freeze-up. All soil temperatures are below -2 °C. The gray dashed line indicates day 365 (end of the year). b) The number of days for freezing the active layer from top to bottom (0.01 m to 1.41 m depth).

Active Layer Thickness

An estimation of the maximal thaw depth of the active layer was calculated for each year, using the Stefan Equation (see equation (8)). The result is presented in Figure 15 together with a linear trend line. Trend analysis over the years 1999 to 2016 suggest a thickening of the layer with 5 ± 0.7 cm/year. While the maximum thawing in 2000 reached 1.04 m below surface, marking the lowest thawing value, the 2 m mark was exceeded in 2016 for the first time. Thaw depths were over 1.5 m for over a decade now.

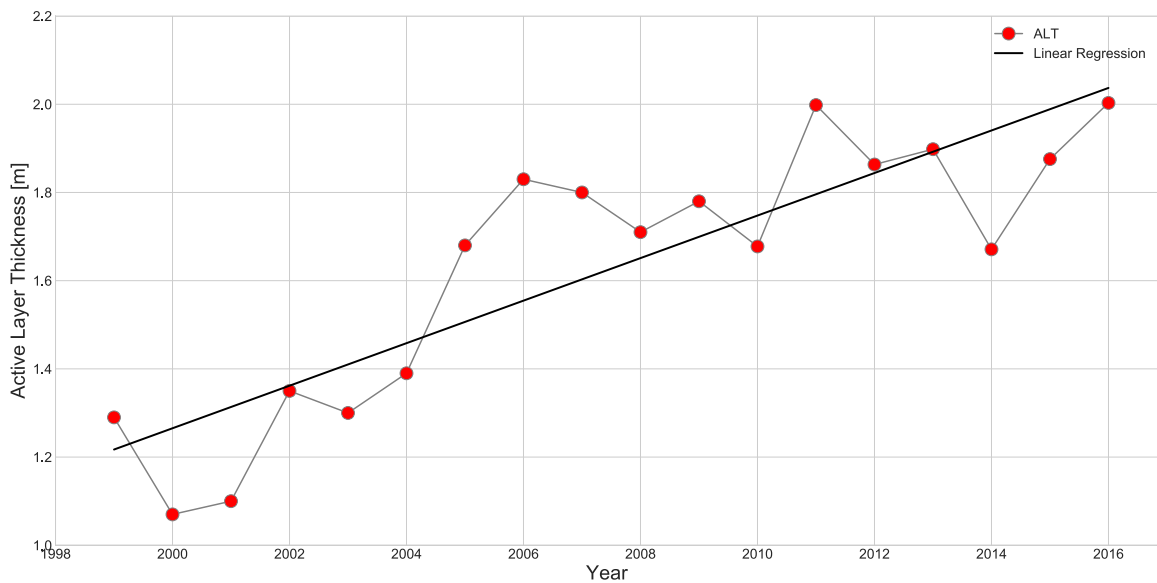


Figure 15: Active Layer Thickness in Bayelva calculated with the Stefan-model. A linear fit (black line) shows a thickness increase of 5 ± 0.7 cm/year.

5.3.2 Permafrost

Temperatures were aggregated and visualized according to Figure 4 in the 20-year record publication by Boike et al. [2017] to be able to compare trends (see Fig. 16). According to AMAP [2017], permafrost temperatures that are already warm (between -1 and -5°C), like in Bayelva, show less warming than colder permafrost regions. Nonetheless there are already areas on Svalbard, that have been thawed all the way through and by definition do not count as permafrost anymore [AMAP 2017; AWI 2017]. Small warming trend in warm permafrost regions thus lead to complete depletion.

Results of trend analysis for the depth 2.5, 5.5 and 9 m are shown in Figure 16, while complete results are shown in Table 5 in the appendix. Highest warming in yearly and winter averages are shown at a depth of 2.5 m below surface. Summer mean values show highest warming at a depth of 5.5 m.

The depth of zero amplitude introduced in chapter 3 is visible in depths 5.5 m and 9.0 m. Both show an increasing trend in the annual, winter and summer aggregations. Summer and winter trends are similar, while the respective trends in a depth of 2.5 m differ. Here the seasonality is reflected.

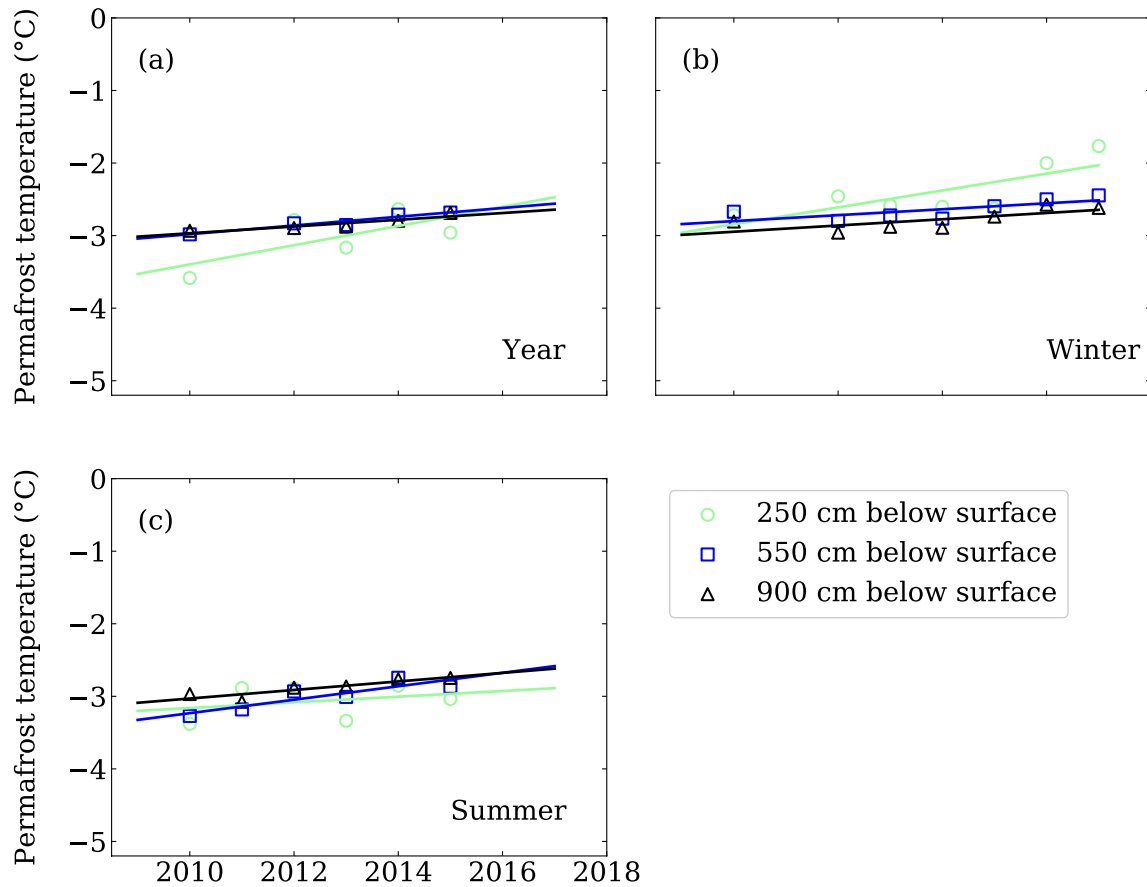


Figure 16: Permafrost Temperatures from 2009 to 2017 for 3 different depths (2.5, 5.5 and 9.0 m) with regression lines. a) yearly mean temperatures, b) winter mean temperatures include the months December, January and February, and c) summer mean temperatures include the months June, July and August.

5.4 Linkage between Climate, Snow and Soil Characteristics

In the final sub-chapter of the result part, all the components described so far were cross-correlated to each other. The result serves as basis for comparisons of the Bayelva data-set with other study sites in the next chapter. When presenting results of correlation analyses, the pearson-coefficient for standard correlation analyses is given to show the level of significance. The pearson-values are between -1 and 1, 0 meaning no correlation. Steps between 0 and 1/-1 are interpreted as follows:

- 0 to 0.3 (-0.3): small positive (negative) correlation,
- 0.3 to 0.5 (-0.5): weak positive (negative) correlation,
- 0.5 to 0.7 (-0.7): moderate positive (negative) correlation,
- 0.7 to 1 (-1): strong positive (negative) correlation.

Positive values describe changes of the variables in the same direction (i.e. increasing variable x correlates with increasing variable y). Negative values act in the opposite direction.

Figure 17 presents the result of a pearson-correlation analysis, limited to correlations with p-values higher than 0.69 and lower -0.69, suggesting strong positive and negative linear correlations. Values close to zero weak to no correlation of the respective variables. The complete spectrum as well as a description of the variables are shown in Figure 27 and Table 6 in the appendix. Darker shadings of both colors on the heatmap refer to strong positive/negative correlations, while lighter colors show correlations close to 0.7, which is still in the range of moderate positive relations.

Against the hypotheses of the effective snow depth stated in chapter 4.4, no strong positive correlation is observed between $S_{\text{depth,eff}}$ values (*Snow_ESD*) and any ground temperature sensors in Bayelva. A p-value of 0.7 between $S_{\text{depth,eff}}$ (*ESD*) and the final day of active layer freeze-back (*Final_Freezeback*), and $S_{\text{depth,eff}}$ to the mean snow height of the cooling season (*Snow_Mean*, $p = 0.9$) are the only significant relations of $S_{\text{depth,eff}}$ results to other variables. Thawing degree-day index (*TDD*) correlates positively with active layer temperatures in 0.01 m depth (*AL_summer_Ts1*), as well as winter temperatures of permafrost depths 2.5 and 3.5 m depths (*Ts_250_winter* and *Ts_350_winter*).

The hypothesis of a depth of zero amplitude (depth in which seasonality diminishes) below 5.5 m (previously mentioned in chapter 5.3.2), is supported by those results since warm air temperature signals included in TDD calculations are only represented in soil layers above 5.5 m. Additionally, winter active layer temperatures (*AL_winter*) correlating with summer permafrost temperatures (*Ts_ _winter*) to a depth of 7.5 m, strengthens the conjecture of the depth of zero amplitude being between the sensors at depths 5.5 and 7.5 m. Summer permafrost temperatures at a depth of 9 m correlate to winter active layer temperatures at a depth of 1.41 m and summer permafrost temperatures in depths of 5.5 and 7.5 m. Those results on the other hand counteract with that hypothesis, especially a p-value of 0.8 with

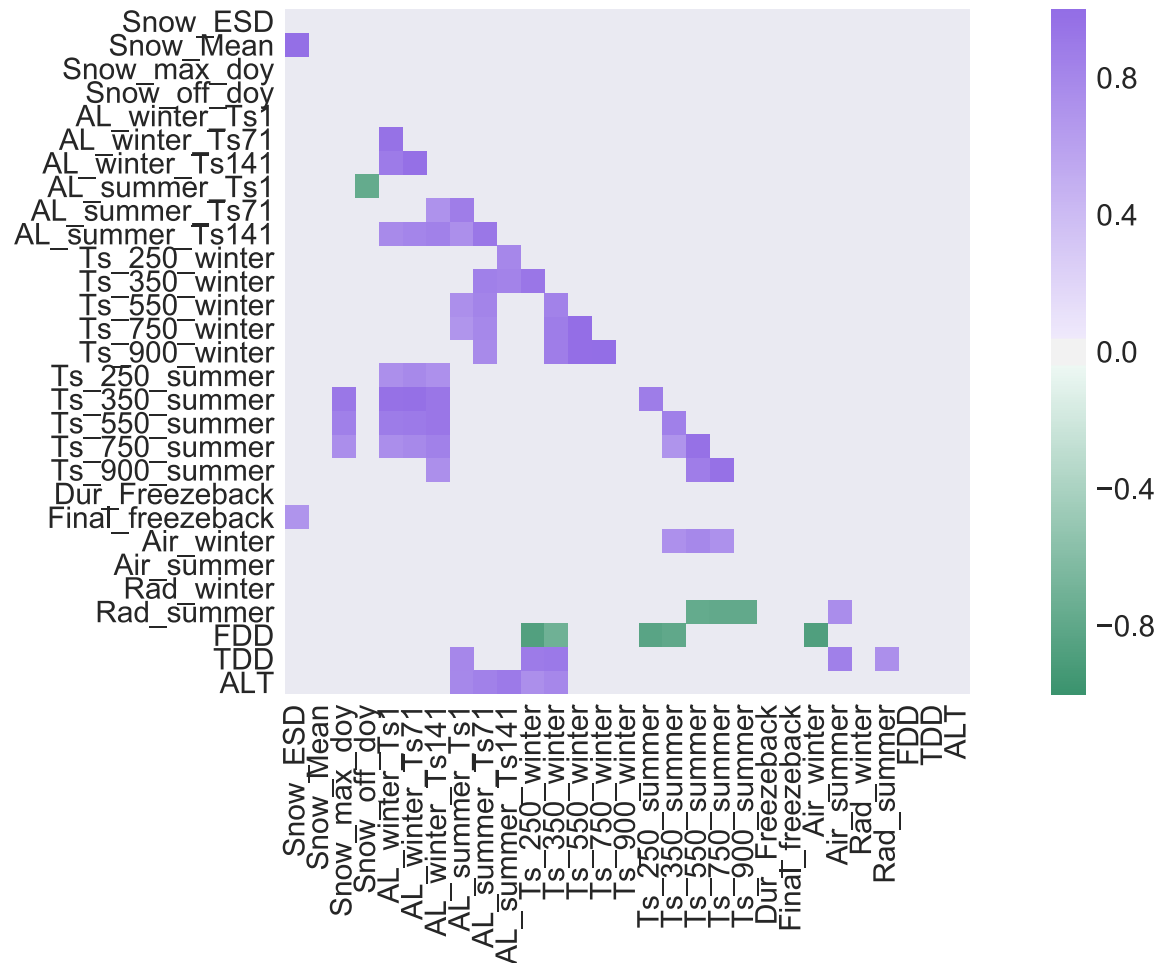


Figure 17: Heatmap of many parameters analyzed in this thesis. Background is a pairwise standard correlation (pearson-value), resulting in values between -1 (strong negative correlation) and 1 (strong positive correlation). The color indicates the level of correlation as shown in the legend on the left. Purple colors represent positive values, green values represent negative values. Only correlation results between $0.69 < p < -0.69$ are shown (statistically significant correlations).

depths 7.5 and 5.5 m.

The Freezing degree-day index (*FDD*), as opposed to the TDD, shows strong negative correlations. Cooling signals from the air temperatures seem to be connected to permafrost winter and summer temperatures at depths 2.5 and 3.5 m in opposite directions, meaning that years with a high FDD, winter, as well as summer temperatures at those depths are low. Absolute temperature values in the calculation of FDD, explain the opposite direction of those correlations, but in general represent expected processes. Very cold air temperatures during cooling months are represented in soil layers. Surprisingly, there is no strong correlation between FDD and active layer temperatures. Looking at Figure 27, a moderate negative correlation can be observed for FDD and active layer temperatures in summer and winter and all depths. Absolute snow depth maxima are positively connected to permafrost summer temperatures (p between 0.7 and 0.9), meaning that years with high snow maxima, summer permafrost temperatures were high as well. Low snow maxima on the other hand occurred in years with low summer permafrost temperatures. Moderate negative correlation of snow maxima with summer active layer temperatures (p-values between 0.5 and 0.7) can be observed, describing a correlation in opposite directions than with the permafrost temperatures. The snow cover thus seems to have different impacts on the active layer and permafrost summer temperatures.

Correlations between different soil sensors will not be described in detail at this point, but can be followed in Figures 17 and 27.

The following chapter takes the results of the Bayelva dataset analyses and discusses them in respect to other observations in the Arctic.

6 Discussion

The discussion part of this thesis is divided into two parts. In a first section, the results of the long-term analyses of climate, soil and snow cover features from the Bayelva research station will be compared to global average developments, Arctic trends, and individual research sites in the Arctic. The second part focuses on the role of the snow cover characteristics analyses and the effective snow depth in snow cover modeling.

6.1 Comparison to other sites

When comparing Svalbard climate, soil and snow characteristics to other High-Arctic regions, there is always the unique feature of Svalbard being semi-arid, compared to other High-Arctic sites with mostly arid conditions (e.g. Siberia). The influence of the West Spitsbergen Ocean Current is visible in air temperatures (comparatively warm), radiation components (through higher air moisture content) and snow cover characteristics (comparatively high, see section 6.1.3). Each climate feature will at first be compared to other trend observations in the Arctic, then a more close insight in different publications of Svalbard will be given.

6.1.1 Climate

Air Temperature

Data quality for air temperature analysis is very good, due to the gap-filling with the AWIPEV data stream. Uncertainties resulting from missing values could thus be reduced.

Førland et al. [2011] state skepticism towards linear trend analysis for temperature development, since changes do not necessarily occur in a linear way. In contrary, the climate system is of chaotic nature, causing climate models to be incapable of predicting long-term trends [Benestad 2003]. Linear trend analysis thus only depict a first-order approach to describe changes in the natural environment.

The air temperature trend of $+1.4\text{ }^{\circ}\text{C}$ per decade in Bayelva for the past 18 years is higher than the global temperature trend. The Fifth Assessment Report of the IPCC states a global air temperature rise of $0.85\text{ }^{\circ}\text{C}$ from 1880 to 2012. The average global air temperature between 2003 and 2012 is $0.78\text{ }^{\circ}\text{C}$ warmer than the average of 1850 to 1900 [IPCC 2013b; IPCC 2013c]. In general, the Arctic has shown a higher air temperature rise, than the global average [Førland et al. 2011; AMAP 2017]. Highest measured air temperature trends in the Arctic are recorded in Barrow, Alaska with $0.29\text{ }^{\circ}\text{C}$ per decade from 1940 to 2005 [Hinzman et al. 2005]. The years 2011 to 2015 have been the warmest ever recorded with an increasing frequency of unprecedented regional warm events [AMAP 2017]. The past ten years in Bayelva show a higher annual temperature increase as well, just as absolute maximum temperatures.

Linear air temperature trends in Ny-Ålesund from 1920 to 2011 were published by Førland et al. [2011]. The authors divided the observed timespan into four approx. 23-years periods. The period overlapping most with the timespan of air temperature recordings in Bayelva – from 1989 to 2011 – shows an increase of $0.99\text{ }^{\circ}\text{C}$ per decade. Other sites on Svalbard, namely Svalbard Airport (in Longyearbyen), Hopen and Bjørnøya show linear trends of 1.25, 1.21 and $0.91\text{ }^{\circ}\text{C}$ per decade respectively (for location see Fig. 28 in appendix). The comparatively high trend in Bayelva is due the high annual air temperatures in the last ten years, especially the high annual mean in 2016 of $-1.8\text{ }^{\circ}\text{C}$. A second publication by Gjelten et al. [2016] reports similar long-term developments on Svalbard. Ny-Ålesund time-series from 1934 to 2015 (1941 to 1946 missing due to WW II) show an increase of $0.16\text{ }^{\circ}\text{C}$ per decade and $0.96\text{ }^{\circ}\text{C}$ per decade for the years from 1979 to 2015. Both linear trends lie within the 5% significance level. The publication stresses the increased temperature warming in recent years in all six meteorological datasets used for their study (Hornsund, Isfjord Radio, Barentsburg, Svalbard Airport, Pyramiden, Ny-Ålesund). Isaksen et al. [2016] examine this most recent warming concerning variations in large-scale atmospheric circulation (AC), changes in air mass characteristics, and sea ice concentration (SIC). Their study includes regional changes around Spitsbergen, but also local phenomena in three specific fjords (Isfjorden, Kongsfjorden, and Hornsund, see Fig. 28 in appendix). Data basis for the analysis are surface air temperature recordings at five stations (Hornsund, Isfjord Radio, Barentsburg, Svalbard Airport and Ny-Ålesund plus one extra station for sea ice concentration analyses: Janssonhaugen, 270 m asl). For atmospheric circulation patterns, the 'Niedźwiedz Classification' (Niedźwiedz 2013 in Isaksen et al. [2016]) comprising 21 AC types, is used. To distinguish between changes in air temperature due to changes in AC or changes in air mass characteristics, the period from 1971 to 2000 is used as the normal period for the present climate. The reference time period used in the study is 2001 to 2015. Frequency of AC types in both periods as well as mean air temperatures for one AC type in both periods are compared to each other. For collecting SIC information two different sources are used:

- (1) 1979 to 2015: Passive microwave satellite data from the European Organisation for the Exploitation of Meteorological Satellites (EUMETSAT) Ocean and Sea Ice Satellite Application Facility (OSI SAF)
- (2) 1969 to 2015: Ice charts from the Norwegian Ice Service, using analogue Infra Red satellite images up to 2007, and afterwards high-resolution synthetic aperture radar satellite data

The results show a mean air temperature increase of $1.8\text{ }^{\circ}\text{C}$ from the normal period 1971 - 2000 to 2001 - 2015, which the authors could mainly relate to changes in air mass characteristics. Only six of the 21 atmospheric circulation types are shown to have a significant influence on air temperatures. The main reason for changes in air mass characteristics is the observed decrease of sea ice around Svalbard. Sea ice coverage in the Isfjorden for example has decreased from 58% in 1997 to 6% in 2015.

Maturilli et al. [2013] published time-series from 1993 to 2011 of the meteorology parameters air temperature, humidity and pressure in Ny-Ålesund. Linear regression yields an air temperature increase of 1.35 ± 0.92 K per decade, with the warmest year being 2006 with an annual mean of -2.8 °C. For the overlapping period from 1998 to 2010 the Bayelva dataset also shows 2006 as the warmest year even though 1999 the annual mean in Bayelva has been similarly high. After 2010 all years except 2013 have been warmer than 2006, reflecting the recent observed warming all over the Arctic that has been mentioned before. Maturilli et al. [2013] observe the increasing air temperatures together with increasing air humidity of 0.22 ± 0.14 g/kg per decade. The authors likewise state atmospheric circulation patterns and sea ice coverage as possible reasons for the reported humidity increase.

Radiation

The SWIPA report from 2017 names downward longwave radiation as one major factor in snow cover processes [AMAP 2017]. It responds to changes in the atmospheric moisture content and air temperatures, as well as the concentration of aerosols and greenhouse gases and the occurrence of clouds. From 1973 to 2008 a global increase of downward longwave radiation of 2.2 W/m² per decade was observed. Maturilli et al. [2015] observe an increase of downward longwave radiation especially in winter months (DJF) from 1992 to 2012 of 15.6 ± 11.6 W/m² per decade in Ny-Ålesund. The reason for that increase is the coupling of downward to upward longwave radiation, which then is tied to changes in both the snow cover and winter air temperatures.

A detailed comparison of Bayelva radiation recordings to Ny-Ålesund radiation recordings (presented in Maturilli et al. [2015]) follows. This serves as data quality assessment for the Bayelva set-up. In a first step, monthly mean values of the four components will be compared, followed by the evaluation of annual mean values and the resulting linear regression (all shown in Fig.7).

Monthly mean values of downward/upward shortwave and longwave radiation in Bayelva were aggregated for the years 2010 to 2017. Maturilli et al. [2015] report unusual low values of upward shortwave radiation in 2006, which is not covered by the Bayelva dataset. Nonetheless, the explanation for the low values in 2006, could be transferred to the low values recorded in 2016 in Bayelva: warm temperatures in early April caused an early onset of snow melt that changed the reflectance of the surface. Even though air temperatures in spring 2016 (MAM) were high in comparison to previous years (see Fig.25 in the appendix), snow cover offset was not until the 13th June. Other than that, reflected shortwave recordings between the two stations show similar behavior, concerning maximum values in May or June and a general high variability of summer month mean values between the years. Similar is the comparison of downward shortwave radiation: the high variability in summer months is explained by the changing cloud situation each year. This factor could be excluded by only using clear-sky condition data, but since there are only little hours without cloud-coverage on Svalbard, the data set would become too small for statistical representation. Thus both the Bayelva and

Ny-Ålesund analyses include all-sky conditions.

Both downward and upward longwave radiation recordings behave similar to the Ny-Ålesund recordings. The variability of longwave fluxes has been explained in section 5.1.1. High air temperatures in autumn (SON) and winter (DJF) month explain the slightly higher downward longwave values in 2016 (pink).

Still following Maturilli et al. [2015], net radiation budget analyses were conducted following to data procession done for the Ny-Ålesund dataset. Within the data- and measurement uncertainties, the Bayelva trend analyses results align with the AWIPEV results, showing a net radiation increase of $3.3 \pm 2.7 \text{ W/m}^2$ per decade from 1999 to 2016, the trend in Ny-Ålesund being $4.9 \pm 2.9 \text{ W/m}^2$ per decade from 1993 to 2012. On Samoylov Island in Siberia – an additional AWI research site – the annual net radiation budget is similarly to Bayelva with a mean net radiation of 18 W/m^2 for the years 1998 to 2011 [Boike et al. 2013].

The trend analysis of the mean annual net radiation in Bayelva needs to be interpreted with care, since the error is high ($\pm 2.7 \text{ W/m}^2$ per decade). Averaging annual means with such high inter-annual variations together with the missing years 2002, 2009 and 2012 are reasons for that high uncertainty. Therefore seasonal mean values were calculated and trend analyses show positive trends in spring, summer and autumn averages (see Fig. 29 in the appendix). The highest increase occurs in summer net radiation means with 14.69 W/m^2 per decade, the standard error being $\pm 0.62 \text{ W/m}^2$ per decade. Standard errors for all seasons are distinctly smaller than for annual means since inner-seasonal variations are smaller as well as the amount of missing years in each data stream. Data quality in Ny-Ålesund is in general better for the following reasons: all sensors are installed twice and a year-long daily maintenance by the AWIPEV personnel ensures consecutive data-recording. Furthermore, rime formation is removed through a ventilation system. The overall site set-up after BSRN standards ensures comparability in a broad data network.

6.1.2 Soil

Permafrost temperatures as well as ALT are indicators for the thermal state of permafrost [AMAP 2017]. The analyses regarding these two variables in Bayelva both show positive trends. Permafrost temperatures were rising from 2009 to 2016 and the active layer has been thickening from 1998 to 2016 (see chapter 5.3.2). During the Fourth International Polar Year IPY from 2007 to 2009, a broad network of permafrost boreholes was established in the Arctic [IPY 2018; Christiansen et al. 2010; AMAP 2017]. Mean permafrost temperatures in Scandinavian lowland, peat plateaus and mountains are close to $0 \text{ }^\circ\text{C}$, while in high mountain areas, Greenland and Svalbard permafrost mean temperatures are a few degrees below $0 \text{ }^\circ\text{C}$. Those relatively warm areas are most sensitive to climatic changes [Christiansen et al. 2010].

Figure 30 from the 2017 SWIPA report shows mean ground temperatures at depths between 9 to 26 m below surface for cold continuous and discontinuous permafrost research sites in the Arctic. To detect warming trends, permafrost temperatures with little annual fluctuation give the best estimate. In Bayelva, temperatures at the deepest depth of 9 m temperatures are 0.24 °C warmer today, compared to 2009. This trend agrees with the observations in Nordic regions as well as Siberia, where current temperatures are compared to temperatures during the IPY [AMAP 2017].

Since permafrost temperatures in Bayelva are close to 0 °C already, warming has immediate results of a thickening of the active layer. The trend estimated with the Stefan-Model in Bayelva shows a thickening of 0.5 m per decade. While there were variations in ALT observations in the Arctic, the past five years show thickening trends for most regions, only Russian observation sites show little to no AL thickening [AMAP 2017].

Studies conducted on the North-West coastal line of Spitsbergen show an AL thickening of 0.13 to 0.25 m per decade from 1996 to 2012 [Sobota and Nowak 2014]. Åkerman and Johansson [2008] published results of ALT studies in the Sub-Arctic Sweden. The authors present mean summer air temperatures, mean air temperatures from October to May, TDD in May summer precipitation and snow depths from October to May as relevant climate parameter for AL thickening. Even though mean annual air temperatures in Bayelva are lower (approx. -5 °C) than in the Sub-Arctic Sweden (approx. -0.6 °C), ALT change rates are higher in Bayelva, than in Sweden (change rate = 0.07 to 0.13 m per decade). Our dataset only represents 18 of the 29 years in Sweden and particular high ALT values in Bayelva over the last 10 years explain this difference. The 2017 SWIPA report connects thickening of the AL to variations in summer air temperatures. The correlation analysis of this study yields a moderate positive correlation of ALT and summer air temperature means ($p = 0.6$). The correlation coefficient for ALT and TDD is $p = 0.7$, which means a moderate to strong relationship. This aligns with findings of Schuh et al. [2017], who used the Advanced Terrestrial Simulator (ATS) model to determine the role of soil moisture content on the inter-annual active layer temperature. In-situ measurements of active layer temperature and soil moisture permafrost temperature and thaw depth progressions in Adventdalen on Svalbard are connected to the model, which is then run under different soil moisture retention characteristics. Model runs suggest that the soil water content has little effect on long-term thaw depth developments. Thaw depth was measured through steel probing eight to fifteen times between May and September and the results show a stronger correlation between ALT and winter soil temperatures than variable summer conditions.

A land surface model (CHANGE), run on pan-Arctic areas by Park et al. [2015] estimates an ALT increase of 0.23 m per decade for the timespan from 1901 to 2009. The model examined changes in ALT connected to changes in snow depth and air temperature. The authors state that changes in ALT due to changes in snow depth appear mostly in southern boundary permafrost regions, while in more northern regions (60° N - 80° N) snow depth changes lead

to a permafrost temperature rise. For Bayelva (78° N) the correlation analysis is different: pearson-values for snow depth to winter permafrost temperatures range between 0 and -0.7, while ALT and snow depth correlate with $p = 0.3$. The big variation of negative p-values for permafrost temperatures allows no distinct statement, same as the weak positive correlation of ALT to snow depths. ALT to $S_{\text{depth,eff}}$ also shows a weak positive correlation ($p = 0.3$). The variability of the snow cover between the years in Bayelva together with a small amount of observed years could explain the difference of our results to the publication by Park et al. [2015].

Ling and Zhang [2003] used a one-dimensional heat transfer-model with phase change including the surface energy balance equation to link changes in snow cover characteristics to active layer and permafrost temperatures. Using meteorological data from Barrow, Alaska as basis, results show that the ground thermal regime reacts sensitively on changes in snow cover timing. As presented in chapters 5.2.1 and 5.3, an earlier date of the end of the snow cover as well as warming soil temperatures can be observed in Bayelva. Simple linear correlation analysis in chapter 5.4 shows only a small positive correlation.

Regarding the date of final freeze-up, Bayelva air temperatures show warming in both summer and winter periods, with more warming of winter temperatures. Thus the date of complete freeze-up of the active layer is thus shifted back by almost two months [Hinzman et al. 2005; AMAP 2017]. In Bayelva the day of final freeze-up was between late November and December for the years from 1998 to 2004 (except 2001) and has been shifted to dates after January of the next year. The latest day of final-freeze up occurred in May 2013. The results from Bayelva align with the general trend reported by the 2017 SWIPA report, regarding the last decade. Only 18 of the 30 years are represented our dataset though. The overall duration of the re-freezing of the active layer also shows an increase since 2005, aligning with the SWIPA statement, that warming has been especially strong during the last decade.

In conclusion, trend analyses on soil properties in Bayelva align well with general processes observed in the Arctic. Temperature warming trends as well as AL thickening and re-freeze properties are above average which can be explained by the unique climatic situation in Svalbard, being influenced by the warm West Spitsbergen Ocean Current. Correlation analysis of this study can not always support findings of other Arctic regions, which is mostly due to the small sample size as well high variability of all variables.

Regarding permafrost temperatures, the study of Isaksen et al. [2007] is used here to discuss the results of my work. The authors present data from three deep boreholes (> 100 m) in Svalbard and Scandinavia: Janssonhaugen (270 m asl) on Svalbard has been introduced in the discussion of air temperatures, Tarfalaryggen (1550 m asl) is a north-south oriented mountain ridge in northern Scandinavia and Juvvasshøe (1894 m asl) a mountain plateau in the southern part of Scandinavia. The three study sites differ in mean annual air temperatures (Janssonhaugen being the coldest with -8 °C), annual average precipitation values (highest values on Juvvasshøe: 800 to 1000 mm per year), type of ground surface, and altitude (see

above). In Janssonhaugen the bedrock consists of a fine-grained porous sandstone with a high silt content. The bedrock is traversed by thin shale interbeds. On Tarfalaryggen blocks of regolith with a lot of chasms make up the upper 4 m of the ground. On Juvvasshøe medium gray quartz mozonorite form the bedrock. These soil properties are very different in their ability to store water, thus showing different freezing and thawing characteristics. In Janssonhaugen for example no zero-curtain effect was observed except in 2000, after heavy rainfall in September and October. Snow depths are very low at all three sites, mostly due to wind blow. A thin layer occurs in some winters in Tarfalaryggen. Analysis of data from six years (2000 to 2005) shows warming permafrost temperatures at all sites with rates between 0.04 to 0.07°C/year. Greatest warming was observed in Svalbard. All sites show high correlations of air and ground surface temperatures at 0.2 m depth. The absent or very thin snow layer in Janssonhaugen distinguishes this study site from Bayelva. The missing insulating cover results in highly variable winter temperatures to a depth of 1.6 m. Annual temperature amplitude starts to diminish at a depth of 10 m (compared to 5.5 m in Bayelva) but is only completely gone at a depth of 20 m. Comparison of the three boreholes gives insight that exposed bedrock shows the most direct impact of climate change signals [Isaksen et al. 2007; Smith and Riseborough 1996].

6.1.3 Snow Cover Characteristics

Snow Depth and Duration

Averaging the beginning and end date of snow cover in Bayelva gives a mean duration of eight months, from October to May. As mentioned before, mean snow cover duration on the Northern Hemisphere is six months, usually from October to March. While relations of snow cover changes to air temperature warming and increased precipitation are still highly variable in the Arctic, more and more evidence arises, that an earlier end date of snow cover appears with global warming [AMAP 2017]. Lawrence and Slater [2010] suggest a shortening of the snow season of -14 ± 7 days for terrestrial northern high-latitude regions due to earlier melt-off in spring. Snow cover onset in autumn is assumed to be delayed by $+20 \pm 9$ days. Those results are based on a Community Climate System Model simulation of the twentieth and twenty-first century. The 2017 SWIPA report states a shortening of -2 days per year in the Arctic, based on observations. The results of this study are lower (-0.17 and -0.46 days per year), but also suggest earlier melt-off. Shortening of the snow covered period in spring allows for more soil warming due to more absorption of incoming shortwave radiation. Park et al. [2015] predict a shortening of the snow season, based on six models run with the IPCC A2 scenario, for the period 2049 to 2060. A shorter snow-season is intuitively connected to a warming of global air temperatures, which leads to midwinter snow melt as well as compaction of the snow pack [Park et al. 2015]. Correlation analysis of annual mean air temperatures and the end of snow cover day of year however show a weak negative relation

($p = -0.3$), supporting the high uncertainty of linking end of snow cover observations and air temperatures. Regional and seasonal differences together with highly complex inner-snow processes, which are difficult (so far even impossible) to measure, are not yet understood well enough at this point to find statistically significant connections. Projections of snow cover duration under IPCC emission scenarios RCP4.5 and RCP 8.5 suggest a shortening of 10% and -20% respectively compared to the years 1986 to 2005 for all Arctic non-glacier areas [AMAP 2017].

Lawrence and Slater [2010] find positive correlations (based on simulations) of snow mean depth and the length of snow season, which is not examined in this study, since beginning of snow cover dates could only be detected with high uncertainties. Nonetheless with a maximum observed snow depth of 2.2 m, Bayelva exceeds most other High-Arctic regions, and even other study sites on Svalbard. In Adventdalen, close to Longyearbyen the capital of Svalbard, maximal snow depth in 2010 has been 0.69 m, while average snow depths in that area are between 0.2 and 0.3 m [Watanabe et al. 2017]. On Samoylov Island in Siberia, maximal snow depth of 0.44 m was observed in 2007 and in the Trail Valley Creek in the Northwest Territories in Canada, maximum depths between 2013 and 2016 were between 0.5 and 0.77 m [Boike et al. 2013; Anders 2017]. Even if maximum depths in Bayelva vary from year to year, a mean snow depth of 0.6 m is above average, due to the semi-arid circumstances unusual for such high latitudes, needing more energy to melt off in spring. The importance of knowledge on melt processes to understand snow thermal characteristics will be discussed in the following.

Snow melt

Woo [2012] state, that snow melt in temperate latitudes, the southern limits of permafrost regions, starts in April but can be delayed up to two months in the Arctic Islands (e.g. McMaster River, Cornwallis Island, 78° N). The authors state, that even when air and most snow temperatures rose above 0 °C, stream flow only started several days later. This time lag is characteristic for permafrost regions with a cold environment, but melt energy supplied on the snow surface through high incoming shortwave radiation. In 2013 an automated camera was installed at the climate station in Bayelva in order to detect pattern and timing of the snow melt better [Boike et al. 2017].

Onset and duration of snow melt in Bayelva were only determined through negative snow depth change rates. Additionally, air temperatures above 0 °C indicate snow melt from the surface. Through the volumetric water content in the soil, melt water can be detected to a certain degree, but without knowledge on the snow water equivalent (SWE), exact snow melt rates are impossible to determine.

A sensitivity analysis with the GEOtop model, a soil model that uses thermal and hydraulic characteristics, was applied on the Bayelva dataset by Stern [2017]. The results show two counteracting processes concerning the maximum snow depth: the final ablation date gets shifted to later dates with a higher maximum snow cover, shortening the snow-free period

with high shortwave radiation values. On the other hand the snow cover insulates the soil from extreme cold temperatures, leading to mild temperatures during the cold season.

The complexity of snow melt processes is mentioned at this point, since there are only little information about them in Bayelva, but they play an important role for soil temperatures and represent high uncertainties in snow cover modeling, which will be subject of the last sub-chapter of the discussion.

Even though there have been great advances in understanding snow-processes in the Arctic, the SWIPA assessment of 2017 [AMAP 2017] still identifies knowledge gaps, that lead to high uncertainties, when advising decision makers on snow-related topics.

6.2 Difficulties in snow cover modeling

Both the 2017 SWIPA and 2013 IPCC report model future developments of soil temperatures, snow cover and permafrost states. Future snow trends were modeled as a function of air temperature, snowfall rates, circulation and radiation components [Lawrence and Slater 2010], but when implementing relationships of air and soil temperatures under a seasonal snow cover, there is still a high degree of inaccuracy. In this study, one approach of describing this relationship was applied on the Bayelva soil and air temperature measurements [Slater et al. 2017]. The results were presented in chapter 5.2.2. This chapter discusses the results as well as deficiency of the approach itself.

The surface offset between annual air and ground surface temperatures in Bayelva is $\Delta T = 3.19^\circ\text{C}$, with $T_{surf}^{ann} = -1.34^\circ\text{C}$ and $T_{air}^{ann} = -4.53^\circ\text{C}$. Annual surface and air temperatures in Ivotuk, Alaska are -1.4°C and -10.3°C respectively ([Romanovsky 2007] in [Lawrence and Slater 2010]). In Franklin Bluffs, Alaska, Zhang [2005] observed daily mean temperature differences of up to 20°C . To understand the role of the snow cover on those temperature differences, a correlation of $S_{depth,eff}$ and A_{norm} was done in this study.

Slater et al. [2017] use the exponential relationship of $S_{depth,eff}$ and A_{norm} to quantify land model skills (see Eq. (14)). A snow and heat transfer metric SHTM is developed, to describe how different model insulation curves depart from the observed curve. SHTM calculates as follows:

$$SHTM = 1. - \sqrt{[2 \cdot (ModelA_{norm,i} - ObservedA_{norm,i})]^2} \quad (16)$$

The land models vary widely which is attributed to structural weaknesses of the models. Another deficiency lies in the exponential fit of the $S_{depth,eff}$ and A_{norm} relationship shown in Figure 18b). Figure 18a) shows the results of the analysis with Bayelva data, 18b) the corresponding figure of the underlying study by Slater et al. [2017]. Bayelva results are presented for all $S_{depth,eff}$ values between 0 and 1 m, while the original only uses $S_{depth,eff}$ values below 0.5 m, stating that the thermo-insulation effect of snow diminishes after a

$S_{\text{depth,eff}} = 0.5$ m. The vertical gray line in 18 marks the 0.5 m margin. It is visible, that half of the results are above $S_{\text{depth,eff}} = 0.5$ m, still showing high variability.

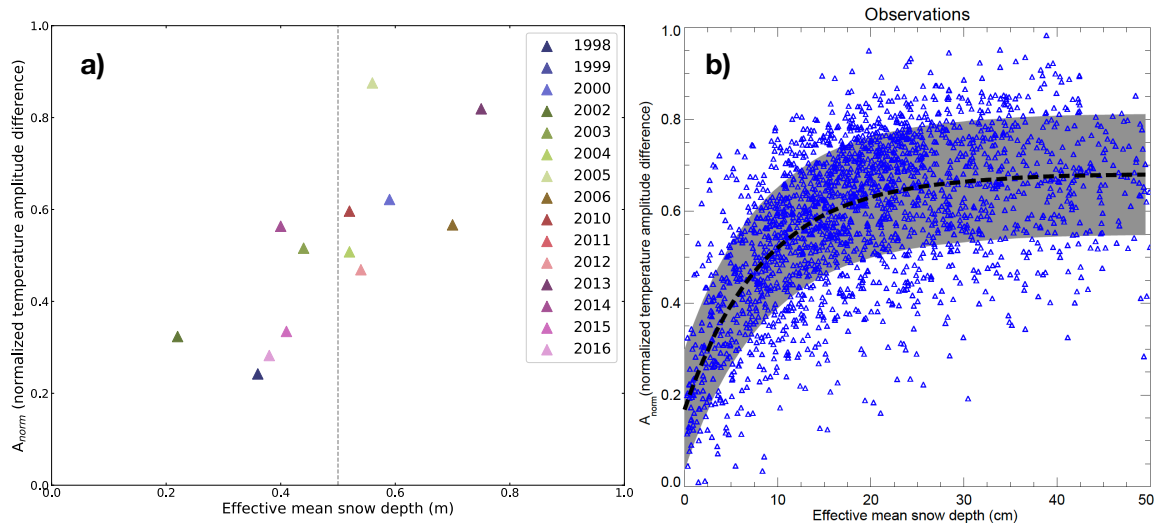


Figure 18: a) Results of $S_{\text{depth,eff}}$ and A_{norm} observed relationship in Bayelva. Vertical gray line indicates 0.5 m $S_{\text{depth,eff}}$. b) Relation of $S_{\text{depth,eff}}$ and A_{norm} from Slater et al. [2017] along with the resulting exponential fit (dashed black line). The gray shading shows the median fit plus/minus the mean scatter of all fits.

$S_{\text{depth,eff}}$ and A_{norm} correlation in 18b) shows high variability as well, which is explained by the authors through three main reasons:

- (1) Climate conditions as well as snow regimes (timing and metamorphism) vary greatly on the Northern Hemisphere
- (2) Moisture content of the soil
- (3) Uncertainties of the measurements themselves

Those error sources will be discussed in the following.

Changes in snow cover timing, duration and depth in Bayelva show high variability, similar to the results of other studies in the Arctic (see chapter 6.1.3). Therefore uncertainties exist both in year-to-year comparisons of one site and between different sites. The second reason, regarding the moisture content of the soil at 0.2 m depth is crucial as well. The soil at 0.2 m depth undergoes a phase change from liquid to solid during freeze-back, which was shown to continue far into the cooling period (January/February). Using soil temperatures at 0.2 m depth to represent the soil surface is thus highly critical. It represents a major source for the high scattering in the correlation plot (Fig. 18b).

The third reason listed by the authors, measurement uncertainties, are always part of analyses with different data sources and measuring techniques. In this kind of setting they are hard to diminish, since no uniform measurement technique exists.

All of those error sources lead to a scattering of the correlation analysis. The exponential fit

of equation (14) needs to be observed with care. As seen in Figure 18b), observed correlation scatter widely, thus are bound to subjectivity. Reproduction of the results is difficult. Implementing the exponential relationship on a model is thus assessed highly critical at this point. Westermann [2010] states the SWE as an additional important factor regarding the insulation properties of the snow cover. However exact estimated are hard to retrieve. The average snow density can be calculated through snow depth and SWE giving the volumetric heat capacity. Measuring the SWE can be done by manually analyzing snow samples on their stratigraphy, which is related to a high work load and time consumption. Especially during the melting phase, changes in SWE would need to be monitored on a daily basis at least, to record ice lens formation after a temperature drop. This process is typical for the snow cover in Bayelva [Westermann 2010], complicating the estimate of SWE even more. Westermann [2010] estimated the SWE for Bayelva by using the theory of conductive heat flow. That approach gives a solid representation of a thicker snow pack, but lacks with smaller snow depths. He suggest heated-needle probing of the snow pack, after Sturm [2002], which again is related to field work under hard conditions.

The difficulty of achieving good results for SWE values was explained now. However, that variable is one of many complications, when investigating snow thermal processes.

The complexity of the relationship between air and soil temperatures with a seasonal snow cover can be seen in Figure 19 as well. Here, daily amplitudes of air and soil temperatures on one day are plotted against the respective snow depth. All years from 1998 to 2017 are included.

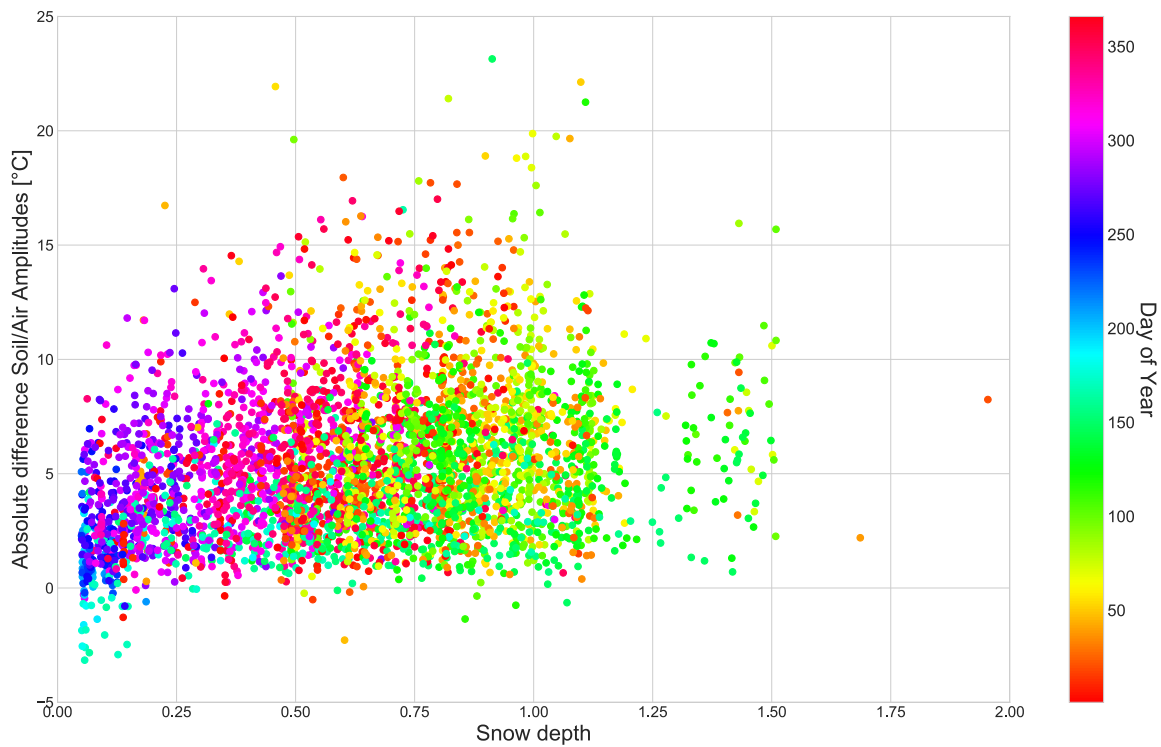


Figure 19: On the y-axis the absolute difference of daily air and soil (at 0.01 m depth) temperature amplitudes are shown against the respective snow depth of that day on the x-axis. Turquoise and blue data points are summer days with little or no snow cover, bright green data points show spring days with the highest snow covers.

Color-coding the respective day of year, allows to follow snow cover built up over the course of a snow season. Snow cover onset occurs after day 200 (blue colors) and reaches maximum values in spring (days 75 to 150, bright green). Interestingly the absolute difference of daily soil and air temperature amplitudes is not increasing with an increasing snow depth. Maximum amplitude differences can be seen at a snow depth around 1 m. Color-codes for the highest amplitude difference values indicate late winter, early spring dates. This observation aligns with the assumption, that while air temperatures in spring have high daily amplitudes, following a day/night rhythm, soil temperatures are still 'shielded' from these short-term changes by the snow cover. In autumn (blue/purple colors) air temperatures show a similar day/night behavior, but the soil is then not protected by a thick enough snow cover, so it follows air temperature processions.

Another interesting part of Figure 19 are data points above a snow depth of 1.25 m that range are connected to a wide range of amplitude difference values (between 0 and 15 °C). The dominating color is green, showing spring days. Here the onset of snow melt could play an important role again.

The aim of introducing Figure 19 at the end of the discussion chapter was to illustrate the high complexity a seasonal snow brings to the thermal relationship of atmosphere and lithosphere. All the parameters analyzed in this work are represented in this figure: air and soil temperature via their daily amplitudes, radiation components and their procession over a year are hidden in the day of year color-coding, together with snow depth and timing characteristics. The wide scattering of the data points represents the variability of single parameters in Bayelva as well as hidden relationships, that are not yet known.

The following final chapter of this work summarizes the previous chapters and gives an outlook on further research in Bayelva.

7 Summary and concluding remarks

The research site Bayelva is characterized by unique climatic conditions, resulting from the warm West Spitsbergen Ocean Current. Aiming to give insight on the development of meteorological, subsurface and snow parameters from 1998 to 2016, this study constitutes a status report of this exceptional study site. Additionally, recent approaches to gain insight in the thermo-insulation effect of a seasonal snow cover were tested on the Bayelva snow cover.

This study showed that air temperatures and soil temperatures at all depths measured (0.01 to 9 m depth) were warming from 1998 to 2016. Soil warming lead to a thickening of the active layer. The resulting trends align with observations in other Arctic regions, and are even slightly higher than the Arctic averages.

The correlation of different climate, soil and snow cover parameters are only statistically significant to a certain degree. The most important results of the correlation analysis were on one hand the validation of the effective snow depth as influencer of freeze-back dates of the active layer, and on the other hand the connection of the ALT to summer AL temperatures and winter permafrost temperatures.

Even though the snow cover in Bayelva could be characterized in this study, its role as thermal insulator is still fraught with high uncertainties and should thus be handled with care when implementing on land surface models. Obtaining better estimates for the SWE is crucial in this context. Using remote sensing in this field of research has been improving the quality of SWE estimates in recent years. One of the most important advantages of using remote sensing in snow related issues, is the coverage of whole areas, compared to point representations of manual in-situ measurements. Bigger areas can be recorded, giving a bigger sample size for correlation analyses. Additionally the spacial variability of snow would be accounted for. Bayelva can be used as a look into the future for colder permafrost regions that are currently warming. It can be observed, that the single parameters show an even higher inner-annual variability, thus making year-to-year comparisons more difficult.

Further analysis with the existing data set from Bayelva would be to analyze the snow temperature measurements. Temperature sensors were installed at different heights over the 18-year period and could give insight to snow melt processes. In general, a more complex statistical analysis of the parameters used for this work could give more specific answers to the research questions asked at the beginning of this work. As shown in Figure 19, there are many more interesting connections hidden in the data set than the time frame of a master thesis allows to look at.

Acknowledgment

This thesis would not have been possible without the help of many great persons.

I have had the great luck of having three supervisors, who supported my work each in their individual way:

Prof. Dr. Bernhard Höfle, Dr. Julia Boike and Prof. Kurt Roth, thank you all very much for the always encouraging words, the right questions at the right time, and the great insight you gave me on scientific research. A special thank to the working group of Kurt Roth, for welcoming me so kindly!

Since there have been so many more persons involved in the process of this work and I'm too afraid of missing anyone right now I'll just promise to bring cake to each and everyone in the near future.

Bibliography

- Aalstad, Kristoffer, Sebastian Westermann, Thomas Vikhamar Schuler, Julia Boike, and Laurent Bertino (July 2017). “Ensemble-based assimilation of fractional snow covered area satellite retrievals to estimate snow distribution at a high Arctic site”. en. In: *The Cryosphere Discussions*, pp. 1–37. ISSN: 1994-0440. DOI: 10.5194/tc-2017-109.
- Åkerman, H. Jonas and Margareta Johansson (July 2008). “Thawing permafrost and thicker active layers in sub-arctic Sweden”. en. In: *Permafrost and Periglacial Processes* 19.3, pp. 279–292. ISSN: 10456740, 10991530. DOI: 10.1002/ppp.626.
- AMAP (2017). *Snow, Water, Ice and Permafrost in the Arctic (SWIPA) 2017*. Arctic Monitoring and Assessment Programme (AMAP).
- Anders, Katharina (2017). “Multitemporal 3D Point Clouds for Thaw Subsidence Monitoring. Methods for Quantifying Ground Surface Displacement in Tundra Landscapes using Terrestrial Laser Scanning in Trail Valley Creek, Canada”. Master Thesis. Heidelberg University.
- AWI (2017). *Direkter Draht in den Permafrost - AWI*. <https://www.awi.de/im-fokus/permafrost/direkter-draht-in-den-permafrost.html>.
- Barry, Roger G. and Thian Yew Gan (2011). *The global cryosphere: past, present, and future*. eng. 1. publ. Cambridge [u.a.]: Cambridge Univ. Press. ISBN: 978-0-521-76981-5 978-0-521-15685-1.
- Benestad, Rasmus E. (2003). “What can present climate models tell us about climate change?” In: *Climatic Change* 59.3, pp. 311–331.
- Boike, Julia (2003). “Seasonal snow cover on frozen ground: Energy balance calculations of a permafrost site near Ny-Ålesund, Spitsbergen”. en. In: *Journal of Geophysical Research* 108.D2. ISSN: 0148-0227. DOI: 10.1029/2001JD000939.
- Boike, Julia, Inge Juszak, Stephan Lange, Sarah Chadburn, Eleanor Burke, Pier Paul Overduin, Kurt Roth, Olaf Ippisch, Niko Bornemann, and Lielle Stern (2017). “A 20-year record (1998–2017) of permafrost, active layer, and meteorological conditions at a High Arctic permafrost research site (Bayelva, Spitsbergen): an opportunity to validate remote sensing data and land surface, snow, and permafrost models, Earth Syst. Sci. Data Discuss”. In: *Earth System Science Data Discussions* 1, p. 86.
- Boike, J. et al. (Mar. 2013). “Baseline characteristics of climate, permafrost and land cover from a new permafrost observatory in the Lena River Delta, Siberia (1998–2011)”. en. In: *Biogeosciences* 10.3, pp. 2105–2128. ISSN: 1726-4189. DOI: 10.5194/bg-10-2105-2013.
- Christiansen, H. H. et al. (Apr. 2010). “The thermal state of permafrost in the nordic area during the international polar year 2007-2009: Thermal state of permafrost in the Nordic area”. en. In: *Permafrost and Periglacial Processes* 21.2, pp. 156–181. ISSN: 10456740. DOI: 10.1002/ppp.687.

- Cook, Benjamin I., Gordon B. Bonan, Samuel Levis, and Howard E. Epstein (July 2008). “The thermoinsulation effect of snow cover within a climate model”. en. In: *Climate Dynamics* 31.1, pp. 107–124. ISSN: 0930-7575, 1432-0894. DOI: 10.1007/s00382-007-0341-y.
- Derksen, C. and E. LeDrew (2000). “Variability and change in terrestrial snow cover: data acquisition and links to the atmosphere”. In: *Progress in Physical Geography* 24.4, pp. 469–498.
- Førland, Eirik J., Rasmus Benestad, Inger Hanssen-Bauer, Jan Erik Haugen, and Torill Engen Skaugen (2011). “Temperature and Precipitation Development at Svalbard 1900–2100”. en. In: *Advances in Meteorology* 2011, pp. 1–14. ISSN: 1687-9309, 1687-9317. DOI: 10.1155/2011/893790.
- Gjelten, Herdis M., Øyvind Nordli, Ketil Isaksen, Eirik J. Førland, Pavel N. Sviashchennikov, Przemyslaw Wyszynski, Uliana V. Prokhorova, Rajmund Przybylak, Boris V. Ivanov, and Alexandra V. Urazgildeeva (Jan. 2016). “Air temperature variations and gradients along the coast and fjords of western Spitsbergen”. en. In: *Polar Research* 35.1, p. 29878. ISSN: 1751-8369. DOI: 10.3402/polar.v35.29878.
- Harris, S. A. and National Research Council of Canada Permafrost Subcommittee Associate Committee on Geotechnical Research, eds. (1988). *Glossary of permafrost and related ground-ice terms*. Technical Memorandum / National Research Council, Canada 142. OCLC: 20504505. Ottawa, Ontario, Canada. ISBN: 978-0-660-12540-4.
- Hinzman, Larry D. et al. (Oct. 2005). “Evidence and Implications of Recent Climate Change in Northern Alaska and Other Arctic Regions”. en. In: *Climatic Change* 72.3, pp. 251–298. ISSN: 0165-0009, 1573-1480. DOI: 10.1007/s10584-005-5352-2.
- Hodson, Andy, Martyn Tranter, Angela Gurnell, Mike Clark, and Jon Ove Hagen (2002). “The hydrochemistry of Bayelva, a high Arctic proglacial stream in Svalbard”. In: *Journal of Hydrology* 257, pp. 91–114.
- IPCC (2013a). “IPCC, 2013: Annex III: Glossary”. In: *Climate Change 2013: the Physical Science Basis. Contribution of Working Group I to the Fifth Assessment Report of the Intergovernmental Panel on Climate Change*. Ed. by Serge Planton. Cambridge, United Kingdom and New York, NY, USA: Cambridge University Press.
- IPCC (2013b). *IPCC, 2013: Climate Change 2013: The Physical Science Basis. Contribution of Working Group I to the Fifth Assessment Report of the Intergovernmental Panel on Climate Change*. Ed. by Thomas F. Stocker, Dahe Qin, Gian-Kasper Plattner, Melinda Tignor, Simon K. Allen, Judith Boschung, Alexander Nauels, Yu Xia, B. Bex, and B. M. Midgley. Cambridge University Press.
- IPCC (2013c). “Summary for Policymakers”. In: *Climate Change 2013: The Physical Science Basis. Contribution of Working Group I to the Fifth Assessment Report of the Intergovernmental Panel on Climate Change*. Ed. by T. F. Stocker, D. Qin, G. K. Plattner, M. Tignor, S. K. Allen, J. Boschung, A. Nauels, Y. Xia, V. Bex, and B. M. Midgley. Cambridge, United Kingdom and New York, NY, USA: Cambridge University Press.

- IPY (2018). *Arctic Zone: About International Polar Year (IPY)*. <https://www.pmel.noaa.gov/arctic-zone/ipy.html>.
- Isaksen, K., Ø. Nordli, E. J. Førland, E. Łupikasza, S. Eastwood, and T. Niedźwiedź (Oct. 2016). “Recent warming on Spitsbergen-Influence of atmospheric circulation and sea ice cover: RECENT WARMING ON SPITSBERGEN”. en. In: *Journal of Geophysical Research: Atmospheres* 121.20, pp. 11, 913–11, 931. ISSN: 2169897X. DOI: 10.1002/2016JD025606.
- Isaksen, Ketil, Johan Ludvig Sollid, Per Holmlund, and Charles Harris (Feb. 2007). “Recent warming of mountain permafrost in Svalbard and Scandinavia”. en. In: *Journal of Geophysical Research* 112.F2. ISSN: 0148-0227. DOI: 10.1029/2006JF000522.
- Klene, Anna E., Frederick E. Nelson, Nikolay I. Shiklomanov, and Kenneth M. Hinkel (May 2001). “The N-Factor in Natural Landscapes: Variability of Air and Soil-Surface Temperatures, Kuparuk River Basin, Alaska, U.S.A.” In: *Arctic, Antarctic, and Alpine Research* 33.2, p. 140. ISSN: 15230430. DOI: 10.2307/1552214.
- Larsen, J.N., Oleg Anisimov, A. Constable, A.B. Hollowed, N. Maynard, P. Prestrud, T.D. Prowse, and J.M.R Stone (2014). “Polar Regions”. In: *Climate Change 2014: Impacts, Adaptation, and Vulnerability. Part B: Regional Aspects. Contribution of Working Group II of the Fifth Assessment Report of the Intergovernmental Panel on Climate Change*. Ed. by V.R. Barros et al. Cambridge, United Kingdom and New York, NY, USA: Cambridge University Press, pp. 1567–1612.
- Lawrence, David M. and Andrew G. Slater (June 2010). “The contribution of snow condition trends to future ground climate”. en. In: *Climate Dynamics* 34.7-8, pp. 969–981. ISSN: 0930-7575, 1432-0894. DOI: 10.1007/s00382-009-0537-4.
- Ling, Feng and Tingjun Zhang (Apr. 2003). “Impact of the timing and duration of seasonal snow cover on the active layer and permafrost in the Alaskan Arctic”. en. In: *Permafrost and Periglacial Processes* 14.2, pp. 141–150. ISSN: 1045-6740, 1099-1530. DOI: 10.1002/ppp.445.
- Lloyd, C. R. (2001). “On the physical controls of the carbon dioxide balance at a high Arctic site in Svalbard”. In: *Theoretical and Applied Climatology* 70.1, pp. 167–182.
- Lüers, J., S. Westermann, K. Piel, and J. Boike (Nov. 2014). “Annual CO₂ budget and seasonal CO₂ exchange signals at a high Arctic permafrost site on Spitsbergen, Svalbard archipelago”. en. In: *Biogeosciences* 11.22, pp. 6307–6322. ISSN: 1726-4189. DOI: 10.5194/bg-11-6307-2014.
- Mastrandrea, Michael D., Christopher B. Field, Thomas F. Stocker, Ottmar Edenhofer, Kristie L. Ebi, David J. Frame, Hermann Held, Elmar Kriegler, Katharine J. Mach, and Patrick R. Matschoss (2010). “Guidance note for lead authors of the IPCC fifth assessment report on consistent treatment of uncertainties”. In:
- Maturilli, M., A. Herber, and G. König-Langlo (Apr. 2013). “Climatology and time series of surface meteorology in Ny-Ålesund, Svalbard”. en. In: *Earth System Science Data* 5.1, pp. 155–163. ISSN: 1866-3516. DOI: 10.5194/essd-5-155-2013.

- Maturilli, Marion, Andreas Herber, and Gert König-Langlo (Apr. 2015). “Surface radiation climatology for Ny-Ålesund, Svalbard (78.9° N), basic observations for trend detection”. en. In: *Theoretical and Applied Climatology* 120.1-2, pp. 331–339. ISSN: 0177-798X, 1434-4483. DOI: 10.1007/s00704-014-1173-4.
- meteoblue (2018). *Klima Baffin Island*. https://www.meteoblue.com/de/wetter/vorhersage/modelclimate/baffin-island_kanada_5889292.
- Outcalt, Samuel I., Frederick E. Nelson, and Kenneth M. Hinkel (1990). “The zero-curtain effect: Heat and mass transfer across an isothermal region in freezing soil”. In: *Water Resources Research* 26.7, pp. 1509–1516. DOI: 10.1029/WR026i007p01509.
- Park, Hotaek, Alexander N. Fedorov, Mikhail N. Zheleznyak, Pavel Y. Konstantinov, and John E. Walsh (May 2015). “Effect of snow cover on pan-Arctic permafrost thermal regimes”. en. In: *Climate Dynamics* 44.9-10, pp. 2873–2895. ISSN: 0930-7575, 1432-0894. DOI: 10.1007/s00382-014-2356-5.
- Phillips, Marcia, Sarah M. Springman, and Lukas U. Arenson, eds. (2003). *Permafrost: proceedings of the 8th International Conference on Permafrost, Zurich, Switzerland, 21-25 July 2003*. OCLC: ocm52357583. Lisse [Netherlands] ; Exton, PA: A.A. Balkema Publishers. ISBN: 978-90-5809-582-4 978-90-5809-584-8 978-90-5809-585-5.
- Romanovsky, V. (2007). *Daily Average Soil, Air and Ground Temperatures - Ivotuk Shrub Site. Version 1.0*. en. DOI: 10.5065/D6GQ6VX7.
- Roth, Kurt and Julia Boike (2001). “Quantifying the thermal dynamics of a permafrost site near Ny-Ålesund, Svalbard”. In: *Water Resources Research* 37.12, pp. 2901–2914. ISSN: 0043-1397. DOI: 10.1029/2000WR000163.
- Schuh, Carina, Andrew Frampton, and Hanne Hvidtfeldt Christiansen (Feb. 2017). “Soil moisture redistribution and its effect on inter-annual active layer temperature and thickness variations in a dry loess terrace in Adventdalen, Svalbard”. en. In: *The Cryosphere* 11.1, pp. 635–651. ISSN: 1994-0424. DOI: 10.5194/tc-11-635-2017.
- Slater, Andrew G., David M. Lawrence, and Charles D. Koven (Apr. 2017). “Process-level model evaluation: a snow and heat transfer metric”. en. In: *The Cryosphere* 11.2, pp. 989–996. ISSN: 1994-0424. DOI: 10.5194/tc-11-989-2017.
- Smith, M. W. and D. W. Riseborough (1996). “Permafrost Monitoring and Detection of Climate Change”. In: *Permafrost and Periglacial Processes* 7, pp. 301–309.
- Smith, M. W. and D. W. Riseborough (Mar. 2002). “Climate and the limits of permafrost: a zonal analysis”. en. In: *Permafrost and Periglacial Processes* 13.1, pp. 1–15. ISSN: 1045-6740, 1099-1530. DOI: 10.1002/ppp.410.
- Smith, Sharon L., Daniel W. Riseborough, Philip P. Bonnaventure, and Caroline Duchesne (May 2016). “An ecoregional assessment of freezing season air and ground surface temperature in the Mackenzie Valley corridor, NWT, Canada”. en. In: *Cold Regions Science and Technology* 125, pp. 152–161. ISSN: 0165232X. DOI: 10.1016/j.coldregions.2016.02.007.

- Sobota, Ireneusz and Marcin Nowak (June 2014). “Changes in the dynamics and thermal regime of the permafrost and active layer of the high arctic coastal area in north-west spitsbergen, svalbard”. en. In: *Geografiska Annaler: Series A, Physical Geography* 96.2, pp. 227–240. ISSN: 0435-3676, 1468-0459. DOI: 10.1111/geoa.12045.
- Sokratov, Sergey A. and Roger G. Barry (May 2002). “Intraseasonal variation in the thermoinsulation effect of snow cover on soil temperatures and energy balance: THERMOINSULATION OF SOIL BY SNOW COVER”. en. In: *Journal of Geophysical Research: Atmospheres* 107.D10, ACL 13–1–ACL 13–6. ISSN: 01480227. DOI: 10.1029/2001JD000489.
- Stern, Lielle (2017). “Hydraulic and Thermal properties of Permafrost in Svalbard, Analysis and Modelling using GEOtop”. MA thesis. University Heidelberg.
- Sturm, Matthew (2002). “Thermal conductivity and heat transfer through the snow on the ice of the Beaufort Sea”. en. In: *Journal of Geophysical Research* 107.C10. ISSN: 0148-0227. DOI: 10.1029/2000JC000409.
- Takala, Matias, Kari Luojus, Jouni Pulliainen, Chris Derksen, Juha Lemmetyinen, Juha-Petri Kärnä, Jarkko Koskinen, and Bojan Bojkov (Dec. 2011). “Estimating northern hemisphere snow water equivalent for climate research through assimilation of space-borne radiometer data and ground-based measurements”. en. In: *Remote Sensing of Environment* 115.12, pp. 3517–3529. ISSN: 00344257. DOI: 10.1016/j.rse.2011.08.014.
- Watanabe, Tatsuya, Norikazu Matsuoka, Hanne H. Christiansen, and Stefanie Cable (Apr. 2017). “Soil Physical and Environmental Conditions Controlling Patterned-Ground Variability at a Continuous Permafrost Site, Svalbard: Patterned Ground Variability at a Continuous Permafrost Site, Svalbard”. en. In: *Permafrost and Periglacial Processes* 28.2, pp. 433–445. ISSN: 10456740. DOI: 10.1002/ppp.1924.
- Weismüller, J., U. Wollschläger, J. Boike, X. Pan, Q. Yu, and K. Roth (Sept. 2011). “Modeling the thermal dynamics of the active layer at two contrasting permafrost sites on Svalbard and on the Tibetan Plateau”. en. In: *The Cryosphere* 5.3, pp. 741–757. ISSN: 1994-0424. DOI: 10.5194/tc-5-741-2011.
- Westermann, Sebastian (2010). “Sensitifty of Permafrost”. PhD thesis. University Heidelberg.
- Westermann, Sebastian, Johannes Lüers, Moritz Langer, Konstanze Piel, and Julia Boike (2009). “The annual surface energy budget of a high-arctic permafrost site on Svalbard, Norway”. In: *The Cryosphere* 3.2, p. 245.
- Winther, Jan-Gunnar, Sebastian Gerland, J.B. Ørbæk, Boris Ivanov, Alberto Blanco, and Julia Boike (1999). “Spectral reflectance of melting snow in a high Arctic watershed on Svalbard: some implications for optical satellite remote sensing studies”. In: *Hydrological Processes* 13, pp. 2033–2049.
- Woo, Ming-ko (2012). *Permafrost hydrology*. eng. Berlin ; Heidelberg [u.a.]: Springer. ISBN: 978-3-642-23461-3.
- ZAMG (2018). *Geschichte — ZAMG*. <https://www.zamg.ac.at/cms/de/klima/informationsportal-klimawandel/klimaforschung/klimamessung/geschichte>.

Zhang, Tingjun (2005). "Influence of the seasonal snow cover on the ground thermal regime: An overview". en. In: *Reviews of Geophysics* 43.4. ISSN: 8755-1209. DOI: 10.1029/2004RG000157.

Appendix

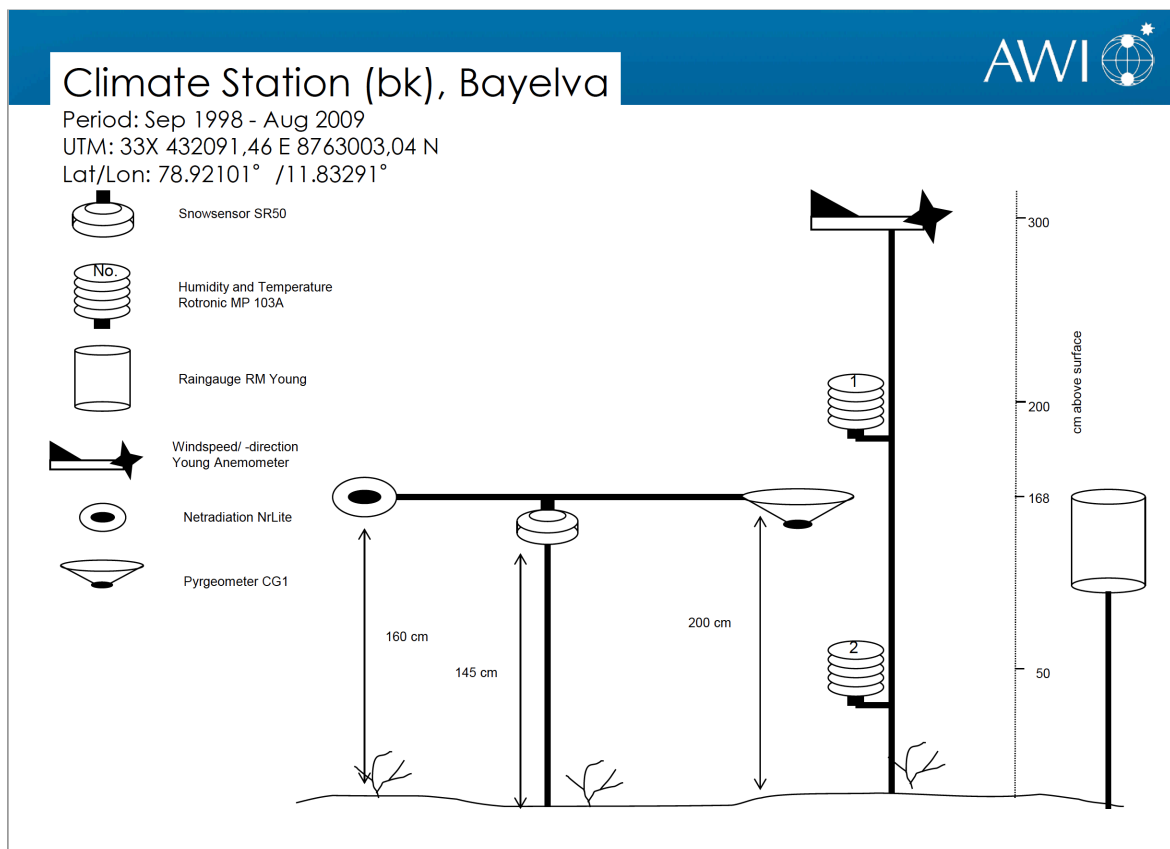


Figure 20: Schematic set-up of the Bayelva climate station running from 1998 to 2009.

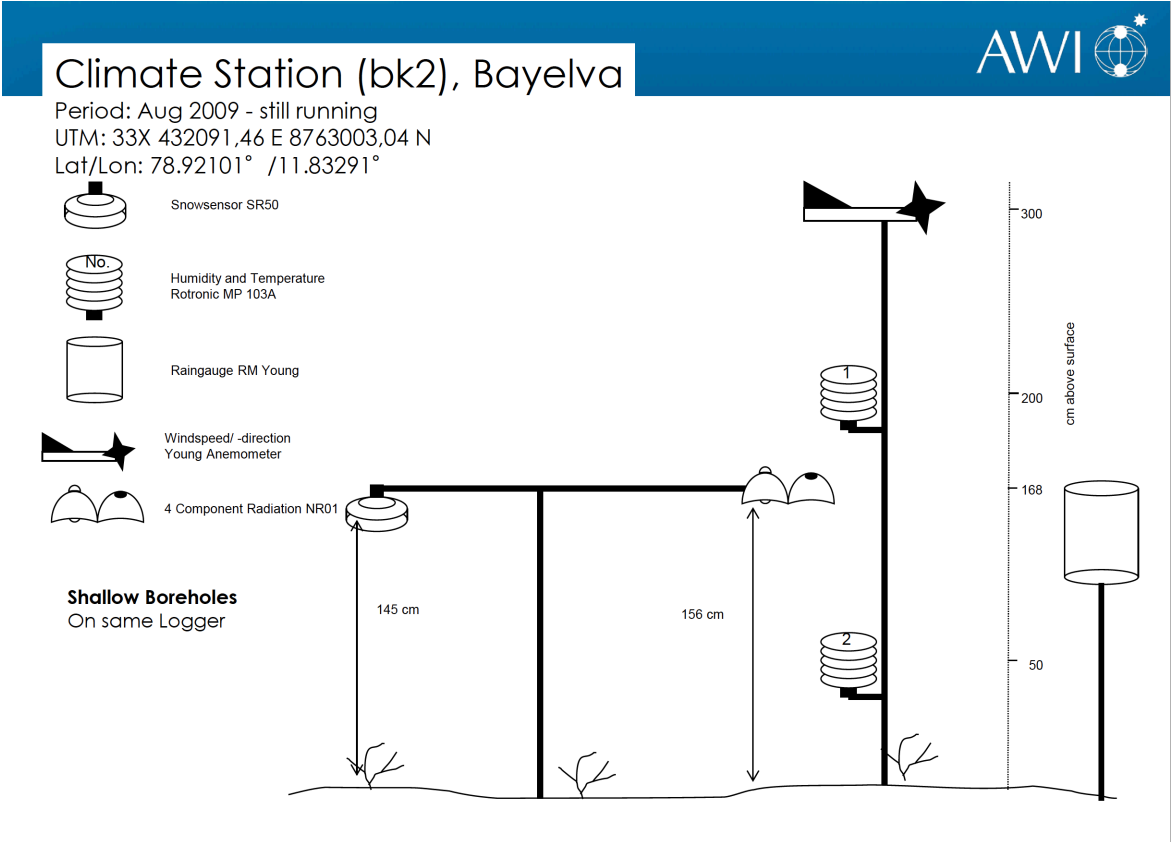


Figure 21: Schematic set-up of the Bayelva climate station running from 2009 to now.

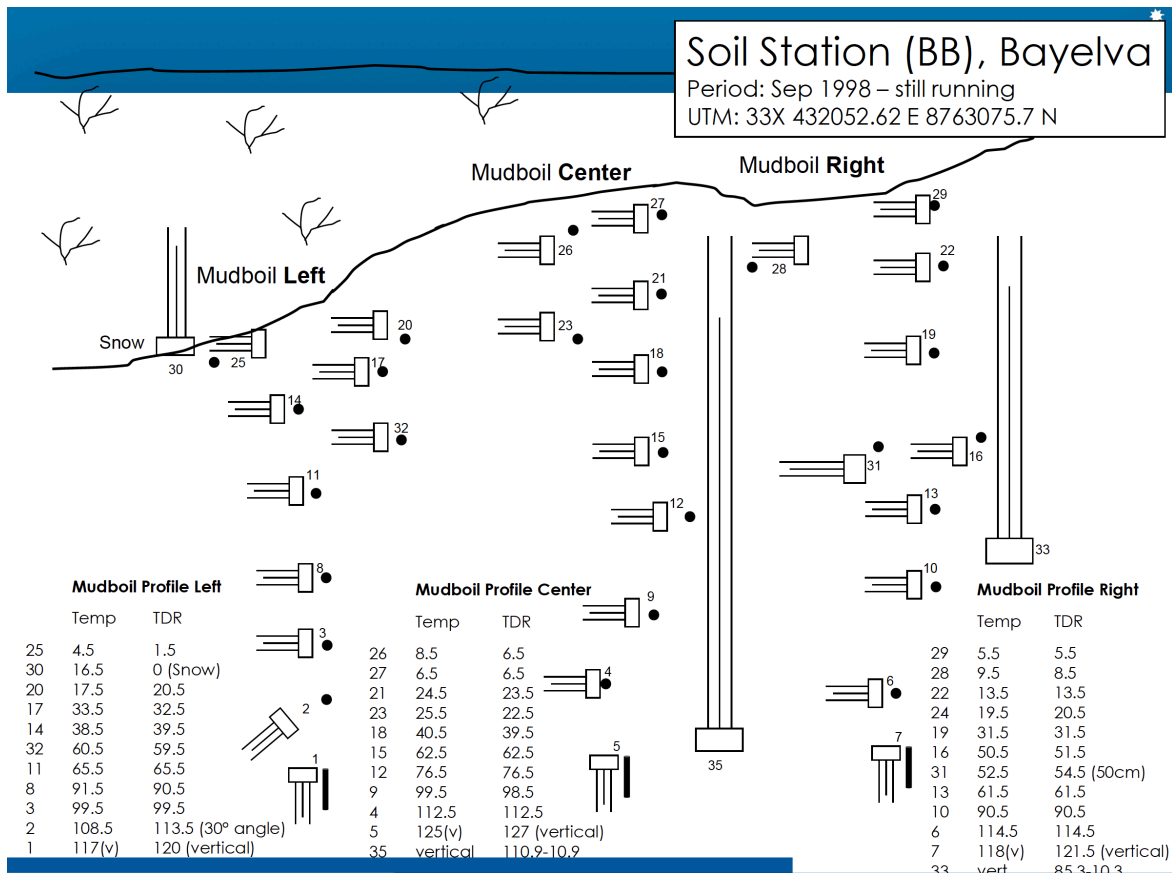


Figure 22: Schematic set-up of the Bayelva 2D soil profile running from 1998 to now. Cross-section of a mudboil.



Figure 23: a) Temperature and TDR sensor set-up at the soil profile installed in 2009. b) Schematic description of sensor location at the profile installed in 2009. Data collection is still ongoing.

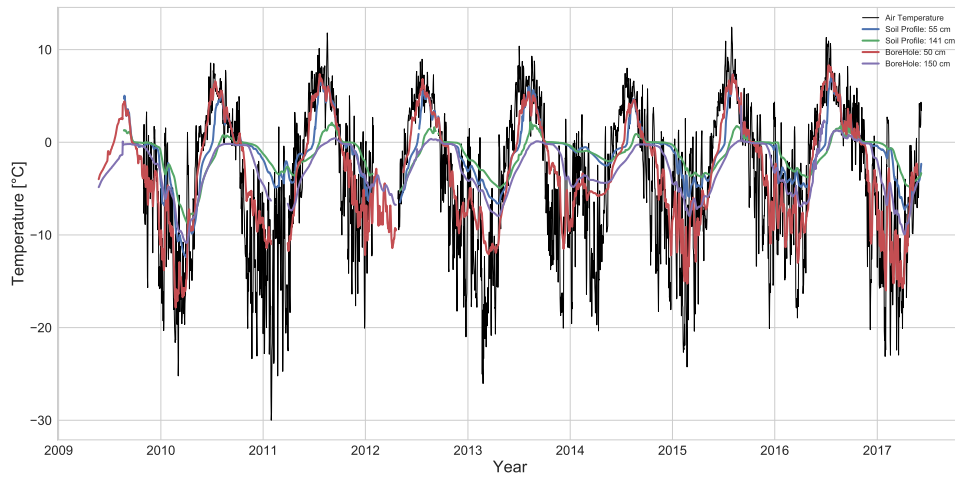


Figure 24: Temperature measurements from the temperature chain in the borehole in depths of 0.5 and 1.5 m are compared to temperatures from the soil profile at depths of 0.55 and 1.41 m for the period from 2009 to 2017. Air temperatures are shown, to explain high amplitudes in borehole temperatures at 0.5 m depth with high amplitudes in air temperatures.

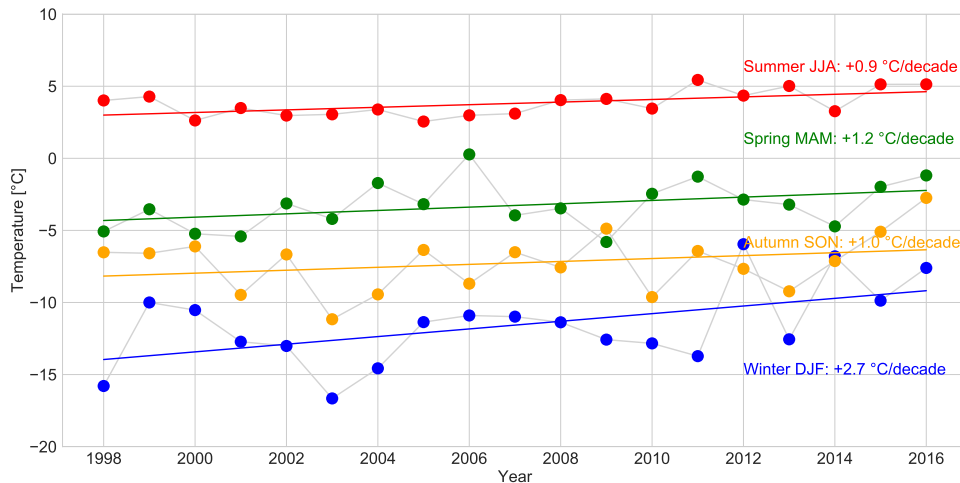


Figure 25: Seasonal mean air temperatures for the years 1998 to 2016 with linear regression lines. Standard error of summer regression (red) is $\pm 0.32^\circ\text{C}/\text{decade}$, for spring (green) $\pm 0.64^\circ\text{C}/\text{decade}$, for autumn (orange) $\pm 0.83^\circ\text{C}/\text{decade}$ and winter (blue) $\pm 1^\circ\text{C}/\text{decade}$.

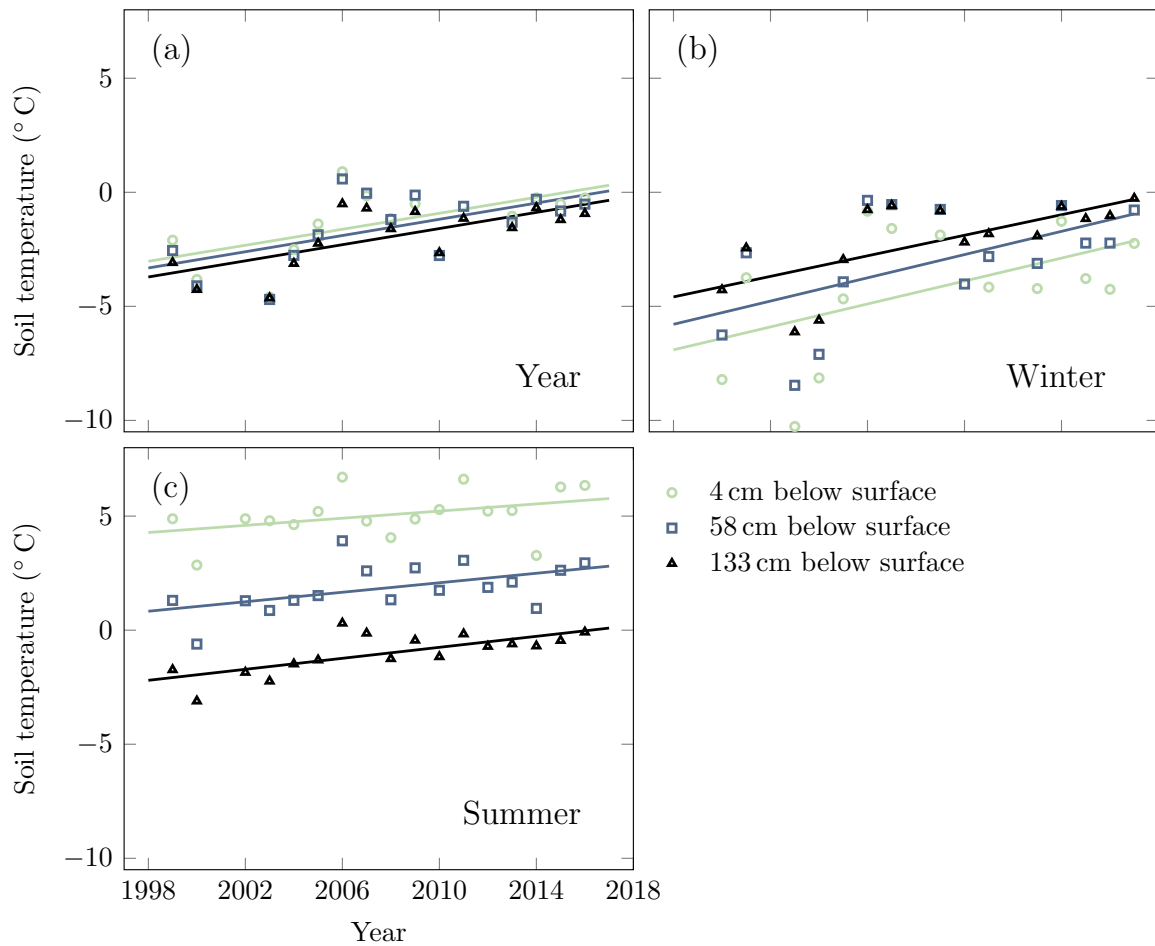


Figure 26: Bayelva soil temperature trends for three depths from 1998 - September 2017, using Level 2 soil temperatures. a) yearly trends at all three depths of 4, 58, 138 cms are $0.18\text{ }^{\circ}\text{C}/\text{year}$ (standard error of trends: $\pm 0.07, 0.06, 0.05\text{ }^{\circ}\text{C}/\text{year}$), b) winter trends (months December, January, February) are $0.25, 0.25, 0.23\text{ }^{\circ}\text{C}/\text{winter}$ (standard errors of trends: $\pm 0.12, 0.11, 0.07\text{ }^{\circ}\text{C}/\text{winter}$) and c) summer trends (months June, July, August) are $0.08, 0.1, 0.12\text{ }^{\circ}\text{C}/\text{summer}$ (standard error of trends: $\pm 0.05, 0.04, 0.03\text{ }^{\circ}\text{C}/\text{summer}$) [Boike et al. 2017].

Table 3: Maximum Soil Temperatures: Absolute annual maximum soil temperatures at depths 0.1, 0.71 and 141 m.

UTM	Ts1		Ts71		Ts141	
	depth	date	depth	date	depth	date
1999	12.8207	18.07.99	3.8495	24.07.99	0.1376	07.09.99
2000	7.993	12.08.00	2.7014	19.08.00	-0.5494	17.11.00
2001	9.2719	27.07.01	2.7205	15.08.01	-0.3209	10.11.01
2002	10.1543	13.07.02	4.199	19.08.02	0.3235	19.10.0
2003	9.8665	13.07.03	3.529	09.08.03	0.151	10.09.03
2004	11.1474	12.07.04	3.7522	30.07.04	0.312	10.10.04
2005	11.3607	07.07.05	4.3938	02.08.05	0.3924	05.09.05
2006	11.8052	23.07.06	5.5484	26.07.06	1.8604	20.08.06
2007	11.9309	03.08.07	6.5931	08.08.07	2.2536	12.08.07
2008	10.415	23.07.08	3.7617	27.08.08	1.0257	22.09.08
2009	11.5241	02.08.09	5.2914	06.08.09	1.384	21.08.09
2010	16.69	13.07.10	4.535	07.08.10	0.765	12.08.10
2011	16.79	19.07.11	5.674	23.07.11	2.164	03.09.11
2012	16.46	21.07.12	4.601	30.07.12	1.95	03.09.12
2013	15.7	03.07.13	5.088	08.08.13	3.152	11.08.13
2014	13.23	15.07.14	3.941	19.08.14	1.458	13.09.14
2015	16.72	01.08.15	6.242	05.08.15	1.754	18.08.15
2016	16.88	11.07.16	5.746	21.07.16	3.287	19.09.16

Table 4: Minimum Soil Temperatures: Absolute annual minimum soil temperatures at depths 0.1, 0.71 and 141 m.

UTM	Ts1		Ts71		Ts141	
	depth	date	depth	date	depth	date
1999	-8.6581	18.04.99	-7.9533	19.04.99	-7.0133	22.04.99
2000	-16.0972	07.03.00	-12.791	14.03.00	-10.5472	16.03.00
2001	-9.1914	17.04.01	-7.528	17.04.01	-6.9521	01.05.01
2002	-10.3048	26.10.02	-7.0219	14.05.02	-6.513	15.05.02
2003	-15.6492	01.02.03	-13.9998	03.02.03	-11.7122	07.02.03
2004	-9.1182	12.02.04	-8.7164	07.03.04	-7.6345	08.03.04
2005	-8.1272	23.03.05	-7.6654	31.03.05	-6.0361	31.03.05
2006	-3.3589	05.04.06	-2.7638	06.04.06	-2.8671	26.04.06
2007	-3.1645	01.05.07	-3.077	10.05.07	-2.758	10.05.07
2008	-7.2646	03.04.08	-6.1867	08.04.08	-4.9415	02.05.08
2009	-8.41	12.10.09	-3.6961	05.05.09	-2.9549	08.05.09
2010	-14.25	24.03.10	-11.78	01.04.10	-8.72	06.04.10
2011	-10.07	15.11.11	-4.579	14.02.11	-3.607	24.04.11
2012	-9.31	01.01.12	-6.377	02.05.12	-5.252	02.05.12
2013	-7.803	12.04.13	-6.31	22.04.13	-4.95	25.04.13
2014	-6.127	30.10.14	-2.415	09.05.14	-2.06	18.05.14
2015	-8.87	13.02.15	-5.543	16.02.15	-3.774	16.04.15
2016	-13.59	12.01.16	-4.617	22.04.16	-3.786	27.04.16

Table 5: Permafrost Temperatures: Results of trend analysis.

	Ts250	±	Ts350	±	Ts550	±	Ts750	±	Ts900	±
Year	0.132	0.080	0.102	0.046	0.060	0.010	0.056	0.010	0.046	0.012
Spring	0.172	0.197	0.131	0.078	0.048	0.014	0.039	0.018	0.029	0.017
Summer	0.039	0.060	0.098	0.059	0.093	0.025	0.074	0.014	0.059	0.015
Autumn	0.076	0.023	0.062	0.020	0.055	0.020	0.061	0.023	0.054	0.019
Winter	0.116	0.043	0.075	0.025	0.041	0.017	0.045	0.020	0.043	0.019
January	0.165	0.053	0.084	0.024	0.049	0.016	0.055	0.019	0.051	0.017
February	0.092	0.052	0.094	0.030	0.042	0.016	0.045	0.019	0.044	0.017
March	0.141	0.139	0.105	0.038	0.044	0.015	0.049	0.018	0.043	0.017
April	0.160	0.170	0.156	0.063	0.064	0.017	0.057	0.018	0.046	0.018
May	0.270	0.199	0.239	0.114	0.073	0.024	0.044	0.025	0.032	0.027
June	0.084	0.103	0.147	0.088	0.093	0.024	0.062	0.016	0.048	0.020
July	0.020	0.056	0.090	0.057	0.097	0.026	0.076	0.015	0.060	0.015
August	0.083	0.046	0.092	0.031	0.091	0.018	0.093	0.013	0.075	0.011
September	0.077	0.029	0.062	0.027	0.055	0.026	0.055	0.028	0.048	0.022
October	0.074	0.023	0.061	0.020	0.055	0.020	0.062	0.023	0.054	0.019
November	0.079	0.022	0.064	0.019	0.053	0.019	0.059	0.021	0.053	0.019
December	0.121	0.035	0.069	0.019	0.050	0.017	0.056	0.020	0.052	0.019

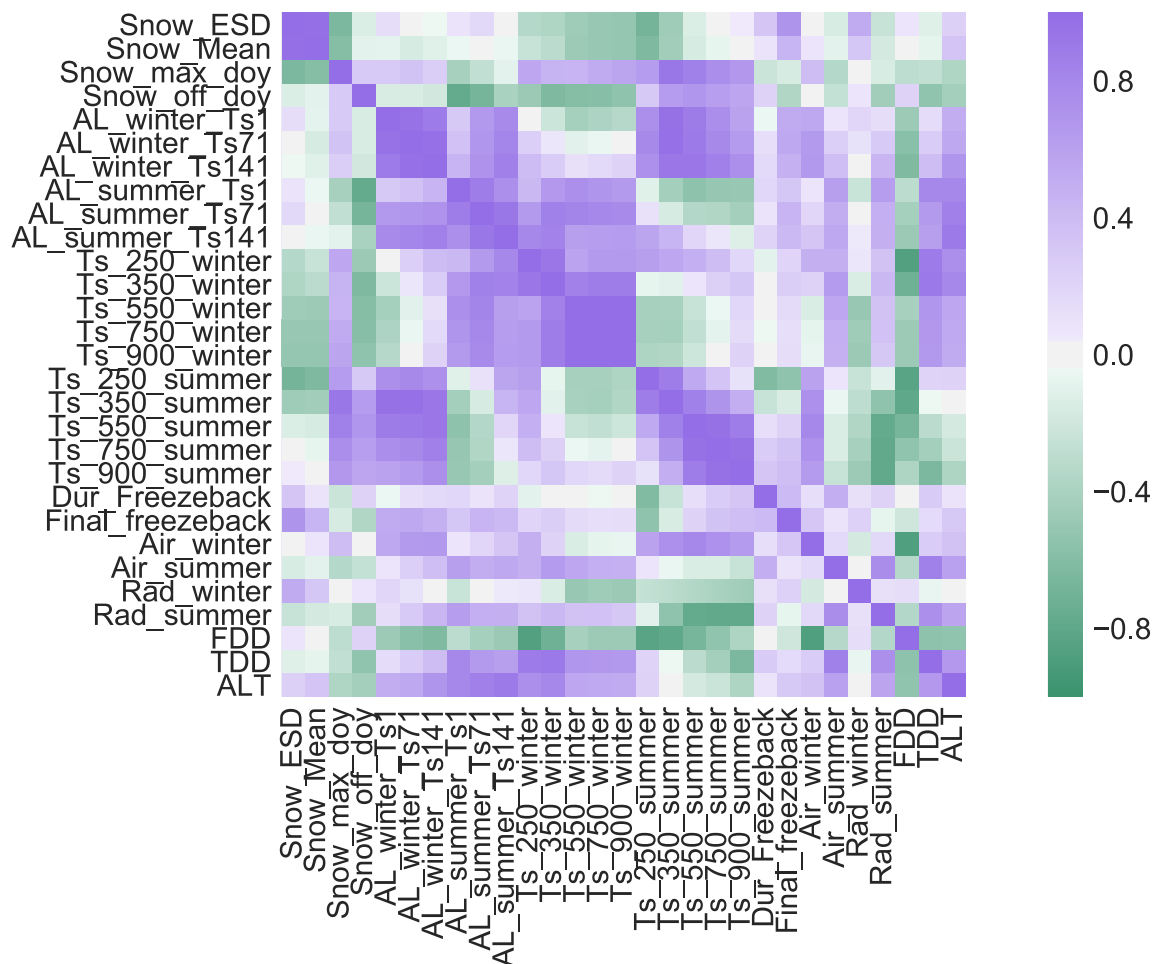


Figure 27: Heatmap of many parameters analyzed in this thesis. Background is a pairwise standard correlation (pearson-value). The color indicates the level of correlation as shown in the legend on the left. Purple shades are positive correlations, green shades negative correlations. Description of the variables can be found in table 6.

Table 6: Correlation Variables: Name and description of variables used for correlation analysis.

Variable	Description
Snow_ESD	Effective Snow Depth after Slater et al. 2017
Snow_Mean	Mean Snow depth of Cooling Season
Snow_max_doy	Absolute maximum Snow Depth
Snow_off_doy	End of Snow Cover (given in Day of Year)
AL_winter_Ts1	Active Layer winter Temperature at depth of 0.01 m
AL_winter_Ts71	Active Layer winter Temperature at depth of 0.71 m
AL_winter_Ts141	Active Layer winter Temperature at depth of 1.41 m
AL_summer_Ts1	Active Layer summer Temperature at depth of 0.01 m
AL_summer_Ts71	Active Layer summer Temperature at depth of 0.71 m
AL_summer_Ts141	Active Layer summer Temperature at depth of 1.41 m
Ts_250_winter	Winter Permafrost Temperature at depth of 2.5 m
Ts_350_winter	Winter Permafrost Temperature at depth of 3.5 m
Ts_550_winter	Winter Permafrost Temperature at depth of 5.5 m
Ts_750_winter	Winter Permafrost Temperature at depth of 7.5 m
Ts_900_winter	Winter Permafrost Temperature at depth of 9 m
Ts_250_summer	Summer Permafrost Temperature at depth of 2.5 m
Ts_350_summer	Summer Permafrost Temperature at depth of 3.5 m
Ts_550_summer	Summer Permafrost Temperature at depth of 5.5 m
Ts_750_summer	Summer Permafrost Temperature at depth of 7.5 m
Ts_900_summer	Summer Permafrost Temperature at depth of 9 m
Dur_Freezeback	Duration of complete freeze-up of Active Layer
Final_freezeback	Day of final freeze-up
Air_winter	Winter Air Temperature
Air_summer	Summer Air Temperature
Rad_winter	Winter Net Radiation
Rad_summer	Summer Net Radiation
FDD	Freezing degree-day Index
TDD	Thawing degree-day Index
ALT	Active Layer Thickness Estimate after Stefan-Model

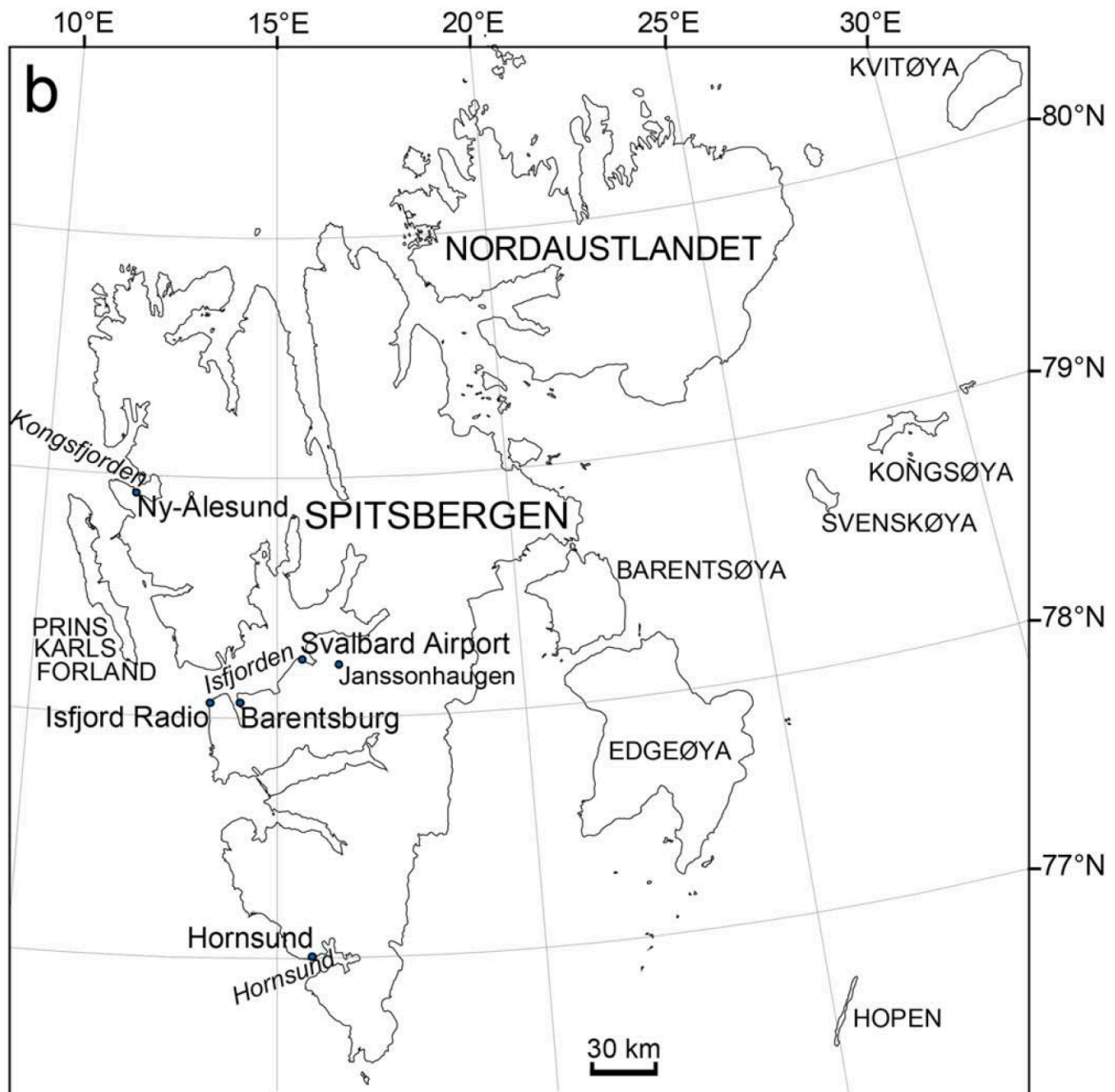


Figure 28: Location of meteorological stations on Svalbard [Isaksen et al. 2016].

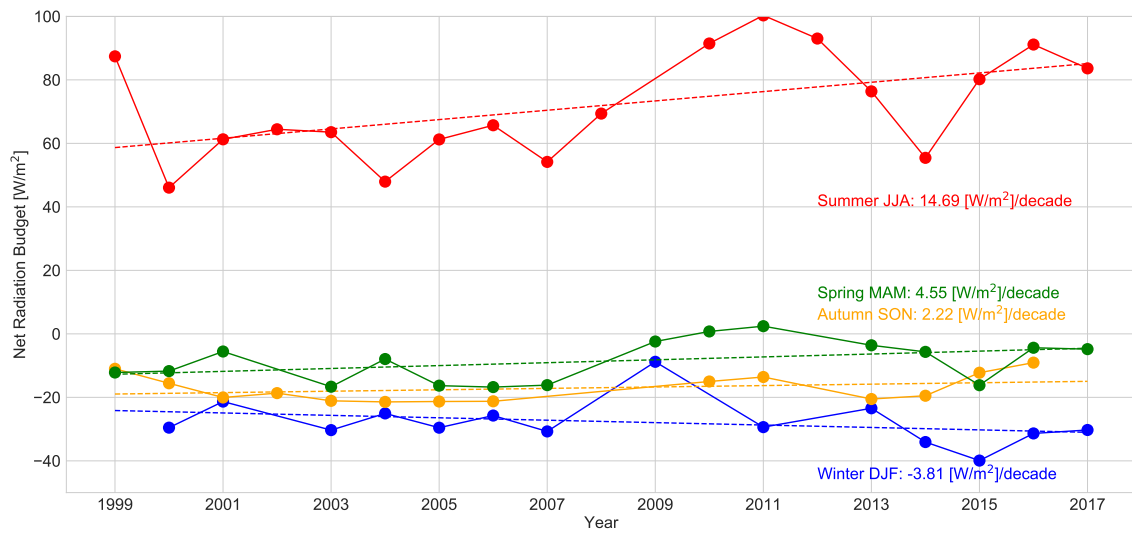


Figure 29: Seasonal trend analysis of the net radiation budget for the years 1999 to 2017. Summer mean values (red) show a positive trend of 14.69 W/m^2 per decade (standard error: $\pm 0.62 \text{ W/m}^2$ per decade), spring mean values (green) show a positive trend of 4.55 W/m^2 per decade (standard error: $\pm 0.27 \text{ W/m}^2$ per decade), autumn mean values (orange) show a positive trend of 2.22 W/m^2 per decade (standard error: $\pm 0.20 \text{ W/m}^2$ per decade) and winter mean values (blue) show a negative trend of -3.81 W/m^2 per decade (standard error: $\pm 0.34 \text{ W/m}^2$ per decade).

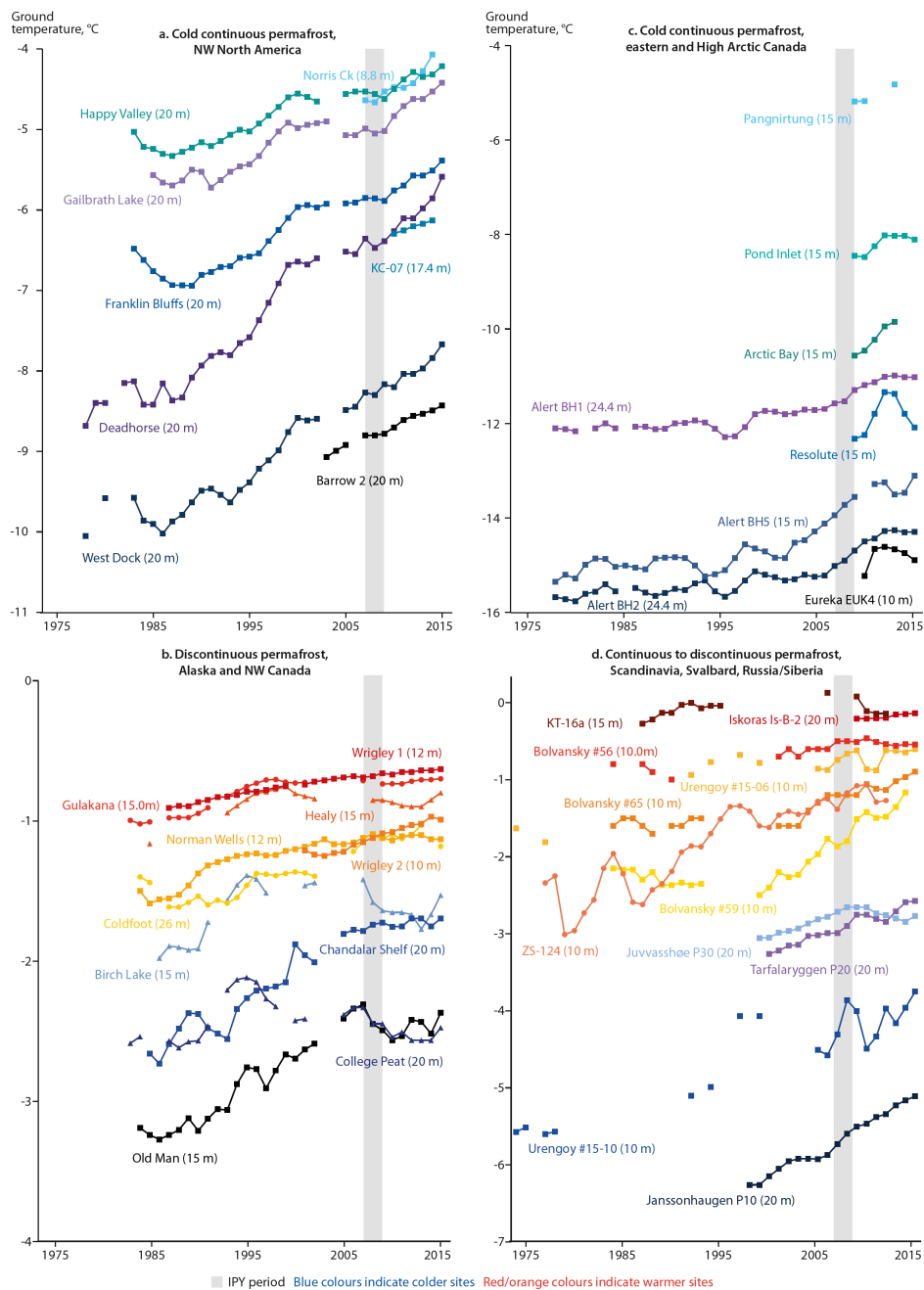


Figure 4.2 Time series of annual mean ground temperature at depths of 9 to 26 m below the surface at selected measurement sites (see Figure 4.1 for locations) that fall roughly into the AACA priority regions: (a) cold continuous permafrost of northwestern North America (Beaufort-Chukchi region); (b) discontinuous permafrost in Alaska and northwestern Canada; (c) cold continuous permafrost of eastern and High Arctic Canada (Baffin Davis Strait); and (d) continuous to discontinuous permafrost in Scandinavia, Svalbard, Russia/Siberia (Barents region). Temperatures are measured at or near the level of zero annual amplitude. Data series are updated from Christiansen et al. (2010), Romanovsky et al. (2014, 2015) and Ednie and Smith (2015).

Figure 30: Mean ground temperatures for several sites in the Arctic from the 2017 SWIPA report [AMAP 2017]